2012

INVESTIGATION OF BAND BENDING IN n- AND p-TYPE GaN

Michael Foussekis
Virginia Commonwealth University

INVESTIGATION OF BAND BENDING IN n- AND p-TYPE GaN

A Dissertation submitted in partial fulfillment of the requirements for the degree of Doctor of Philosophy in Nanoscience & Nanotechnology at Virginia Commonwealth University.

By:

Michael Alexander Foussekis

M.S. Applied Physics, Virginia Commonwealth University, 2009

B.S. Physics, Virginia Polytechnic Institute and State University, 2003

Directors:

DR. MICHAEL A. RESHCHIKOV

ASSOCIATE PROFESSOR, DEPARTMENT OF PHYSICS

&

DR. ALISON A. BASKI

PROFESSOR, DEPARTMENT OF PHYSICS

Virginia Commonwealth University

Richmond, Virginia

May, 2012

Acknowledgements

I would first like to extend my deepest gratitude to Dr. Alison Baski and Dr. Michael Reshchikov. Without their guidance and patience this work would not be possible. I appreciate all of the time spent over the years developing the ideas in this dissertation as a research group.

Dr. Baski, I would like to thank you for all of the stars you have given me over the years, I have really come to fear stars now instead of enjoying them like in elementary school. I always enjoyed getting your perspective on our work, as your brain seemed to reorganize the ideas for the better. Hopefully I can take the organization and logic skills you have taught me to wherever I may go.

Dr. Reshchikov, thank you for always leaving your office door open (especially so we can put stuff under your mouse). It has been a pleasure working in your laboratory for the past 5 years, and I have really enjoyed getting to know more about you. I am still astonished at how much you know, and without your passion and drive for science, this work would not be possible.

To my future wife Katherine Anna Golkow, without your love and support I think I would be in a mental institution right now. Thank you for standing by me for these 5 long years. With the completion of this dissertation, we can begin the rest of our lives together (in the same city for once). Again, thank you for all of your love and support.

To Joy McNamara (spelt correctly), thank you for letting me harass you these past 2 years. I hope you learned some interesting stuff, and I am excited to see what work you continue to do with Dr. Reshchikov. Take care of the Kelvin probe for me. Oh, I hope you find all of those sticky notes!

To all of the other graduate students at VCU in no particular order: Joe, Louis, Matt, Chuck, Steele, Vince, and Anita, I want to wish you the best of luck to you all of you on your future endeavors. Thank you for all of the support you have shown me over the years here at VCU. You all will be sorely missed. Let’s try to stay in touch!

And just because I have to……FIRST!

Table of Contents

List of Figures (captions)

Abstract

INVESTIGATION OF BAND BENDING IN n- AND p-TYPE GaN

By Michael Alexander Foussekis

A Dissertation submitted in partial fulfillment of the requirements for the degree of Doctor of Philosophy in Nanoscience & Nanotechnology at Virginia Commonwealth University.

Virginia Commonwealth University, 2012

Major Directors:

Dr. Michael A. Reshchikov

Associate Professor, Department of Physics

&

Dr. Alison A. Baski

Professor, Department of Physics

This dissertation details the study of band bending in n- and p-type GaN samples with a Kelvin probe utilizing different illumination geometries, ambients (air, oxygen, vacuum 10^{-6} mbar), and sample temperatures (77 – 650 K). The Kelvin probe, which is mounted inside an optical cryostat, is used to measure the surface potential. Illumination of the GaN surface with band-to-band light generates electron-hole pairs, which quickly separate in the depletion region due to a strong electric field caused by the near-surface band bending. The charge that is swept to the surface reduces the band bending and generates a surface photovoltage (SPV). Information about the band bending can be obtained by fitting the SPV measurements with a thermionic model based on the emission of charge carriers from bulk to surface and vice versa.

The band bending in freestanding n-type GaN templates has been evaluated. The Ga-polar and N-polar surfaces exhibit upward band bending of about 0.74 and 0.57 eV, respectively. The surface treatment also plays a major role in the SPV behavior, where the SPV for mechanical polished surfaces restores faster than predicted by a thermionic model in dark. When measuring the photoluminescence (PL) signal, the PL from mechanically polished surfaces was about 4 orders of magnitude smaller than the PL from chemically mechanically polished surfaces. The PL and SPV behaviors were explained by the presence of a large density of defects near the surface, which quench PL and aid in the restoration of the SPV via electron hopping between defects.

Temperature-dependent SPV studies have also been performed on doped n- and p-type GaN samples. In Si-doped n-type GaN, the estimated upward band bending was about 1 eV at temperatures between 295 and 500 K. However, in p-type GaN, the downward band bending appeared to increase with increasing temperature, where the magnitude of band bending increased from 0.8 eV to 2.1 eV as the temperature increased from 295 to 650 K. It appears that heating the p-type GaN samples allows for band bending values larger than 1 eV to fully restore. Pre-heating of samples was of paramount importance to measure the correct value of band bending in p-type GaN. The slope of the dependence of the SPV on excitation intensity at low temperatures was larger than expected; however, once the temperature exceeded 500 K, the slope began to reach values that are in agreement with a thermionic model.

Chapter 1: Introduction to Material System and Kelvin Probe

1.1 Motivation and Introduction

Light-emitting diodes (LEDs) based on gallium nitride (GaN) have recently attracted a great amount of attention as an energy efficient means for commercial lighting. One major application of GaN-based films was the development of high-brightness LEDs.[1] With the creation of these LEDs, it became possible to develop GaN-based LED displays and other commercial devices that require a light-emitter. GaN can also be synthesized into laser diodes, which have currently been implemented in "Blu-ray" disc technology.[2] In these devices, a GaN-based laser diode is used to read information stored on "Blu-ray" discs. This technology may become the next standard for storing optical data, since the Blu-ray discs hold about five times the amount of data than a standard DVD.[2]

Semiconductors with electronic band gaps larger than ~2 eV are classified as "wide-bandgap", and they are well suited for LEDs and high power applications. GaN is a semiconductor with a band gap of approximately 3.4 eV at room temperature. Along with its fairly large bandgap, GaN films have many other physical properties which make them promising for use in optoelectronics, high-power and frequency devices, LEDs, and laser diodes.[3] The melting point of GaN is about 2500^{o}C, and its thermal conductivity is about 1300 W/mK.[4] GaN films are also chemically stable at high temperatures and are extremely resilient to wet chemical etching.[5] The chemical, thermal, and inherent structural stability of GaN films make them appealing for use in devices or as protective coatings.[6]

Progress is currently being made in the understanding of the bulk and surface defects in GaN. The presence of defects in GaN-based devices is detrimental to their quantum efficiency

and reliability.[7] Gaining an understanding of the surface and bulk defects and their roles on device performance will aid the development of higher-quality GaN films for use in future devices. Despite tremendous progress in understanding of the bulk and surface defects in GaN, their effect on device performance is not yet completely understood.[8]

This dissertation is divided into nine chapters: (1) an introduction to the material system and experimental technique, (2) an extensive literature review on how band bending in GaN has been previously studied by others, (3) the experimental details of our setup, (4) the overview of a thermionic model used to fit surface photovoltage (SPV) data, (5) the SPV behavior of Si-doped n-type GaN, (6) the SPV behavior of polar, bulk undoped GaN, (7) the SPV behavior of Mg-doped p-type GaN, (8) X-ray photoelectron spectroscopy and the Hall effect measurements of GaN films, and finally (9) conclusions and future directions.

1.2 GaN

Gallium nitride was successfully grown in 1932 by Johnson *et al*.,[9] and was shown to be a mechanically and chemically stable semiconducting material. The growth of high-quality GaN films for use in devices is not an easy task; one of the major challenges is the high density of extended defects that occur during film growth. When GaN is grown as a thin film on a variety of substrates, it tends to have a high density of threading dislocations due to a poor match of the lattice parameters between GaN and its substrate.[10]

Gallium nitride naturally forms a wurtzite crystalline structure under ambient conditions.[10] This structure is the combination of two hexagonal closed-packed (HCP) lattices which are intermeshed. The unit cell of the GaN crystal structure is shown in Figure 1.

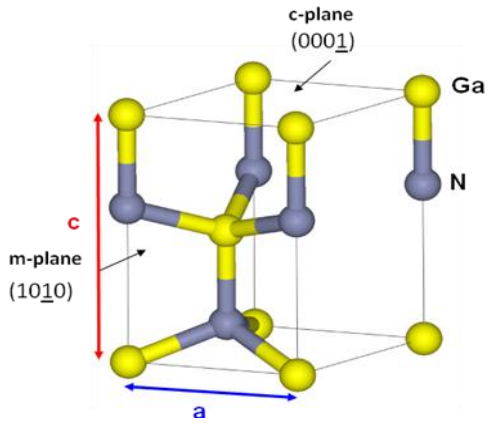

Figure 1 Unit cell of the wurzite structure of GaN. Lattice constant values: a = 3.19Å and c = 5.19Å.

The c-axis is polar, where one surface will terminate with Ga atoms and N atoms, which will introduce a spontaneous polarization inside of the crystal. Generally, c-plane sapphire or silicon carbide is used as a substrate for the epitaxy of c-plane GaN films.[11,12] The c-plane is the most commonly produced orientation for GaN films due to its low cost. Since there is no material with the same lattice parameters as GaN, the epitaxy of GaN on any substrate will introduce strain to the crystal.

The doping of GaN with shallow acceptors to produce p-type conductivity was a problem that took years to resolve. It was not until the late 1960's that the first electronic devices containing n- and p-type GaN-based films could be successfully synthesized.[13] Amano *et al.*[14] were the first to create Mg-doped GaN with good p-type conductivity by using low energy electron beam irradiation (LEEBI) in 1989. These authors were also able to synthesize the first GaN-based LED using the LEEBI technique to create a p-n junction.[14] In 1996, S. Nakamura *et al.*[15] successfully synthesized the first InGaN-based multiple quantum well structure for blue laser diodes. Even though GaN-based LED structures are routinely produced now, additional research is currently needed to produce higher quality and more cost effective GaN films.

A major issue that is still associated with the growth of GaN films is the high density of point and extended defects, which prove detrimental to device performance.[4,16] Reducing the large number of extended defects has been a goal in the research and development of GaN film growth. Research of the GaN surface has progressed tremendously over the years, but the influence of the surface conditions on device performance is still not completely understood.

As a result of a net negative or positive surface charge, the surfaces of n- and p-type GaN exhibit upward and downward band bending, respectively.[17,18,19] The band bending (Φ_0) gives rise to a depletion region, which affects the optical and electronic properties of GaN-based devices.[20] The dominant source of surface charge responsible for the band bending at the surface of GaN is still unknown, but it may be related to the defects in the GaN crystal.

In this work, we will divide the surface defects in GaN films into two categories: internal and external. The internal defects consist of defects belonging to the GaN crystal such as dangling bonds, impurities, native defects, spontaneous polarization, stress in the crystal lattice, and surface reconstructions. In an attempt to reduce the number of internal defects, GaN films are synthesized by hydride vapor phase epitaxy (HVPE), molecular beam epitaxy (MBE), or metal organic chemical vapor deposition (MOCVD) and are epitaxied onto sapphire, silicon, and silicon carbide substrates.[11,12,21] The presence of a large amount of internal defects along with their poor understanding negatively affects the efficiency and reliability of GaN-based devices.[22]

Along with the internal defects which are related to the crystal structure, the external defects also contribute to poor device performance. The external defects can include a native thin oxide layer and any adsorbed species. It has been established that a monolayer of chemisorbed oxygen exists on the surface of GaN, which may form a thin (~1 nm) oxide layer on the

surface.[23] Work has been performed to determine the properties of the native surface oxide on GaN; however, there is little information about the properties of this oxide layer.[24]

The internal (surface related) and external (adsorbed species) defects in GaN films lower the efficiency of GaN-based devices. Both the internal and external defects may contribute to the net surface charge which is responsible for band bending in GaN films, but the roles of these defects in the magnitude of the near-surface band bending are still unknown.

In this dissertation, the band bending in GaN will be investigated through the surface photovoltage (SPV) behavior measured by a Kelvin probe setup. In particular, the band bending will be estimated by fitting SPV measurements with a thermionic model.

1.3 Kelvin Probe Method

The Kelvin probe technique provides a non-contact, non-destructive measurement of the work function of a given material in reference to a vibrating metal probe. This method is very sensitive to the top most atomic layers, which makes it a valuable tool for surface studies. The Kelvin probe setup is structured like a vibrating capacitor and is able to measure the difference in work functions between two conductive materials. William Thomson (Lord Kelvin) schematically designed the Kelvin probe apparatus and technique around 1861, and N. Knoble was the first person to utilize a constantly vibrating reference probe in 1932.[25] The Kelvin probe measures the contact potential difference (CPD), or potential difference between a surface and probe. This potential difference is proportional to the amount of surface charge. By measuring the surface potential of our samples, we are able to obtain information about the near-surface band bending, as well as about what chemical processes occur at the surface in dark and under

illumination.

Chapter 2: Literature Review

The band bending in GaN can be measured by various techniques. The most common techniques to measure band bending in semiconductors are X-ray photoelectron spectroscopy (XPS), ultraviolet photoelectron spectroscopy (UPS), atomic force microscopy (AFM) in scanning Kelvin probe mode (SKPM), and the Kelvin probe technique. Results from the study of band bending in GaN using these techniques are reported and discussed below.

2.1 XPS and UPS studies of band bending in GaN

X-ray photoelectron spectroscopy (XPS) and ultraviolet photoelectron spectroscopy (UPS) have been used previously to determine the amount of band bending in various semiconductors, including Si and GaAs.[26,27,28,29,30,31] Researchers have used these techniques to also study band bending in both n- and p-type GaN. [32,34,37,39,40,41]

Under X-ray or high energy UV illumination with photon energy $h\nu$, electrons are ejected from GaN into vacuum. In an XPS or UPS setup, these ejected electrons are captured by a electron detector which measures their kinetic energy (KE) based on the field applied. The XPS spectra are commonly plotted as electron counts vs. binding energy (BE), where:

$$BE = h\nu - KE.$$

The electrons that are ejected from the surface and measured by the detector will come from the top 1-10 nm near the surface. Due to the presence of band bending at the surface, the photo-ejected electrons then will originate from the depletion region. It is important to note that the

binding energy is defined as the energy from a given electron orbital to the surface Fermi-level. The surface Fermi-level will be located deeper than the bulk Fermi-level due to the upward or downward band bending.

Figure 2 shows an energy level diagram for the sample and XPS spectrometer, assuming that the measured sample is a conductive material.

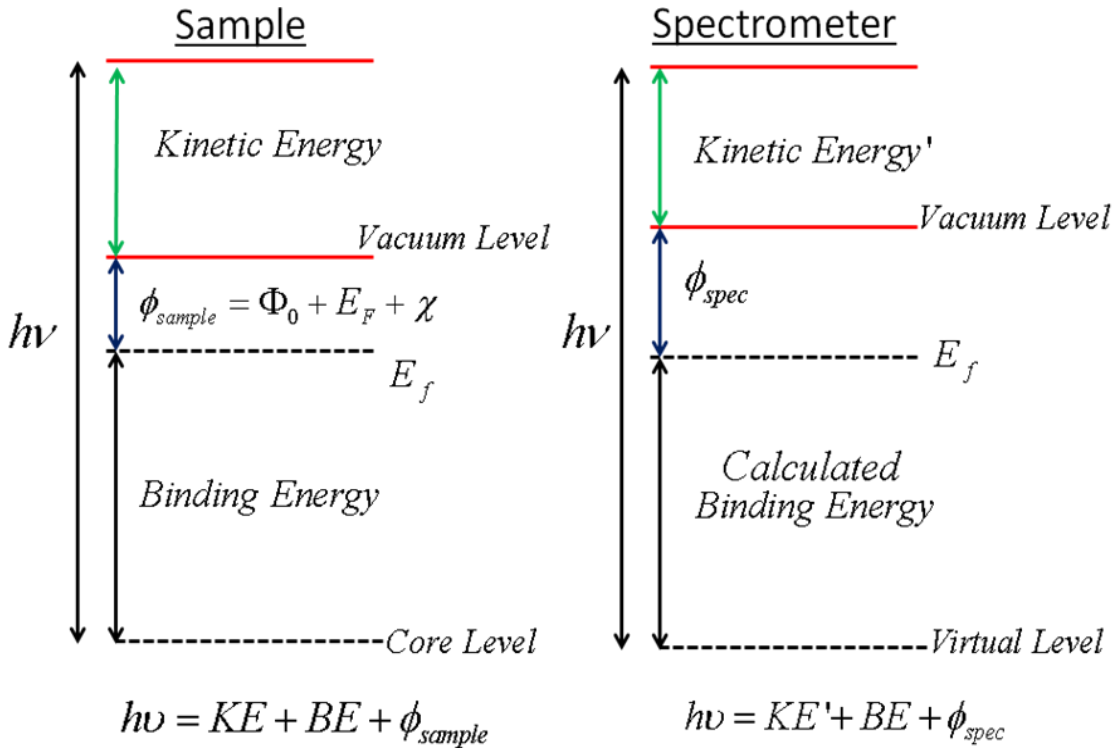

Figure 2 Energy level diagram of sample and XPS spectrometer. In this diagram it is assumed that the sample is conductive, so that the Fermi-levels align.

It is assumed for a conductive sample that the Fermi-levels of the spectrometer and sample are aligned. The kinetic energy measured by the spectrometer, KE', is different than the true value of the kinetic energy of the photo-ejected electron, KE, because it is affected by the work function of the spectrometer, ϕ_{spec}. However, when the Fermi-levels are aligned, one does not need to know the work function of the sample, ϕ_{sample}, and the true value of the kinetic energy,

KE. Instead, the known value of ϕ_{spec} and the measured KE' could be used to calculate the binding energy as:

$$BE = h\upsilon - KE_{measured} - \phi_{spec}.$$

Therefore, it is imperative for the Fermi-levels to be in alignment to measure the absolute values of the binding energy in XPS measurements. If the Fermi-levels are not aligned, the values of the reported values of the binding energy will be shifted. Also for our GaN samples, changing the band bending will additionally shift the values of the binding energy due to changes in the work function of the sample. Another source of error can stem from how stable the work function of the detector is. The adsorption coefficient for Mg-Kα X-rays in GaAs is about 1000 to 10,000 cm^{-1}, which is expected to be similar for GaN.[33] The penetration depth of the X-ray will not play a major role in the number of electrons measured; the limiting factor is the ability for electrons to escape the surface without undergoing collisions (mean free path). This means electrons will be captured from the first few nanometers (up to10 nm) of the material.

By accurately determining the position of an electron orbital relative to the valence band (E_V - *Orbital*), the position of the surface Fermi-level can be estimated as:

$$E_{F\ Surface} = BE - (E_V - Orbital).$$

Using XPS or UPS data, the band bending in GaN can be estimated using the measured position of the Ga_{3d} peak. Figure 3 illustrates how the position of the surface Fermi-level can be obtained from measurement of the Ga_{3d} peak with XPS/UPS.

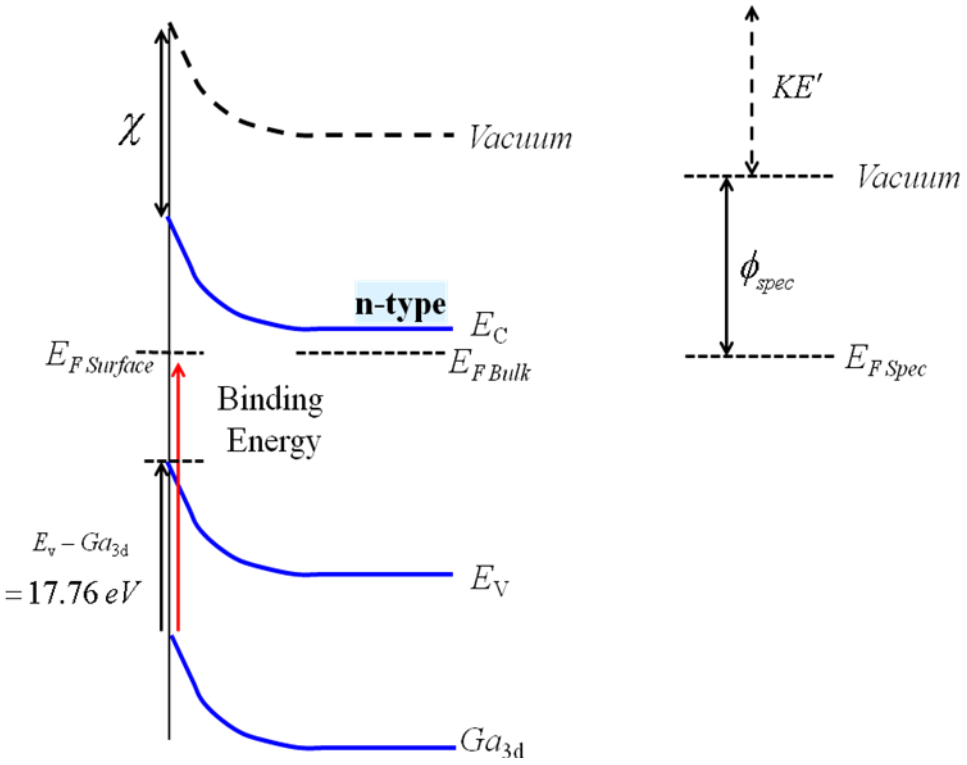

Figure 3 Schematic band diagram of GaN showing the position of the Ga_{3d} orbital. Since the position of the Ga_{3d} peak relative to the valence band is known, the position of the surface Fermi-level can be calculated.

In this example, the binding energy (red arrow) measured from the XPS/UPS setup is defined as the energy from the Ga_{3d} level to the surface Fermi-level. From this figure, it is apparent that the surface Fermi-level position can be estimated as:

$$E_{F\,Surface} = BE_{Ga3d} - 17.76\,\text{eV}.$$

The position of the bulk Fermi-level can be determined from the Hall effect. With the information about the position of the Ga_{3d} peak (therefore the surface Fermi-level) and the bulk Fermi-level, it is possible to estimate the band bending as the difference between the bulk and surface Fermi-levels.

Waldrop and Grant[34] accurately measured the energy difference between the valence band maximum and the energy level of the Ga_{3d} peak to be approximately 17.76±0.03 eV, for an AlN/GaN heterojunction. The results are shown in Figure 4.

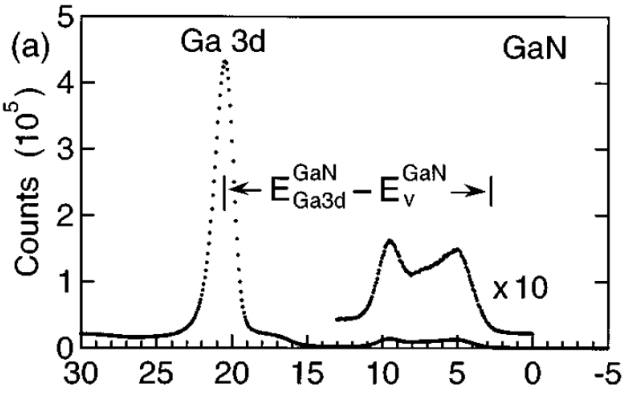

Figure 4 XPS binding energy spectrum for GaN (0001). [34]

The data from this figure was fit with a theoretical broadening of the valence band density of states for GaN (fitting not shown in this figure).[35] The purpose of this fitting was to accurately determine the position of the valence band maximum relative to the Ga_{3d} peak. This type of fitting was performed 15 times in different locations to enhance their accuracy. They believed that the results from this measurement were more accurate than the previously measured 17.1 eV by Martin *et al.*[36] who also used XPS on an AlN/GaN heterostructure. The measurement of the Ga_{3d} peak will provide information about the position of the surface Fermi-level, since photo-generated electrons are ejected from the depletion region close to the surface.

In this work, the position of the position of the surface Fermi-level determined by XPS will be calculated by subtracting the measured value of the Ga_{3d} peak from the value the value of $E_{Ga3d} - E_{Valence\ Band}$ (17.76±0.03 eV), measured by Waldrop and Grant.[34]

This method of calculating band bending has been employed by Tracey *et al*.[37] for clean n- and p-type GaN surfaces. They studied the surfaces of n- and p-type GaN grown on an AlN buffer layer by the metal organic vapor phase epitaxy (MOVPE) technique. The surfaces included an n-type sample with n ~2×10^{17} cm^{-3}, and a p-type sample with N_A-N_D ~3×10^{18} cm^{-3} calculated from the Hall effect and C-V measurements, respectively. In this study, all of the samples were treated with acetone, methanol, and then kept in HCl (37%) for 10 min. Afterwards, all of the samples were rinsed with deionized water for 10 s and loaded into the XPS chamber. The XPS spectra were taken from the samples as-loaded (after the previously described treatment), or were additionally cleaned *in situ* with a chemical vapor cleaning process. The cleaning process involved exposing the samples to ammonia and annealing at 865^{o}C for 15 min. Figure 5 shows the XPS spectra from the as-loaded, and cleaned GaN(0001) surfaces.

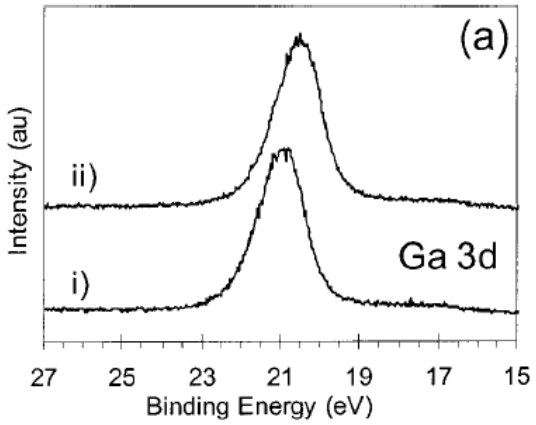

Figure 5 XPS spectra of Ga_{3d} peak for (i) as-loaded GaN(0001) and (ii) clean GaN(0001) surfaces. The spectra were obtained using Mg K_a X-rays. The spectra were offset vertically for ease in viewing. [37]

The Ga_{3d} peak positions for the as-loaded and cleaned surfaces of the n-type GaN samples were 21.0±0.1 eV (FWHM 1.3±0.1 eV) and 20.6±0.1 eV (FWHM 1.3±0.1 eV), respectively. The Ga_{3d} spectra exhibited a similar behavior in the p-type GaN surfaces, where the position of the Ga_{3d}

level was measured to be 19.6±0.1 eV for the as-loaded sample and 18.9±0.1 eV after the cleaning procedure.

The band bending can be calculated from the difference in the positions of the bulk and surface Fermi-levels. In this work, the authors have measured the bulk Fermi-level to be 0.1 eV below the conduction band and 0.3 eV above the valence band for the n- and p-type GaN samples, respectively. Using the spectra of the Ga_{3d} peak, we can calculate the values of the surface Fermi-level to be about 0.19 and 0.59 eV below the conduction band for the as-loaded and cleaned n-type samples, respectively. For the as-loaded sample:

$$E_{CB} - E_{F\ Surface} = (3.43) - (21.0 - 17.76) = 0.19\ \text{eV}.$$

Using the positions of the surface Fermi-levels we calculated, we can estimate the upward band bending to be about 0.09 and 0.49 eV for the as-loaded and cleaned samples, respectively. An example calculation is shown below for the cleaned n-type GaN surface,

$$E_{F\ Surface} - E_{F\ Bulk} = 0.59 - 0.1 = 0.49\ \text{eV}.$$

For the p-type GaN samples using the Ga_{3d} peak positions, we calculate that the surface Fermi-level positions as 1.84 and 1.14 eV above the valence band for the as-loaded and cleaned samples, respectively. Using this data we can estimate the downward band bending in the studied p-type GaN samples to be about -1.54 and -0.84 eV for the as-loaded and cleaned samples, respectively.

In UPS, the surface is illuminated with high energy ultraviolet light instead of X-rays. This is assumed to make the technique more surface sensitive, most likely due to a change in the adsorption coefficient. Since the UPS technique uses a lower photon energy, it can only probe the lower limits of binding energy (< 50 eV). The threshold of the UPS spectra can be used to

identify the valence band maximum, meaning the spectrum can be shifted in reference to the Fermi-level.

Figure 6 shows how Tracey *et al.*[37] measured the valence band maximum from their UPS spectra.

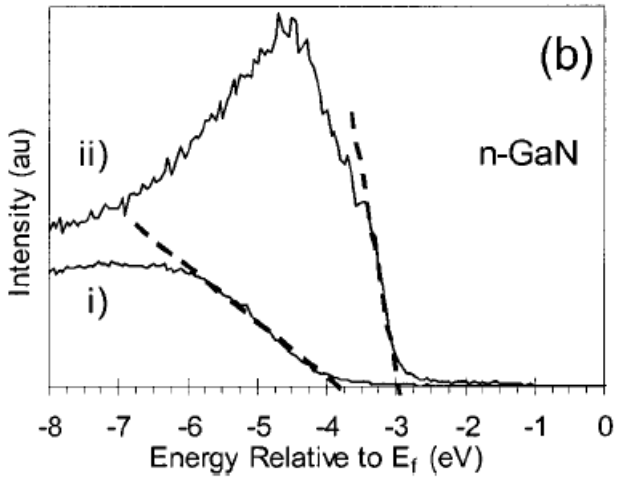

Figure 6 Expanded view of the valence band maximum for as loaded (i) and cleaned (ii) n-type GaN. Ref. [37]

In this figure, the authors decided to use linear fits to determine the position of the valence band maximum. It is possible to fit this data with the broadened valence band density of states, but the authors chose not to.[34,35] This will introduce error in measured position of the valence band maximum, since the fits added to the figures in Ref. [37] did not require any calculations.

The position of the valence band maximum in reference to the Fermi-level for the cleaned surfaces using UPS was determined to be about 3.0±0.1 eV for n-type GaN and 1.1±0.1 eV for p-type GaN. These measurements were also performed on the as-loaded samples and provide values of 3.9±0.1 eV and 3.0±0.1 eV for n- and p-type GaN, respectively. The authors commented that the values of the valence band maximum for the as-loaded samples appeared very unreliable. They attributed this to oxide formation, and cite similar results by King *et al.*[38]

Since the curves were fit linearly, and not with any type of model, I believe that this introduces error in their estimates. Also, the value of 3.9 eV measured for the valence band maximum of the as-loaded surface is entirely unreasonable, this means that the surface Fermi-level has to be located about 0.5 eV above the conduction band. Figure 7 summarizes the results from their study.

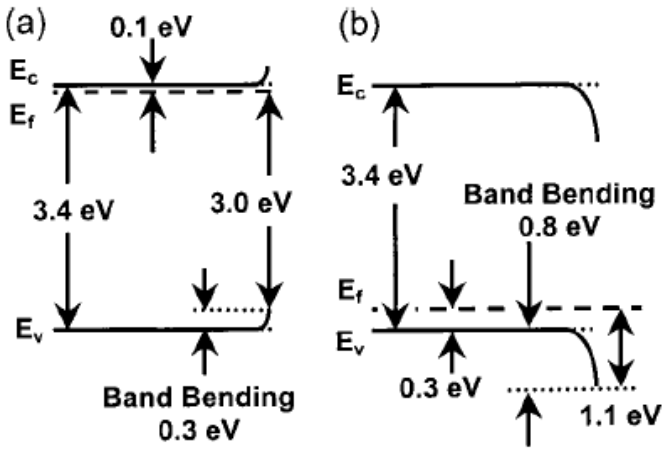

Figure 7 Schematics of the band of (a) n-type GaN and (b) p-type GaN. On the left side is the flat band condition, and on the right side is the band bending measured from the cleaned surfaces in their study. [37]

Using the UPS measurements to determine the position of the surface Fermi-level, the authors report that there exists upward bend bending of about 0.3 eV and downward band bending of -0.8 eV for the cleaned n- and p-type GaN samples, respectively. The authors did not comment on the band bending of the as-loaded samples, most likely due to the fact the results would be unreasonable.

To summarize, we will compare how the authors measured band bending in this work, with the calculations we performed using the data provided. The authors used the results from the UPS experiments to determine the band bending in their cleaned samples. We additionally used the position of the Ga_{3d} peak to estimate the near surface band bending. Table I summarizes

the results presented in Ref. [37] and the additional calculations done by us using the data provided in this work.

Table I: Band bending reported and calculated for n- and p-type GaN samples from Ref. [37].

Sample	**Φ_0 from UPS reported by authors (eV)**	**Ga3d position reported by authors (eV)**	**Bulk Fermi-level position by authors (eV)**	**Surface Fermi-level position from Ga_{3d} calculated by us (eV)**	**Φ_0 Calculated using Ga_{3d} by us (eV)**
Cleaned: n	0.3	20.6	0.1	0.56	0.49
Cleaned: p	-0.8	18.9	0.3	1.14	-0.84
As-loaded: n	—	21.0	0.1	0.16	0.09
As-loaded: p	—	19.6	0.3	1.84	-1.54

The data obtained for the band bending in the cleaned surfaces made by us using the Ga_{3d} peak position (XPS technique) and made by the authors using for the (UPS technique) are in agreement. However, the estimates of band bending for the as-loaded samples using the Ga_{3d} peak provides values that are 0.4 eV smaller for n-type GaN and -0.7 eV larger for p-type GaN. For the as-loaded n-type GaN surface, it appears that there is almost no upward band bending (0.09 eV), and this result disagrees with other reports.[17] For the p-type GaN sample, it appears that the downward band bending increased to about -1.54 eV.

Performing these additional estimates of the band bending using the XPS data indicates the potential error in XPS or UPS when estimating the band bending. The estimates of the band bending for clean surfaces are within 0.1 eV; however, the estimates for the as-loaded surfaces vary more than 0.4 eV. This may indicate that XPS or UPS is extremely sensitive to surface conditions, and contribute to the measured differences in the band bending in these two surfaces.

There is an additional inherent problem with measuring the near-surface band bending using the XPS technique. For n-type GaN, the incoming X-rays eject electrons from the

depletion region and create holes. These remaining holes are then swept to the surface, which generates a surface photovoltage (SPV) that reduces the net upward band bending.[39] The magnitude of the SPV generated will increase with the illumination power density of the incident X-ray beam. The illumination of p-type GaN with X-rays will also generate a SPV, since electrons will be ejected and holes will be swept from the depletion region to the bulk. The resulting electrons that flow towards the surface from the bulk may generate a SPV. Tracey *et al.*[37] kept this in consideration and believed that their estimates gave the lower limit of band bending in their n- and p-type GaN samples.

Suzer *et al.*[40] measured the effect that an external light has on the measured peak positions in their XPS setup. In this study, the sample was additionally illuminated by directing a laser beam inside of their XPS chamber to the same position as the incident X-ray beam. The authors believed that their 50 mW at 405 nm laser would generate an additional SPV (aside from the SPV generated by the X-rays). The effect of the laser illumination on the measured peak position is shown in Figure 8.

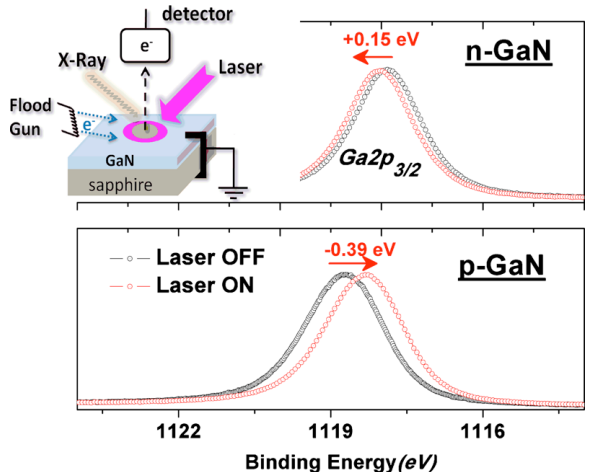

Figure 8 The Ga $2p_{3/2}$ region for the n- and p-GaN samples without and under illumination with a 50 mW 405 nm laser. The experimental set-up is shown as an insert. [40]

The incoming laser beam generated a significant SPV and shifted the measured binding energies in both n- and p-type GaN. The shifts in the peak positions when the laser is on correspond to a decrease of the near-surface band bending, which is consistent with the SPV effect explanation previously described in this dissertation. The laser illumination was able to additionally reduce the band bending by about 0.15 and 0.39 eV for the n- and p-type GaN samples, respectively.

In this work, Suzer *et al*.[40] did not report on the magnitude of band bending in their GaN samples, since their goal was to experimentally verify that an externally-generated SPV can shift the measured binding energies in their XPS spectra. The authors did comment that the SPV generated from below-bandgap excitation was larger for their p-type GaN sample. They attributed the difference in the shifts to the fact that the band bending in p-type GaN is expected to be larger than n-type GaN, and should therefore have a larger SPV. We conclude that XPS and UPS measurements may prove unreliable if the SPV generated from the incoming X-ray beam or any parasitic light is not taken into account.

V. M. Bermudez *et al*.[17,41] performed UPS and XPS measurements to determine the amount of upward band bending in clean GaN-(0001) surfaces. In the Ref. [41], before the UPS and XPS data were taken, the surfaces were cleaned by sputtering with nitrogen atoms, and were subsequently annealed *in situ*. They measured two samples in these studies with free electron concentrations of 1.6×10^{17} and 5.7×10^{17} cm^{-3}. The XPS spectra of the Ga_{3d} peak for clean GaN surfaces are shown in Figure 9.

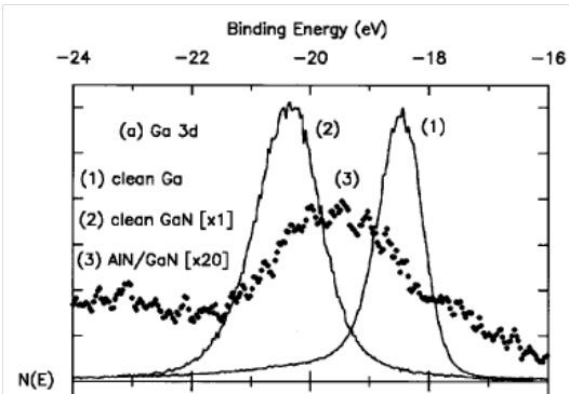

Figure 9 XPS spectra of the Ga_{3d} level for clean GaN surface. ZrMζ = 151.5 eV. [41]

The authors mentioned that their measured binding energies of the Ga_{3d} peak were larger than other values which are reported in the literature. They attributed this to many factors: smaller near surface band bending, surface charging, or a SPV effect caused by the X-ray or UV illumination. Surface charging may play a role, and will shift peaks towards higher binding energies due to the additional energy required to remove electrons from ionized atoms. The results from various studies performed by this group are shown in Table II.

Table II: Summary of the Ga3d peak positions from various reports. [41]

Binding Energy Ga_{3d}(eV)	E_F - E_V (eV)	Surface Preparation
20.3	1.9	MOCVD on sapphire; Ga-flux annealed in UHV
19.2	—	Gas-source MBE on sapphire
20.0	—	Gas-source MBE on SiC
19.5	< 0.5	N_2-ion bombardment of GaAs
19.7	—	Nitrogen sputtering of Ga onto Si
19.7	2.0	Vapor-phase epitaxy on sapphire, wet etching, in situ annealing
17.1	—	Gas-source MBE on sapphire

Along with the spectrum of the Ga_{3d} peak, Bermudez *et al.*[41] also measured the work function and electron affinity in their GaN sample with their low energy X-ray XPS setup to be $\phi = 4.2 \pm 0.2$ eV, and $\chi = 2.7 \pm 0.3$ eV, respectively. This was done by identifying the valence band maximum, and therefore surface Fermi-level position. With the position of the surface Fermi-level, and the position of the first observed peak, which is equal to the work function, ϕ, the electron affinity can be calculated as their difference.

The position of the bulk Fermi-level in their sample was estimated to be about 0.07 eV below the conduction band, whereas the surface Fermi-level was estimated to be at 1.9 eV above the valence band. Using these values, the upward band bending in their n-type GaN samples was calculated to be about 1.4 eV.

In this report, the authors used a value of 18.4 eV for the energy distance from the Ga_{3d} peak to the valence band maximum. If instead they used the value measured by Waldrop *et al.*,[34]

they would have estimated the band bending to be about 0.8 eV. Calculated the band bending using the latter values provide an estimate that is in better agreement with values measured with our Kelvin probe setup.

The surface cleaning in Ref. [17] was performed by depositing a thick layer of Ga metal onto the surface, followed by an anneal at ~900^{o}C *in situ*. The details of the sample cleaning can be found in Ref. [41]. In this work, Bermudez performed the same series of XPS measurements on a similar GaN sample. He revised his previous estimate of the near-surface band bending by correcting the measured value of the electron affinity to be $\chi = 3.2 \pm 0.2$ eV and the measured position of the valence band maximum. This change in the electron affinity accounted for the observation of surface states in their UPS spectra, which lead to Fermi-level pinning (E_F-*VBM)* at the surface. They also estimated that the Ga_{3d} level is 17.9 eV below the valence band, not 18.4 which was used in the previous report. This correction reduces the calculated band bending from 1.4 to about 0.9 eV (18.4 – 17.9 eV). This calculated value of band bending agrees strongly with estimates done by others, as well as with our Kelvin probe measurements.

They were also able to use the Ga_{3d} peak to estimate the band bending for cleaned and practical surfaces. By comparing the relative positions of the Ga_{3d} peaks for the cleaned and practical surface, the relative band bending could be estimated. Performing this quick calculation yields values that the band bending for the practical surfaces is about 0.5 eV smaller than for the cleaned surface; i.e., $\Phi_0 \sim 0.4 \pm 0.2$ eV for the practical surface.

2.2 AFM

An atomic force microscope (AFM) in scanning Kelvin probe microscopy (SKPM) mode has been previously used to locally map the surface potential of various films.[42,43,44] With the local surface potential values, some sample parameters, and the work function of the probe, the band bending can be calculated.[45] In a work by Reshchikov *et al.*,[46] the surfaces of two undoped MBE-grown GaN samples were measured with SKPM while being illuminated by a laser. The laser beam generates a SPV, which is measured as a change in the surface potential in dark and under illumination. Information about band bending could be calculated from the magnitudes of the SPV generated as a function of excitation intensity. The SPV decay is shown in Figure 10.

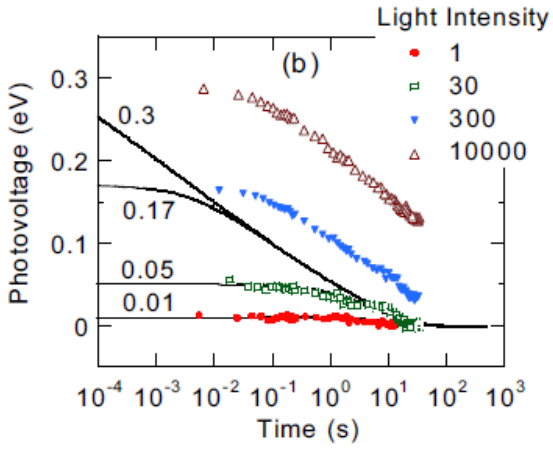

Figure 10 SPV decay after illumination with a pulsed laser. The decays were fit by a thermionic model developed in Ref. [46].

The decay rates were fit by a thermionic model, which indicated that external processes affected the restoration rate at higher excitation intensities. The slower than predicted restorations were explained by the photo-induced adsorption or desorption of ions from the ambient or the charging of the oxide layer. The band bending in the undoped GaN samples was estimated to be about 0.8 and 1.1 eV from the measured dark surface potential values. These values are in

agreement with the SPVs generated, since the band bending must be larger than the SPV generated.

In a work by Koley and Spencer,[47] SKPM was performed on GaN films with different types of doping. The study included two intentionally doped samples, an undoped sample, and a semi-insulating film. In this study, they estimated the work function of their two AFM tips by measuring the surface potentials of Al, Pt, Ni, and Au.

Since their GaN samples were exposed to the ambient, they decided to use a "practical" value of the electron affinity in their calculation of the band bending. The electron affinity of a practical surface was measured by Smart *et al.*[48] to be about 4.1 eV; this value is ~0.7 eV larger than the measured electron affinity in vacuum (3.4 eV). Table III shows the calculated values of the band bending for GaN films with various growth conditions, using the practical value of the electron affinity.

Table III: Summary of results in Ref. [47] from SKPM study of various GaN films with different growth conditions.

Material Type	Growth Method	Free carrier Concentration (cm^{-3})	Φ_0 (eV)
n-type GaN	MOCVD	~1×10^{18}	0.59±0.05
n-type GaN	MBE	~8×10^{17}	0.57±0.05
Undoped GaN	MOCVD	~5×10^{16}	0.70±0.05
Semi-insulating GaN	MOCVD	< 1×10^{16}	1.40±0.05

The calculated upward band bending was about 0.6 eV for the doped samples, about 0.7 eV for the undoped sample, and about 1.4 eV for the semi-insulating sample. In the same study, the observed difference in the band bending was insignificant between a MBE-grown and MOCVD-

grown GaN films. In this study, the band bending appeared to decrease with an increasing concentration of free electrons.

Sabuktagin *et al.*[49] measured the band bending using AFM for a set of samples in which the carrier concentration was varied by about 5 orders of magnitude. The band bending as a function of carrier concentration is shown in Figure 11.

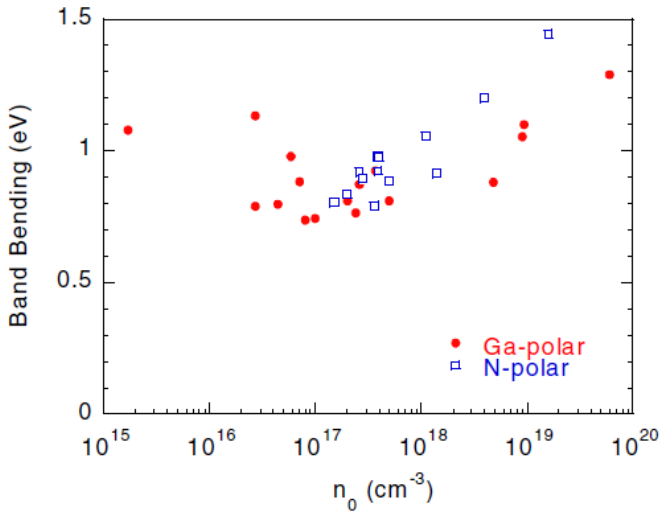

Figure 11 Dependence of the upward band bending in MBE grown GaN as a function of the concentration of free carriers. [49]

In this work, it appears that the band bending increases with increasing carrier concentration above ~10^{17} cm^{-3}. In this work, the band bending in their Ga- and N-polar MBE samples did not show a dependence on polarity. However, when they measured the band bending from bulk templates, and they observed that the N-polar surface had 0.2 eV smaller band bending as opposed to the Ga-polar surface (not shown in the figure). These data were fit by a model which attributed the polarity dependent band bending and the increase of the band bending with increasing concentration of free electrons to surface traps.[50]

Barbet *et al.*[51] performed a series of SKPM measurements on MOCVD grown n- and p-type GaN films. They observed that the Fermi-level was pinned at the surface in all of their samples. Tables IV and V show the results from the Hall effect and surface potential measurements of their n- and p-type GaN samples.

Table IV: Hall effect and SKPM measurement results for the different n-type GaN samples. [51]

Free electron Concentration (cm^{-3})	SKPM surface potential (V)	Surface Band Bending Φ_0 (eV)	Depletion Charge (e/cm^{-2})	Depletion Length (nm)
2.0×10^{18}	0.28±0.04	1.32	5.27×10^{12}	22.9
1.0×10^{19}	0.13±0.12	1.47	1.24×10^{13}	10.2
2.0×10^{19}	0.32±0.18	1.28	1.64×10^{13}	7.25

Table V: Hall and SKPM measurement results for the different p-type GaN samples. [51]

Density of free holes (cm^{-3})	N_A-N_D (cm^{-3})	SKPM surface potential (V)	Surface Band Bending Φ_0 (eV)	Depletion Charge (e/cm^{-2})	Depletion Length (nm)
7.18×10^{16}	4.14×10^{17}	-0.52±0.32	-1.11	-2.13×10^{12}	50.4
6.00×10^{16}	2.99×10^{17}	-0.18±0.18	-1.44	-2.13×10^{12}	59.3
7.70×10^{16}	4.70×10^{17}	-0.08±0.05	-1.55	-2.77×10^{12}	47.3
8.00×10^{16}	5.05×10^{17}	-0.05±0.16	-1.58	-2.89×10^{12}	45.6

The surface potential was measured in a dry nitrogen environment with Pt-coated AFM tips, where gold was used to determine the work function of their tips. The authors noted that the work function of their gold reference and the samples changed daily. They attributed changes in the surface potential to reactions with the environment, in particular, oxygen. They accounted for the daily changes in their reference signal as error bars in their estimates of band bending.

The problem with estimating band bending from a static measurement of the surface potential with SKPM is that any error in the work function or electron affinity will be manifested in the calculated band bending values. The calculated values of band bending using the Hall effect and SKPM data were about 1.3 – 1.5 eV for Si-doped n-type GaN and -1.1 – -1.6 eV for Mg-doped p-type GaN. From the values of band bending and the Fermi-level position, the position of the surface Fermi-level was calculated to be 1.34±0.15 eV below the conduction band and 1.59±0.18 eV above the valence band for n-type and p-type GaN, respectively.

SKPM can also be used to map the surface potential along with measuring the topography. This process involves scanning the topography in order to raise the tip a constant height and retrace the topography during a SKPM measurement. Plotting the surface potential as a function of the topography allows one to observe changes in the local surface potential due to surface features.

Simpkins *et al.*[52] measured the surface potential of HVPE-grown GaN films with different thicknesses, and the results are shown in Figure 12.

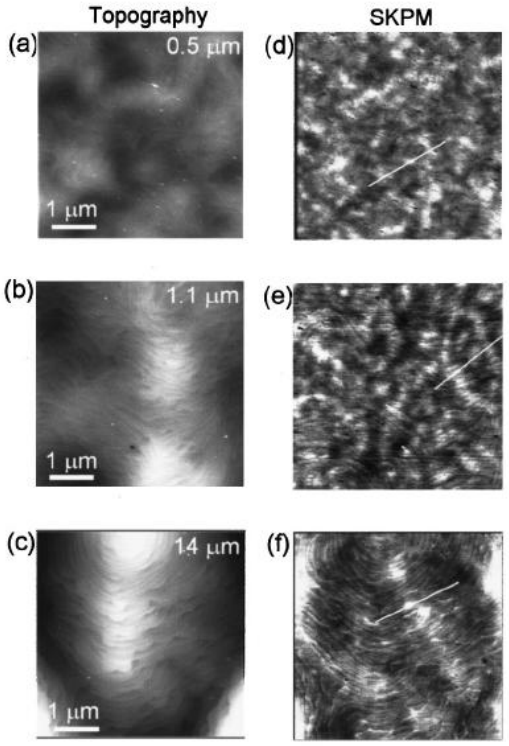

Figure 12 AFM topography(a-c) and surface potential (d-f) images for GaN films with thickness 0.5, 1.1, and 14 μm in thickness. Gray scale is 15 nm for the topography and 0.2 eV for the surface potential images. [52]

From their topography studies, the density of threading dislocations decreases from ~10^6 cm^{-2} for the 0.51 μm and 1.1 μm thick samples down to about zero in the 14 μm thick sample. These estimates seem very small, it is possible that the authors did not correctly measure the density of threading dislocations, since for thicker films the dislocation density should greatly decrease, but not become zero. The SKPM images in Figure 12 also indicate that the local surface potential changes by about 0.1 – 0.2 eV across some topographical features. The authors associated the changes in the surface potential maps with a decrease in the density of threading dislocations and the decrease in the background donor concentration, with increasing film thickness. This report could have been expanded to estimate the band bending in the GaN films; however, this was beyond the scope of their work.

The polarity (or surface termination) of c-plane (0001 or $000\bar{1}$) GaN films is predicted to affect the near-surface band bending, due to the spontaneous polarization inside of the GaN crystal. SKPM measurements of both Ga- and N-polar GaN bulk templates were performed by Wei *et al.*[53] It is important to note that before the surface potential measurements were performed, the samples were cleaned in HF. The steady-state SPV was excited by a "Bluepoint 4" UV source for approximately 5 min, and the SPV transients are shown in Figure 13.

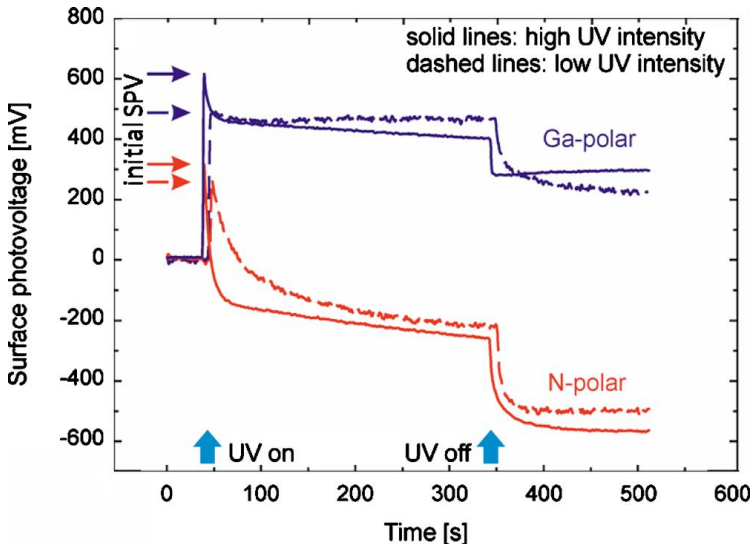

Figure 13 Evolution of SPV for Ga-polar and N-polar GaN surfaces under 360 nm UV light illumination at UV light intensities of 7 μW/cm^2 (dashed) and 70 μW/cm^2 (solid). The initial SPV for each case is indicated by the arrows. [53]

The initial SPV generated in the Ga- and N-polar surfaces was about 0.6 eV and 0.3 eV, respectively. During illumination, the SPV decreased by about 0.2 and 0.5 eV for the Ga- and N-polar samples, respectively. The decrease in the surface potential during UV-illumination was attributed to the photo-induced adsorption of oxygen species. The authors attribute the difference in reactivity between the Ga- and N-polar surfaces to the difference in the total surface charge. It is assumed that the Ga-polar surface is more negative, which would hinder the adsorption of negatively charged oxygen.

The authors did not comment on the absolute values of band bending in their Ga- and N-polar samples, but the authors comment that the band bending can be qualitatively estimated from the magnitude of the SPVs. The difference in the maximum SPV was about 0.2 – 0.3 eV. Thus, assuming that both surfaces have the same depletion region width, it follows from these data that the band bending for N-polar surfaces is smaller by no more than 0.3 eV than Ga-polar surfaces.

2.3 Kelvin probe

The Kelvin probe measures the surface potential using a similar technique as the AFM in SKPM mode. The advantages of this method include a high signal-to-noise ratio and a relatively large sample area. Kronik and Shapira[54] used a Kelvin probe in conjunction with the SPV technique to characterize the electronic structure of semiconductor surfaces. A combination of dark surface potential measurements and SPV data was used to determine the surface properties of various semiconductors. The surface potential signal was measured before, during, and after the surface was illuminated with band-to-band light. To even further characterize the surfaces, the SPV measurements were analyzed along with photoluminescence data, which can provide information about band bending, surface states, and defects. Kronik and Shapira were able to show that the SPV technique is a non-contact, non-destructive approach to characterize the electronic behavior of semiconductors.

Eyckeler *et al.*[55] used a Kelvin probe to measure the contact potential difference (CPD) for both n- and p-type GaN during cesium exposure. The p-type GaN films were grown by plasma-induced MBE to a thickness of 500 nm, with a hole concentration of 1.2×10^{17} cm^{-3} at

room-temperature. In this study, the samples were cleaned by dipping them in HF acid for 1 minute, rinsing them with de-ionized water, loading them into the vacuum chamber, and heating the samples to 800^{o}C while exposing them to Ga atoms for about 30 min. In this study, the work function of the Kelvin probe was calibrated with a freshly cleaved p-type GaN sample stored in vacuum. It is possible that this type of calibration may induce some error instead of measuring a more well known surface. The studied samples were kept in dark during the heating process, and were not subsequently exposed to light before the CPD signal was measured, while the samples were exposed to cesium. Figure 14 shows the position of the Fermi-level during Cs exposure.

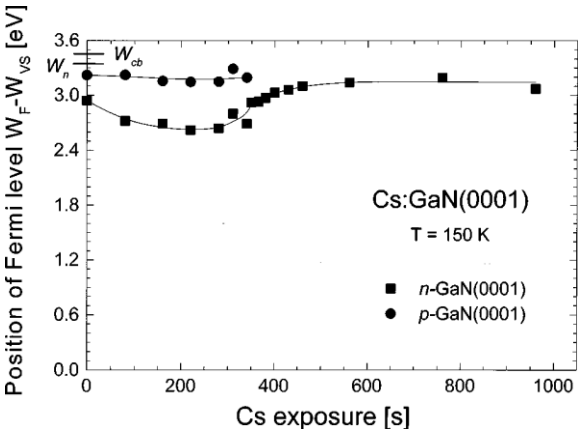

Figure 14 Energy difference between the Fermi-level and valence-band maximum at clean and cesiated n- and p-type GaN (0001) surfaces at 150 K as a function of Cs exposure. [55]

Using information about the surface Fermi-level (measured by the Kelvin probe) and the bulk Fermi-level, which can be calculated from the Hall effect data, the band bending can be estimated as the difference between these Fermi-levels. For the p-type GaN sample, we calculated the position of the Fermi-level at 150 K to be about 0.151 eV above the valence band in the bulk assuming that $N_D = 4.6\times10^{18}$ cm^{-3}, $N_A = 9\times10^{18}$ cm^{-3} and $E_A = 0.18$ eV, and the position of the surface Fermi-level to be about 3.22 eV above the valence band (as reported by authors). Our calculations yield that the downward band bending is about -3.07 eV.

The n-type sample had a concentration of free electrons of about $5\times10^{16}\,cm^{-3}$ at room-temperature. We calculated the position of the bulk Fermi-level to be about 0.05 eV below the conduction band assuming that $N_D = 5\times10^{17}\,cm^{-3}$, $N_A = 4\times10^{17}\,cm^{-3}$ and $E_D = 0.02$ eV, and the measured position (by the authors) of the surface Fermi-level was about 2.94 eV above the valence band, which provides an upward band bending estimate of about 0.53 eV.

$$\Phi_0 = (E_{Gap} - (E_{F\ Surface} - E_{VB}))\,eV - (E_{CB} - E_{F\ Bulk})\,eV$$
$$\Phi_0 = (3.52 - 2.94)\,eV - 0.05\,eV = 0.53\,eV$$

In this work, however, the authors did not comment on the value of band bending and the above calculations were done using the data provided. In their experiment, heating the samples in darkness may have changed the measured value of band bending, especially for p-type GaN.

Shalish *et al.*[56] used a Kelvin probe in conjunction with an Auger electron spectroscopy, XPS, and photoluminescence to measure the effect of HCl etching on band bending. The samples used in this study were grown by MOVPE on (0001) oriented sapphire substrates, with a free electron concentration of about $n \sim 1.2\times10^{17}\,cm^{-3}$. The CPD is plotted as a function of photon energy in Figure 15.

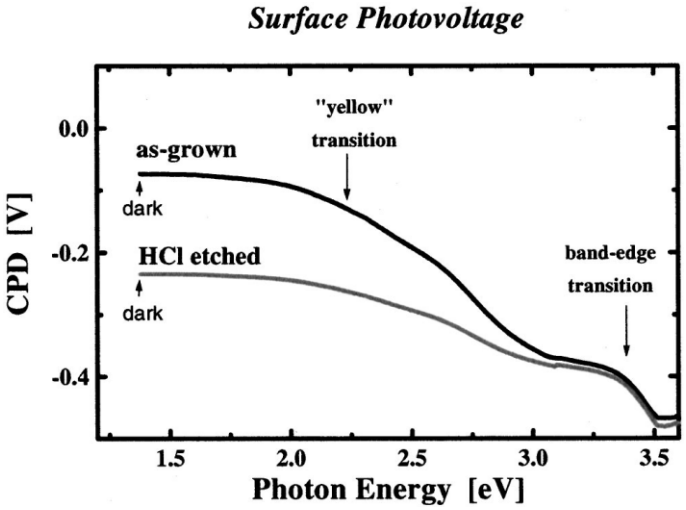

Figure 15 CPD spectra obtained before and after HCl etching from the same GaN film. [56]

The values of the CPD which are labeled "dark" were taken in the absence of light. The samples were illuminated from low to high photon energy. The CPD increased by about ~0.4 and ~0.25 eV for above-bandgap illumination, for the as-grown and HCl etched surfaces, respectively. The authors attribute shoulders in the spectral response to an electron transition from a deep defect to the conduction band (yellow transition) and a band-to-band transition. After about 2 days, the surface potential of the HCl-cleaned surfaces returned to the same value as the as-grown surfaces. Again, the band bending and additional information about the GaN sample surface could have been calculated from the data presented, but was beyond the scope of their work.

2.4 Temperature-Dependent XPS and UPS Measurements

Long and Bermudez[57] performed a temperature-dependent study of GaN using XPS and UPS. In this work, the authors measured the position of the surface Fermi-level for n- and p-type GaN (0001). Using the data provided, the band bending could be determined as the difference between the bulk and surface Fermi-levels. In this study, the authors varied the temperature and

intensity of the X-ray source. When the temperature was increased to 600^{o}C, Long and Bermudez[57] observed shifts in the Fermi-levels towards the same level about 2.5 eV above the v`lence band for both their n- and p-type GaN samples.

The position of the surface Fermi-level is plotted in Figure 16(a) for temperatures from 20 to 700 K. The band diagram in Figure 16(b) illustrates how the position of the Fermi-level is defined. The surface Fermi-level is obtained from the peak positions in XPS data, and the bulk Fermi-level is obtained from the Hall effect measurements. The difference between these two Fermi-levels is the value of band bending during the XPS measurements.

(a) (b)

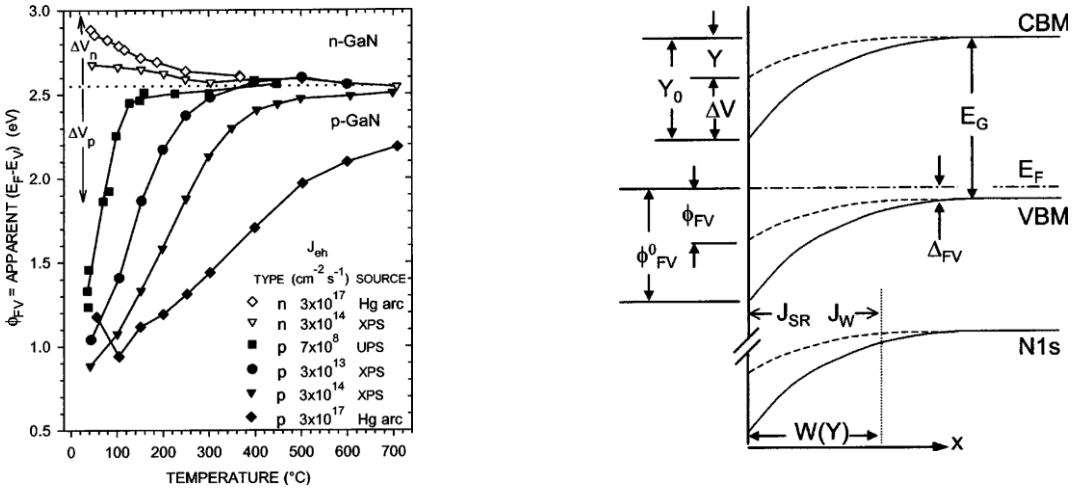

Figure 16 (a) Changes in the surface Fermi-level position with increasing temperature changes from XPS data. (b) A schematic diagram showing the band bending in dark and under illumination. [57]

Although the authors have not provided explicit information about the values of band bending, it can be calculated using the surface Fermi-level position from Figure 16 and the concentrations of free electrons and holes reported in Ref. [57]. The results of these calculations are shown in

Table VI. Band bending in n- and p-type GaN calculated based on the information provided in Ref. [41]

Temperature (K)	N_C **(cm^{-3})**	N_V **(cm^{-3})**	E_C-E_F **n -type (eV)**	E_F-E_V **p-type (eV)**	E_{Gap} **(eV)**	Φ_0**(n-type) (eV)**	Φ_0**(p-type) (eV)**
300	2.6×10^{18}	1.8×10^{19}	0.07	0.13	3.44	0.67	-0.77
700	9.3×10^{18}	6.4×10^{19}	0.20	0.25	3.26	0.64	-2.15

When the temperature was increased from 300 to 700 K, the calculated band bending decreased by about 0.03 eV and increased by about 1.38 eV for n- and p-type GaN, respectively. The experimentally observed increase in band bending for p-type GaN is very interesting, and needs verification. The results appear similar to the Kelvin probe experiment by Eyckeler *et al.*[59]

The effect of oxygen exposure on the position of the surface Fermi-level was measured for n- and p-type GaN. The observed changes in the surface Fermi-level position were attributed to the chemisorption of the oxygen species, which increased and decreased band bending in n- and p-type GaN, respectively.

When the excitation intensity was varied, smaller values of band bending were calculated for larger excitation intensities. This observation confirms that a SPV affects the energy of photo-ejected electrons, as reported by Suzer *et al.*[40] Long and Bermudez[57] were also able to use their excitation dependent, band bending calculations to estimate the size of the generated SPV in their XPS setup, which appeared to be up to 1 eV for p-type GaN.

2.5 Main Results from the Literature and Unsolved Problems

The band bending in GaN has been studied using XPS and Kelvin probe methods. The upward band bending in n-type GaN has been studied thoroughly, and is estimated to be about 1 eV.[37,41,46,47,49,56,58] For n-type GaN, XPS reports have shown that the band bending increases with oxygen exposure.[56] Conversely, there are far fewer reports in the literature on the downward band bending in p-type GaN. The reported values for the downward band bending in p-type GaN vary widely from -0.8 to -3 eV. [37,46,47,59,60] The discrepancies in the values of band bending for p-type GaN have not been discussed in the literature.

Work still needs to be performed to further understand the band bending in n- and p-type GaN. The external mechanisms that affect the SPV behavior, such as adsorption and desorption from the environment, also need to be explored. XPS, AFM and Kelvin probe measurements provide a range of calculated values for band bending in GaN; however, there is no work which compares the accuracy of each technique. The large range of values for the band bending in p-type GaN also requires some consideration. Do the calculated values come from experimental error, or do they originate from some aspect of the experimental method?

All the methods used to estimate band bending have their own disadvantages. In XPS, the X-ray source itself generates a SPV and decreases the band bending, there is potential surface charging, and the measurements rely on values measured in the literature. The major issue with XPS or UPS is that the measurements assume that the Fermi-levels of the sample and spectrometer are in equilibrium. This may not be the case and introduce error in the measurements.

In SKPM measurements with an AFM, the signal-to-noise ratio is high, the data is acquired from a small sample area, and the dark conditions cannot always be achieved. Surface potential measurements taken by Kelvin probe or AFM may have error in the electron affinity and work function, which will be directly related to the error in band bending calculations.

The effect of temperature on band bending also needs to be addressed. There are few studies where band bending is calculated at multiple temperatures, and there are no reports in the literature of the effect on temperature on band bending. Moreover, performing SPV measurements at higher temperatures will allow the bands to restore exponentially faster and provide a better baseline to accurately determine the amount of band bending in darkness.

Chapter 3: Experimental Details

3.1 Kelvin Probe

The Kelvin probe method is very precise (noise ±5 meV), but does not accurately measure the absolute values of the work functions of a material. This low accuracy is due to various changes in the environment or system settings which affect the CPD's absolute value.[61] Exposing the probe or the sample to air, moisture, or any type of gas may dramatically affect the CPD signal. To perform more accurate measurements of the work function, a reference material is generally used to determine the work function of the probe. However, the work function of the reference material could change with time, and this needs to be taken into account. To estimate the work function of our probe, we have measured the CPD from a gold film and compared the values obtained to the calculated band bending from a well studied sample (2015_HN).

In our experiments, the absolute value of the CPD was measured many times over a period of more than six months and was reproducible within an accuracy of 0.05 eV for a single sample. The CPD signal does appear to change greatly when the type of probe is changed, solid versus perforated, the ambient conditions are changed (vacuum or air), and when the sample temperature was changed. We have also noted that the dark value of the CPD signal of GaN sample 2015_HN did appear to change slowly over time with increasing UV-exposure.

Our Kelvin probe acquires data by vibrating a biased reference probe which is parallel to a stationary sample. In principle, one could vibrate the sample while keeping the probe stationary to acquire data, but our Kelvin probe is limited to the vibrating probe approach. When the sample

and probe are isolated from each other, their Fermi-levels have different positions because they are composed of different materials. The first step in measuring the CPD is to bring the sample and probe into electrical contact. This causes electrons to flow between the materials in such a way that the Fermi-levels will align. This flow of electrons generates a current in the circuit, as well as leaves some charge on both the sample and Kelvin probe surfaces. A bias is then applied to the vibrating probe with the intention to reduce the surface charge and current to zero. The voltage that needs to be applied to meet this condition is defined as the contact potential difference (CPD). This process is shown schematically in Figure 17.

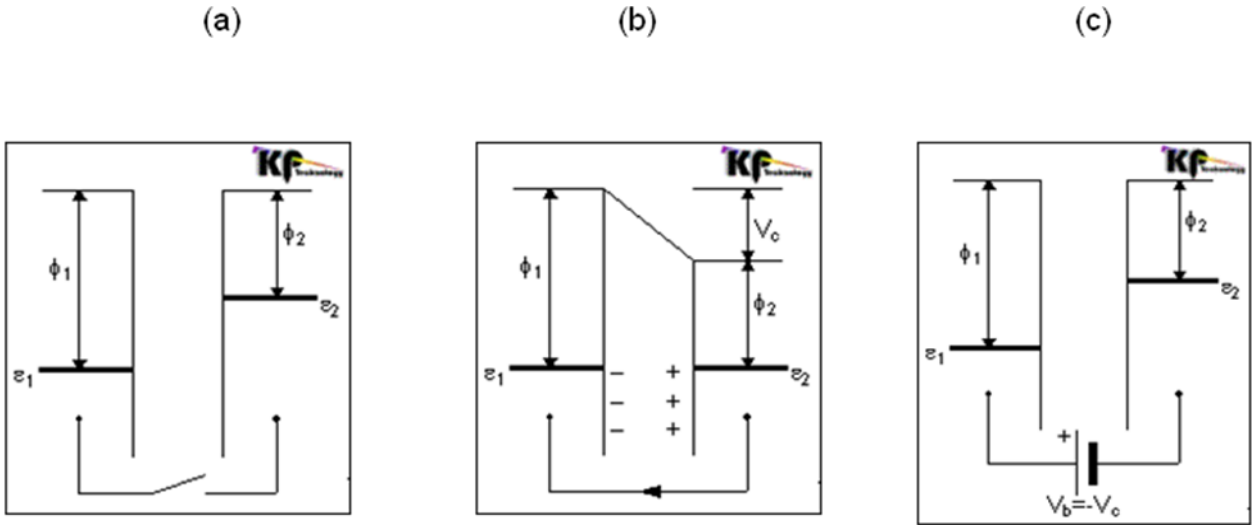

Figure 17 (a) Sample and probe not in electrical contact; (b) Sample and probe brought into electrical contact; (c) Vcpd = Vbacking with no charge/current. Where ϕ_1 is the work function of the probe, ϕ_2 is the work function of the sample and ε_1 and ε_2 are the positions of the Fermi-level for the probe and sample, respectively.[62]

When no backing potential is applied and the sample and probe are in electrical contact, there exists a CPD between the plates due to the difference in work functions (of the sample ϕ_S and the probe ϕ_P). This difference in potential is defined as

$$eV_{cpd} = \phi_S - \phi_P . \tag{3.1}$$

When $V_{backing} = -V_{cpd}$, the electric field between the plates has been nullified; i.e., there is no measureable current output.[26] The accuracy of the Kelvin probe method can be improved by measuring the dependence of the current on different values of the backing potential (large current in the circuit), instead of measuring the null point (little to no current generated in the circuit). In order to cut out additional noise in the circuit, the probe oscillates at a given frequency. Any signals which do not appear at the same frequency at which the probe is oscillating are considered noise by the software. The capacitance *C* between the probe and sample is defined as:

$$\mathrm{C} = \frac{\varepsilon\varepsilon_o A}{d} = \frac{Q}{IR}, \tag{3.2}$$

where *d* is the distance between the sample surface and the probe, *A* is the area of the probe, *I* is the current in the circuit, *R* is the resistance, and *Q* is the charge on the capacitor plates. It follows from Eq. (3.2) that changing the probe-to-sample distance will additionally generate a current if the *Q* and *R* are kept constant. The Kelvin probe exploits a relationship between the current and the CPD so that the null point does not need to be measured. The measured current can be estimated as:

$$I = \frac{dQ}{dt} = \Delta V \frac{dC}{dt} \quad , \tag{3.3}$$

where ΔV is the potential difference between probe and sample. It is important to note that $\Delta V = V_{backing} + V_{cpd}$ in these equations. The distance between the probe and sample is varied sinusoidally as:

$$d = d_o + d_1 \sin(\omega t + \phi). \tag{3.4}$$

After substituting Eq. (3.4) into Eq. (3.2) and then Eq. (3.3), and taking the time derivative of *d*, the current *I* as a function of ΔV is given by:

$$I = -\varepsilon\varepsilon_o A \Delta V \frac{d_1 \omega \cos(\omega t + \phi)}{\left[d_o + d_1 \sin(\omega t + \phi)\right]^2}. \tag{3.5}$$

Equation (3.5) demonstrates that the current is linearly related to the contact potential difference (ΔV). The Kelvin probe exploits this linear relationship by scanning the backing potential while measuring the current. The Kelvin probe software uses interpolation or extrapolation to determine the null point of the current. The voltage at which the current is found to be zero is $V_{backing} = -V_{cpd}$. Therefore, low-noise data can be acquired by exploiting this linear relationship between the CPD and current, and the null point does not need to be directly measured. The Kelvin probe method is an excellent, non-invasive technique used to measure the surface potential of materials.

3.2 Experimental Setup

The experimental setup used to study the SPV behavior of n- and p-type GaN samples consists of a UHV Kelvin probe (McAllister KP-6500), an optical cryostat (Janis VPF-700), and a temperature controller (Lakeshore 331). The experimental setup can operate within the temperature range of 77 to 650 K, while maintaining a high-vacuum (10^{-6} mbar) or controlled gas environment (nitrogen or oxygen). A schematic and a photograph of the experimental setup is shown in Figure 18.

(a) (b)

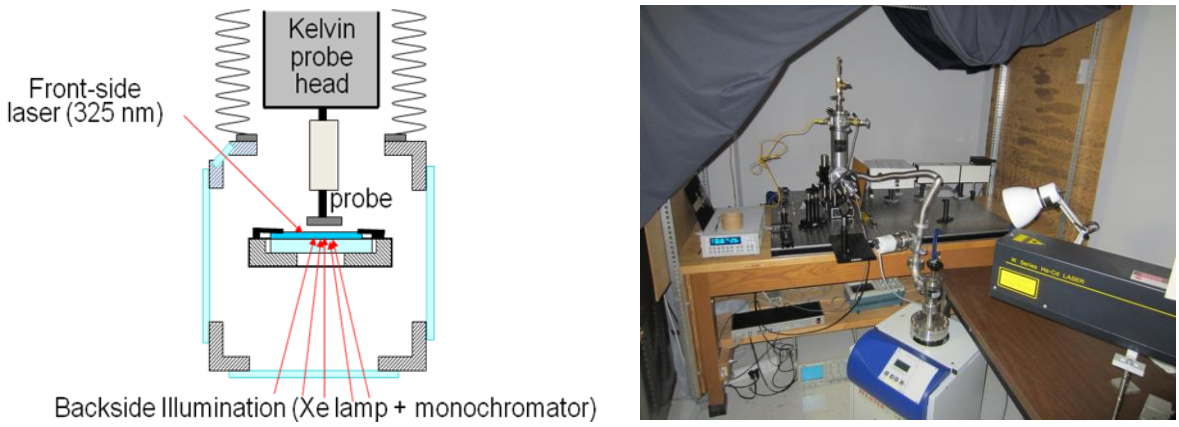

Figure 18 (a) Top-view schematic and (b) a photograph of the experimental setup.

The samples can be illuminated by either a Xe-lamp attached to a monochrometer (with a power density of monochromatic light incident on the sample surface of 0.03 W/cm^2) or a HeCd laser (0.04 W/cm^2 at 325nm incident on the sample surface). After light from the lamp exits the monochrometer, it passes through a series of long-pass filters to further suppress the undesired stray (parasitic) light. The filters play an important role in blocking the parasitic light which may also significantly contribute to the SPV signal. In our setup, two stacked long pass filters are used to decrease the parasitic light intensity by about 8 orders of magnitude. When the light is unfiltered, it is possible that a small fraction of the parasitic light from a monochromator (about 10^{-3} %) can significantly contribute to the measured SPV signal. The excitation power density from either illumination source can be attenuated by calibrated neutral-density filters by up to nine orders of magnitude.

The power density of the laser incident on the surface includes losses due to illumination geometry and light that is able to pass through the perforated probe. The power incident on a

power meter from the laser was measured using the same similar geometry as the Kelvin probe, while the perforated probe was placed in front of the detector in an attempt to account for losses due to the probe. Performing these measurements indicated that about 50% of the power is lost due to the sample angle, and an additional 66% is lost due to light that is not able to pass through the perforated probe. Only about 17% of the initial light intensity is able to reach the surface. This number could be over or underestimated, and a special holder for the Kelvin probe would be needed to measure this value more precisely.

Before measurements begin, the oscillating tip of the perforated Kelvin probe (4 mm dia.) is brought close to the sample surface (sub millimeter) which is mounted in a holder with illumination access from the back or front side (Figure 18). Band-to-band photons absorbed in the depletion region induce a change in the near surface band bending. This is due to the creation of electron-hole pairs which are quickly separated by a strong electric field. The surface potential before, during, and after illumination is monitored by the Kelvin probe in real time.

3.3 GaN Samples

A large number of n- and p-type GaN samples grown by different methods have been studied by Kelvin probe in this work, see Table VII.

The cleaning procedure for samples noted “clean” is listed below:

1) 15 minutes in boiling acetone
2) 5 minutes in acetone, then methanol in an ultrasonic cleaner
3) 15 minutes in hot aqua regia (HNO_3 + HCl)
4) 3 minutes in buffered oxide etch (HF) at room temperature
5) De-ionized water rinse, and nitrogen blow-dry

This cleaning procedure is expected to remove an oxide layer, but not etch any of the GaN surface.

Table VII: Samples studied in this work.

Sample Number	Source of Sample	Growth Method	Sample Doping	Sample Type	$N_A - N_D$ or $N_D - N_A$	Concentration of Free Carriers
750_BN	Morkoç	MBE	Undoped	n		4×10^{16} cm^{-3}
595_BN	Morkoç	MBE	Si-doped	n		7×10^{18} cm^{-3}
2015_HN	TDI	HVPE	Si-doped	n	3.5×10^{17} cm^{-3}	3×10^{17} cm^{-3}
1962_HN	TDI	HVPE	Si-doped	n		3×10^{17} cm^{-3}
863_HP	TDI	HVPE	Mg-doped	p	6.5×10^{18} cm^{-3}	5×10^{16} cm^{-3}
793_MP	Koleske	MOCVD	Mg-doped	p		2×10^{17} cm^{-3}
9600_BP	Calarco	MBE	Mg-doped	p		~10^{17} cm^{-3}
9591_BP	Calarco	MBE	Mg-doped	p		~10^{18} cm^{-3}
9599_BP	Calarco	MBE	Mg-doped	p		~10^{18} cm^{-3}
1412.3_HN	Kyma	HVPE	Undoped	n		~10^{15} cm^{-3}
1412.4_HN	Kyma	HVPE	Undoped	n		~10^{15} cm^{-3}
1305_HN	Kyma	HVPE	Undoped	n		~10^{15} cm^{-3}
2040_MP	SUNY	MOCVD	Mg-doped	p		~10^{16} cm^{-3}

Morkoç – Department of Electrical and Computing Engineering, VCU
TDI Oxford Instruments – Silver Spring, MD
Koleske – Sandia National Laboratories, NM
Calarco – Paul-Drude Institute, Berlin Germany
Kyma – Raleigh, NC
SUNY – Albany, NY

Naming Convention: [Sample#]_[Growth type][Doping]
Growth types: HVPE = H, MBE = B, MOCVD = M
Doping: n-type = N, p-type = P

This sample set allows us to compare the differences in the SPV behaviors for the various types of growths. For n-type GaN samples studied at room temperature, indium has been applied to the sample surfaces to form ohmic contacts. For the temperature-dependent measurements, the samples require different contacts that are able to withstand the high temperatures at which the samples are heated. The high temperature contacts used for the n-type and p-type GaN samples consist of Ti-Al-Ni-Au layers and Ni-Au layers, respectively. After deposition of the contacts, the n-type samples were annealed at 800^{o}C for 1 minute under N_2 flow. The p-type samples were

annealed for 8 min at 600^{o}C in air ambient. These contacts provide flexibility when heating the samples well over 400 K, since the contacts will not melt and potentially alter the surface properties. Varying the surface temperature from 295 to 650 K corresponds to a change in thermal energy from 0.0254 to about 0.0560 eV. This change in thermal energy provides a dramatic change in the SPV behavior of our samples; in particular, the slope of the intensity dependence and the restoration rate should increase with increasing temperature.

Chapter 4: Thermionic Model of the SPV

The surface photovoltage (SPV) behavior for an undoped n-type GaN sample grown by MBE has been studied in detail.[63] In this work, the band bending was determined by fitting SPV data with a thermionic model derived in this work. Some of the possible electronic transitions that are caused by the absorption of band-to-band photons in the GaN films, which will generate a SPV, are shown in Figure 19.

(a) (b)

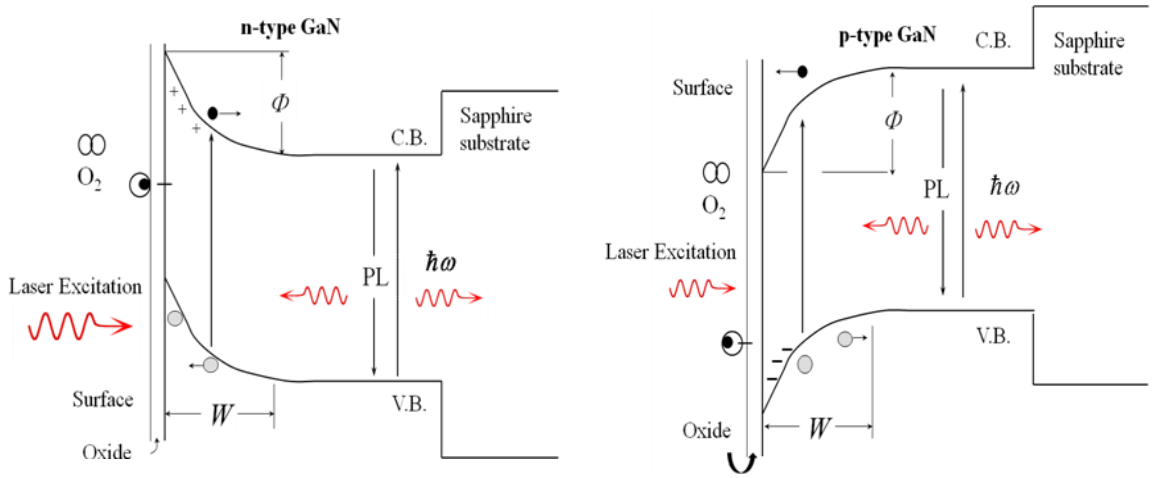

Figure 19 Band diagram for (a) n-type GaN and (b) p-type GaN with main transitions shown. Illumination is incident from the front side. C.B – conduction band, V. B. – valence band, Φ – band bending, and PL – photoluminescence.

Photons with energy greater than the band gap that are absorbed in the depletion region, *W*, generate a SPV. For n-type GaN, holes created in the depletion region are swept to the surface, and reduce the net negative charge responsible for the upward band bending. For p-type GaN, electrons will be swept to the surface and reduce the net positive surface charge. The width of the depletion region can be estimated with the following expression:[64]

n-type:
$$W = \frac{n_s}{N_D - N_A} = \sqrt{\frac{2\Phi_0 \varepsilon \varepsilon_0}{q^2 \left(N_D - N_A\right)}}, \tag{4.1a}$$

p-type:
$$W = \frac{p_s}{N_A - N_D} = \sqrt{\frac{2\Phi_0 \varepsilon \varepsilon_0}{q^2 \left(N_D - N_A\right)}}, \tag{4.1a}$$

with

n-type:
$$n_s(y) = \sqrt{\frac{2(\Phi_0 - y)(N_D - N_A)\varepsilon\varepsilon_0}{q^2}} = \sqrt{\frac{2\varepsilon\varepsilon_0 (N_D - N_A)\Phi_0}{q^2}} \sqrt{1 - \frac{y}{\Phi_0}} = n_s(0)\sqrt{1 - \frac{y}{\Phi_0}}, \tag{4.2a}$$

p-type:
$$p_s(y) = \sqrt{\frac{2(\Phi_0 - y)(N_D - N_A)\varepsilon\varepsilon_0}{q^2}} = p_s(0)\sqrt{1 - \frac{y}{\Phi_0}}, \tag{4.2b}$$

where n_s and p_s are the density of negative and positive charge on the surface, N_D and N_A are the concentration of shallow donors and acceptors, respectively, ε is the static dielectric constant ($\varepsilon = 9.8$ for GaN[65]), Φ_0 is the band bending in dark, and y is the SPV generated by illumination. The near-surface band bending can be calculated from the dark value of the CPD and the steady-state intensity-dependent SPV measurements. The thermionic model used to fit SPV data and the calculations involved to estimate band bending in dark will be explained in detail in this chapter.

4.1 Transient SPV

As previously stated, excess surface charge is responsible for the upward and downward band bending in n- and p-type GaN, respectively. Electrons and holes that leave or arrive at the surface will therefore change the amount of near-surface band bending. There are three processes we can model that affect the charge at the surface of a semiconductor. For an n-type semiconductor, these processes include: (1) holes flowing to the surface, (2) electrons moving

from bulk to surface, and (3) electrons moving from surface to bulk. We will ignore the flow of holes from the surface to the bulk because they have to overcome a very high potential barrier. Below, the rates of these three processes will be estimated.

(1) We are interested in rate at which holes reach the surface under band-to-band illumination, since this is proportional to the SPV generated. We estimate the number of holes that reach the surface to be equal to the number of band-to-band photons that are absorbed in the depletion region. This assumption is justified by a very large electric field present in the depletion region of GaN (on the order of 10^5 V/cm) which forces the holes to reach the surface much faster than they can be captured by defects or recombine with electrons in the depletion region. If illumination is incident on the front surface (surface measured by the Kelvin probe), the number of photons absorbed in the depletion region (P_w) per unit time in a unit area can be approximated as:

$$P_w = \int_0^W \alpha P_0 e^{-\alpha x} dx = P_0(1 - e^{-\alpha W}) = cP_0, \tag{4.3}$$

where W is the width of the depletion region, α is the absorption coefficient, P_0 is the illumination power density (photons per cm^2 per second), and c is a geometrical factor that accounts for the percentage of photons absorbed in the depletion region. Then, the rate at which holes reach the surface, R^*, is

$$R^* = cP_0. \tag{4.4}$$

This expression will remain the same for p-type GaN; however, it estimates the number of electrons that reach the surface under band-to-band illumination instead. Our setup also has the capability to illuminate from the backside, and the number of photons absorbed in the

depletion region in this geometry can be found in Ref. [63]. We generally prefer the front side illumination geometry since we can more accurately estimate the number of photons absorbed in the depletion region.

(2) Electrons that reach the surface will end up increasing the amount of negative charge at the surface for n-type GaN. The rate at which electrons overcome the near surface barrier from bulk to surface for n-type GaN is given by:

$$R_{bs} = C_{n1} N_s^{\circ} N_C \exp\left(-\frac{\Phi_0 + (E_C - F) - y}{kT}\right), \tag{4.5}$$

where C_{n1} is the electron capture coefficient for the surface states, N_s° is the number of unoccupied states at the surface, N_C is the effective density of states in the conduction band, E_C and F are the energies of the conduction band minimum and the Fermi level, respectively, k is Boltzmann's constant, and T is the temperature. It can be seen from Eq. (4.5) that the rate of electrons overcoming the near-surface barrier in darkness, R_0, ($y = 0$) is:

$$R_0 = C_{n1} N_s^{\circ} N_C \exp\left(-\frac{\Phi_0 + (E_C - F)}{kT}\right) \tag{4.6a}$$

$$= s_n N_C \exp\left(-\frac{\Phi_0 + (E_C - F)}{kT}\right). \tag{4.6b}$$

In this expression, s_n is the surface recombination velocity for electrons $\left(C_{n1} N_s^{\circ}\right)$. Using this expression, the rate that electrons move from bulk to surface (R_{bs}) for an n-type semiconductor simplifies to

$$R_{bs} = R_0 \exp\left(\frac{y}{kT}\right). \tag{4.7}$$

The same procedure can be performed to predict the number of holes that move from bulk to surface in p-type semiconductors, and this provides:

$$R_{bs}(holes) = C_{p1} N_s^{\bullet} N_V \exp\left(\frac{\Phi_0 + (E_V - F) - y}{kT}\right), \tag{4.8}$$

where C_{p1} is the hole capture coefficient for the surface states, $N_s^{\bullet}$ is the number of surface states occupied with electrons, N_V is the effective density of states in the valence band, F and E_V are the energies of the Fermi level and the valence band maximum, respectively. In this expression, the rate at which holes overcome the near surface barrier in darkness becomes:

$$R_0 = C_{p1} N_s^{\bullet} N_V \exp\left(\frac{\Phi_0 + \left(E_V - F\right)}{kT}\right) \tag{4.9a}$$

$$= s_p N_V \exp\left(\frac{\Phi_0 + \left(E_V - F\right)}{kT}\right). \tag{4.9b}$$

In this expression s_p is defined as the surface recombination velocity for holes $\left(C_{p1} N_s^{\bullet}\right)$.

(3) Finally, the rate at which electrons travel from surface states over the near surface barrier to the bulk for an n-type semiconductor is given by:

$$R_{sb} = C_{n2} N_s^{\bullet} N_C \exp\left(-\frac{E_C - E_s}{kT}\right), \tag{4.10}$$

where $N_s^{\bullet}$ is the density of surface states occupied with electrons, and E_s is the energy level of a single surface state.

Again, the same treatment can be given for p-type semiconductors, and the number of holes that travel from surface to bulk is given by:

$$R_{sb}(holes) = C_{p2} N_s^{\circ} N_V \exp\left(\frac{E_V - E_s}{kT}\right), \tag{4.11}$$

where N_s° is the density of surface states occupied with holes, and E_s is the energy level of a single surface state.

In this model, the capture coefficients C_{n1}, C_{n2}, C_{p1}, and C_{p2} are related to the electron/hole capture cross-sections σ_{n1}, σ_{n2}, σ_{p1}, and σ_{p2}, respectively, as:

$$C_{n1,2} = \sigma_{n1,2} v_n = \sigma_{n1,2} \sqrt{\frac{8kT}{\pi m_e^*}} \tag{4.12}$$

and

$$C_{p1,2} = \sigma_{p1,2} v_p = \sigma_{p1,2} \sqrt{\frac{8kT}{\pi m_h^*}}, \tag{4.13}$$

where v_n is the average electron thermal velocity, m_e^* is the effective electron mass in the conduction band, v_p is the average hole thermal velocity, and m_h^* is the effective hole mass in the valence band.

In darkness, when the band bending is fully restored, we expect the equilibrium condition $R_{bs} = R_{sb}$ for both n- and p-type semiconductors. In this case, the amount of charge carriers moving from bulk to surface and surface to bulk are equal. This equilibrium condition results in the following relation for n-type and p-type semiconductors, respectively:

$$C_{n1} N_s^{\circ} N_C \exp\left(-\frac{\Phi_0 + E_C - F}{kT}\right) = C_{n2} N_s^{\bullet} N_C \exp\left(-\frac{E_C - E_s}{kT}\right) \tag{4.14a}$$

and

$$C_{p1}N_s^{\bullet}N_V \exp\left(\frac{\Phi_0 + (E_V - F)}{kT}\right) = C_{p2}N_s^{\circ}N_V \exp\left(\frac{E_V - E_S}{kT}\right), \tag{4.15}$$

or

$$C_{n1}N_s^{\circ} = C_{n2}N_s^{\bullet} \tag{4.16a}$$

and

$$C_{p2}N_s^{\bullet} = C_{p1}N_s^{\circ}, \tag{4.16b}$$

if there is a single surface state that pins the Fermi-level.

For n- and p-type semiconductors, the change in the negative and positive surface charge can be expressed by the following equations, respectively:

$$\frac{dn_s}{dt} = R_{bs} - R_{sb} - R^* \tag{4.17a}$$

and

$$\frac{dp_s}{dt} = R_{bs} - R_{sb} - R^*. \tag{4.17b}$$

For n-type semiconductors, the change in the amount of negative surface charge is equal to the rate of bulk electrons that overcome the near-surface barrier and are captured by surface states, the rate of electrons emitted from surface states over the near-surface barrier into the bulk, and the rate at which photogenerated holes arrive at the surface. Plugging in the expressions (4.2), (4.7), (4.10) and (4.16), and simplifying; we get:

n-type
$$\frac{n_s(0)}{2\Phi_0\sqrt{1-\frac{y}{\Phi_0}}}\frac{dy}{dt} = R_0 \exp\left[\frac{y}{\eta kT}\right] - R_0 - R^*, \tag{4.18a}$$

and

p-type
$$-\frac{p_s(0)}{2\Phi_0\sqrt{1-\frac{y}{\Phi_0}}}\frac{dy}{dt} = R_0 \exp\left[\frac{-y}{\eta kT}\right] - R_0 - R^*, \tag{4.18b}$$

where $n_s(0)$ and $p_s(0)$ are the densities of negative and positive surface charge, respectively, y is the SPV generated, and η is added to the expression as an ideality factor that is expected to be close to 1, and which is exactly 1 in this model. The parameter η was added so that our expressions resemble those commonly used by others, and it is important to remember that η has no physical significance. The role of η is only to fit data better.

With Eq. (4.18), we can predict the SPV behavior as a function of time. Using separation of variables, the SPV at any time t under illumination can be found from Eq. (4.18) when illumination begins at $t = 0$ (in the case where $y \ll \Phi_0$):

n-type
$$t \approx \frac{n_s(0)}{2\Phi_0(R_0+cP_0)}\left\{y - \eta kT \ln\left[1+\frac{R_0}{cP_0}\left(1-e^{\frac{y}{\eta kT}}\right)\right]\right\} \tag{4.19a}$$

and

p-type
$$t \approx -\frac{p_s(0)}{2\Phi_0(R_0+cP_0)}\left\{y + \eta kT \ln\left[1+\frac{R_0}{cP_0}\left(1-e^{\frac{-y}{\eta kT}}\right)\right]\right\}. \tag{4.19b}$$

Figure 20 shows the predicted SPV transients for n-type GaN as a function of excitation intensity and temperature calculated using Eq. (4.19a) with the parameters given in the figure caption.

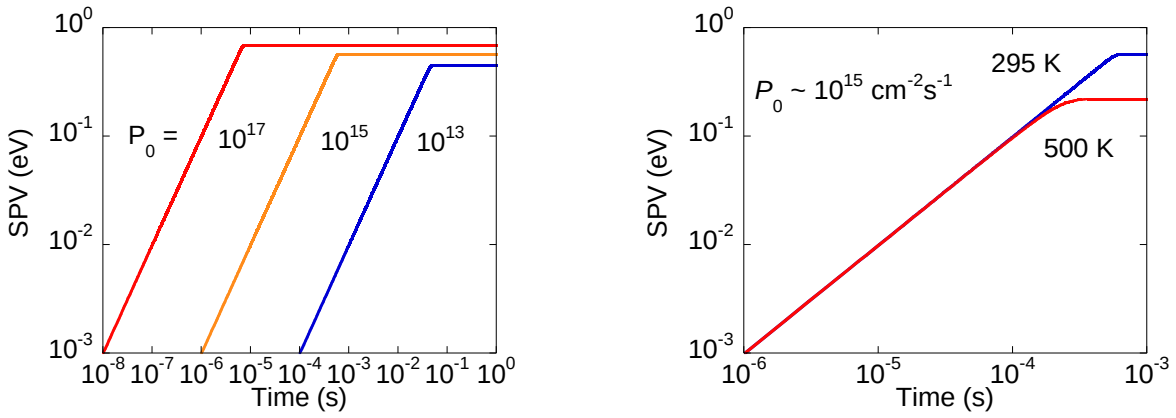

Figure 20 Calculated SPV transients with Eq. (4.19a) under band-to-band illumination with the parameters: Φ_0 = 1 eV, c = 0.5, P_0 = 10^{13}, 10^{15}, and 10^{17} $cm^{-2}s^{-1}$ and R_0 = 10^5 and 3×10^{12} $cm^{-2}s^{-1}$ at 295 K and 500 K, respectively. (P_0=6.5×10^{16} $cm^{-2}s^{-1}$ corresponds to ~40 mW/cm^2.)

From this plot, we observe that increasing the excitation intensity by 2 orders of magnitude will decrease the amount of time it takes the SPV to saturate by 2 orders of magnitude. This will play an important role in our SPV measurements. For example, if the SPV takes approximately 100 s to saturate and the intensity is increased by an order of magnitude, we may expect that the SPV should now saturate after 10 s of exposure. Any observe behavior after 10 s could be attributed to external mechanisms of the SPV (i.e. not related to the thermionic model described above).

With regards to the temperature, we observe that the time the SPV saturates does not change dramatically with increasing temperature. This is due to the fact that the rate the SPV increases in time does not change with increasing temperature [see Figure 20b]. Increasing the temperature will only decrease the amount of time it takes the SPV to saturate, because the maximum SPV generated with increasing temperature is smaller (due to the exponential temperature dependence in the parameter R_0). This type of fitting can be useful to estimate the

amount of time it should take for the SPV to saturate and to avoid external mechanisms that arise from exposing the samples to UV-light for extended periods of time.

4.2 Steady-state SPV

The steady state SPV for an n-type semiconductor is defined as $dn_s/dt = 0$ in Eq. (4.17). The expression can be solved for y which gives:

$$\text{for n-type}: \quad y_0 = \eta kT \ln\left(\frac{cP_0}{R_0} + 1\right) \tag{4.20a}$$

and

$$\text{for p-type}: \quad y_0 = -\eta kT \ln\left(\frac{cP_0}{R_0} + 1\right) \tag{4.20b}$$

where y_0 is the value of the SPV generated by external illumination, kT is the thermal energy, and R_0 is the number of electrons that move over the near surface barrier, from the bulk to the surface, per unit time and per unit area, in dark.

Not shown explicitly in Eq. (4.20) is the exponential temperature dependence in the parameter R_0 [Eqs. (4.6) and (4.9)]. An increase in R_0, due to increased temperatures, will cause the absolute value of the SPV signal to decrease with increasing temperature, if band bending remains constant. Therefore, fitting intensity dependent SPV data to determine the parameter R_0 will allow us to estimate the near surface band bending using a thermionic model.

Figure 21 shows the calculated dependence of the SPV on excitation intensity for n-type GaN using Eq. (4.20) for three values of R_0 and their corresponding band bending values in dark.

(a) (b)

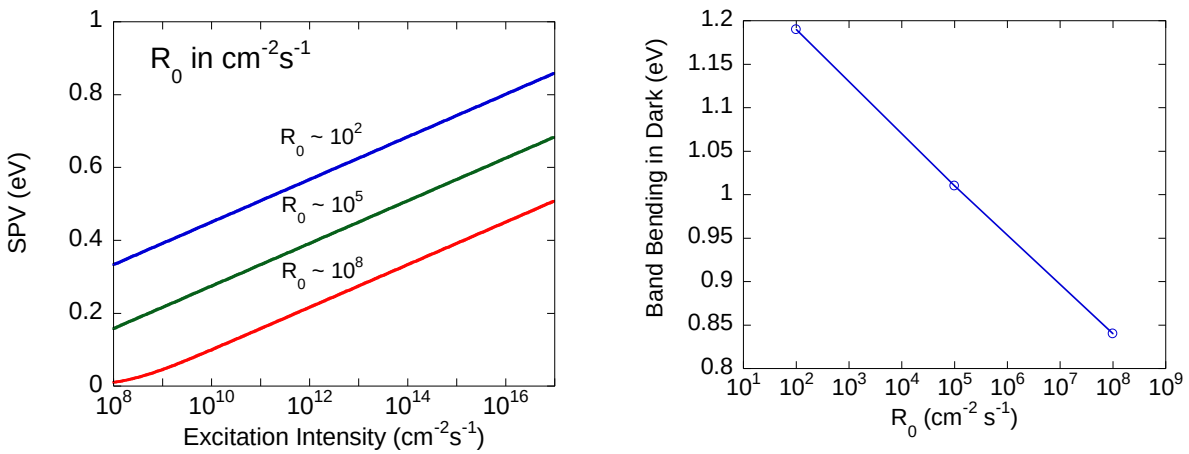

Figure 21 (a) Calculated SPV intensity dependence [Eq. (4.20a)]and (b) band bending values in dark corresponding to different values of R_0 for n-type GaN [Eq. (4.6)]. Parameters used c = 0.5, T = 295 K, n = 2.5×10^{17} cm^{-3}, η = 1, and s_n = 10^5 cm/s.

The plot in Figure 21(a) shows how the maximum SPV is expected to change with changing excitation intensity for different values of R_0. From these R_0 values, the band bending, Φ_0, can be determined using Eq. (4.6). Figure 21(b) shows that even when R_0 changes by orders of magnitude, it has very little effect on the calculated value of band bending. For example, changing R_0 by 3 orders of magnitude only changes the calculated band bending by less than 0.2 eV at room temperature. Fitting the intensity-dependent SPV data with a thermionic model is an accurate way to estimate the band bending in GaN samples. Using the parameters R_0 = 10^5 cm^{-2}s^{-1}, n = 2.5×10^{17} cm^{-3}, T = 295 K, and varying s_n from 10^3 to 10^7cm/s provides values of band bending from 0.9 to 1.13 eV, respectively. We expect that the reasonable range of s_n is 10^3 – 10^7 cm/s for GaN samples of different quality, with the mean value at $s_n \approx 10^5$ cm/s.[66] It shows that an error in s_n does not significantly affect the value of Φ_0 estimated from the SPV intensity dependence.

4.3 Restoration of the SPV

After illumination of the surface is ceased, the band bending is expected to restore with a slope proportional to *kT*. We expect that short UV exposures will be more reliable, since there is less of a chance for external mechanisms to affect the SPV restoration. The restorations can be fit with the following equations:

$$\text{for n-type}: \quad y(t) \approx y_0 - \eta kT \ln\left(1+\frac{t}{\tau}\right) \tag{4.21a}$$

$$\text{with} \quad \tau = \frac{\eta kT}{R_0}\frac{n_s(0)}{2\Phi_0}\exp\left(-\frac{y_0}{\eta kT}\right)$$

and

$$\text{for p-type}: \quad y(t) \approx y_0 + \eta kT \ln\left(1+\frac{t}{\tau}\right) \tag{4.21b}$$

$$\text{with} \quad \tau = -\frac{\eta kT}{R_0}\frac{p_s(0)}{2\Phi_0}\exp\left(\frac{y_0}{\eta kT}\right),$$

where $y(t)$ is the SPV at a given time t, y_0 is the SPV generated right before the illumination is ceased at $t = 0$, and τ is the characteristic delay time after which the logarithmic decay of the SPV begins. After ceasing illumination, the restoration of the SPV becomes noticeable after a duration of time, τ, which strongly depends on the band bending established during illumination; i.e., on $\Phi = \Phi_0 - y_0$. According to Eq. (4.21), the slope of the restoration should increase with increasing temperatures. The calculated restorations of SPVs generated at $T = 295$ and 500 K are shown in Figure 22.

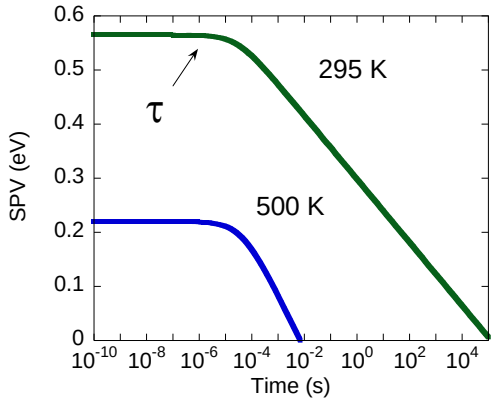

Figure 22 Restoration of the SPV calculated with Eq. (4.21a) with the following parameters: y_0 = 0.684 eV and $\tau = 2.7\times10^{-5}$ s, and y_0 = 0.418 and $\tau = 4.3\times10^{-5}$ s, at 295 and 500 K, respectively. $n_s(0) = 10^{12}$ cm^{-2} and $R_0 = 10^5$ and 3×10^{12} cm^{-2}s^{-1} for T = 295 and 500 K, respectively. Using = Φ_0 = 1 eV, c = 0.5, η = 1, and $P_0 = 10^{15}$ cm^{-2}s^{-1}.

The restoration rate increases with increasing temperature, and the delay time decreases with increasing temperature from 295 to 500 K. It is expected that under high illumination intensity and with reasonable parameters for GaN, the delay time should be less than 1 second. Then, delay times that appear longer than 1 second indicate the affect of external mechanisms on the SPV behavior during illumination. On the other hand, we expect that full restoration will be achieved after a very long time at room temperature (>10^5 s) if $\Phi_0 > 1$. Performing measurements at higher temperatures will provide more accurate baselines for SPV measurements, due to the amount of time it takes for the band bending to restore at 500 K vs. 295 K. It is important to note here that at 500 K the complete restoration of band bending occurs in much less than 1 second.

4.4 Calculation of Band Bending

This subsection will detail how the band bending will be calculated from intensity-dependent SPV measurements, as well as from the CPD signal in dark.

a. Using the Parameter R_0

The parameter R_0 can be found by fitting the experimental dependence of y_0 on P_0 with Eq. (4.20), where R_0 is the only fitting parameter if c is known. The band bending in n- and p-type GaN can then be calculated using information from the experimentally found R_0 values. Then from Eqs. (4.6) and (4.9), the band bending can be estimated by:

$$\Phi_0 = -kT \ln\left(\frac{R_0}{s_n N_C}\right) + \left(E_C - F\right) \tag{4.22a}$$

and

$$\Phi_0 = +kT \ln\left(\frac{R_0}{s_p N_V}\right) - \left(E_V - F\right), \tag{4.22b}$$

for n- and p-type GaN, respectively. The density of states in the conduction and valence band are calculated using:

$$N_C = 2\left[\frac{2\pi m_e kT}{\left(2\pi\hbar\right)^2}\right]^{\frac{3}{2}} \tag{4.23}$$

and

$$N_V = 2\left[\frac{2\pi m_p kT}{\left(2\pi\hbar\right)^2}\right]^{\frac{3}{2}}, \tag{4.24}$$

where $m_e = 0.2\ m_0$[67] and $m_p = 0.8\ m_0$[68] for GaN, and $\hbar$ is Plank's constant. Finally the positions of the Fermi-levels in n- and p-type GaN are given by:

$$E_C - E_F = kT \ln\left(\frac{N_C}{n}\right) \tag{4.25a}$$

and

$$E_F - E_V = kT \ln\left(\frac{N_V}{p}\right), \tag{4.25b}$$

where n and p are the concentrations of free electrons and holes, respectively. The largest error in band bending from these estimates is about ±0.2 eV, which is mostly due to uncertainty of the surface recombination velocity (10^3 – 10^7 cm^2/s). These calculations should be considered the most accurate method to estimate the near-surface band bending using the Kelvin probe setup.

b. Using the Dark CPD

The band bending in n- and p-type GaN can also be calculated from the dark value of the CPD signal using the following expressions:

$$\Phi_0 = \phi_M - \chi - (E_C - F) - qV_{CPD} \tag{4.26a}$$

and

$$\Phi_0 = \phi_M - \chi - \left(E_g + E_V - F\right) - qV_{CPD}, \tag{4.26b}$$

for n- and p-type GaN, respectively, where χ is the electron affinity for GaN (3.2 eV)[69], ϕ_M is the work function of the stainless steel probe (estimated to be 4.8 eV from the measurement of a gold foil), E_g is the energy of the band gap (3.43 eV at 295 K), and qV_{CPD} is the measured contact potential difference multiplied by the electron charge. This method is believed to be less

accurate than using the measured SPV behavior because any error in the parameters used will come out directly in the calculated values of band bending. In particular, if the error in our value of the work function due to the effect of the ambient is about 0.5 eV, then the band bending will have error of at least ±0.5 eV. In reality, the estimates for the value of the electron affinity and the work function could be off by up to 1 eV,[48,69] which may introduce large error in the estimate of band bending using this method.

c. Additional Sample Parameters

The value of the band gap for GaN at 293 to 1237 K can be estimated by[70]

$$E_g = 3.556 - 9.9\times10^{-4}\times\left(\frac{T^2}{T+600}\right), \tag{4.27}$$

where T is the temperature in Kelvin. The following equation will prove useful when information about N_A and N_D is known to calculate the concentration of free electrons or holes, respectively:[71]

$$n + N_A = \frac{N_D}{1+\frac{gn}{N_c}\exp\left(\frac{E_D}{kT}\right)} \tag{4.28a}$$

and

$$p + N_D = \frac{N_A}{1+\frac{gp}{N_V}\exp\left(\frac{E_A}{kT}\right)}, \tag{4.28b}$$

where g in the degeneracy factor (2 for GaN), E_D is the ionization energy for a shallow donor (~20 meV for Si)[72], and E_A is the ionization energy for a shallow acceptor (~180-200 meV for Mg)[73]. These expressions can be solved using the quadratic equation which gives:

$$n = \sqrt{\frac{\left(N_{1n} + N_A\right)^2}{4} + N_{1n}\left(N_D - N_A\right)} + \frac{\left(N_{1n} + N_A\right)}{2} \tag{4.29a}$$

where

$$N_{1n} = \frac{N_C}{g}\exp\left(-\frac{E_D}{kT}\right)$$

and

$$p = \sqrt{\frac{\left(N_{1p} + N_D\right)^2}{4} + N_{1p}\left(N_A - N_D\right)} + \frac{\left(N_{1p} + N_D\right)}{2} \tag{4.29b}$$

where

$$N_{1p} = \frac{N_V}{g}\exp\left(-\frac{E_A}{kT}\right)$$

for the concentration of free electrons and holes, respectively.

Chapter 5: SPV behavior in n-type GaN

In this Chapter we will analyze the SPV behavior from a Si-doped n-type GaN sample grown by HVPE at Oxford Instruments - TDI. (Sample 2015_HN)

5.2 Transient SPV Behavior

The behavior of the SPV signal under band-to-band illumination with the HeCd laser was studied in vacuum and air. Before measurement of the SPV behavior, the sample was cleaned with the procedure outlined in Chap. 3.3, and was loaded into the cryostat within 15 min. The transient SPV behavior for front-side band-to-band illumination of cleaned, Si-doped n-type GaN is shown in Figure 23.

(a) (b)

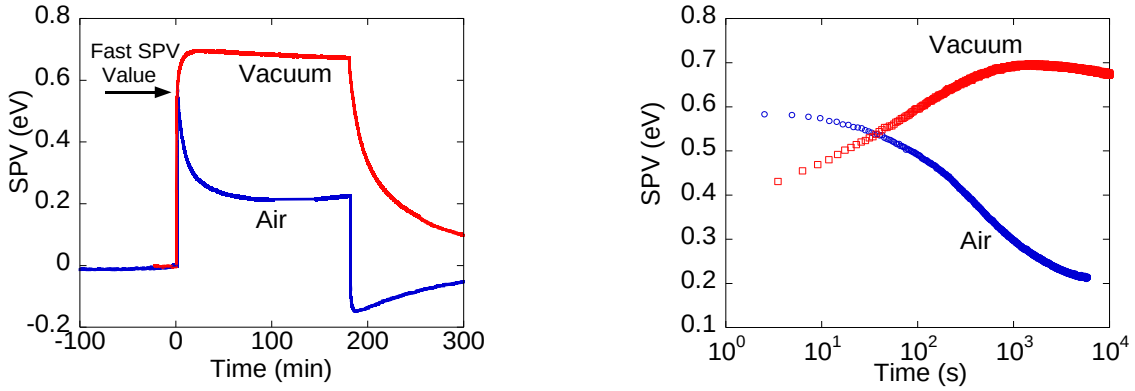

Figure 23 (a)Time dependence of the SPV in air and vacuum for freshly etched n-type GaN, using front-side illumination with band-to-band excitation (325 nm, 40 mW/cm^2). UV illumination begins at t = 0 min and stops after 180 min. (b) SPV plotted as a function of time in a logarithmic scale. Sample 2015_HN.

As expected, when illumination begins the SPV signal quickly rises to a positive value of about 0.5 eV within the first few seconds, due to the accumulation of holes at the surface (internal

mechanism). High excitation intensity and continuous illumination with UV-light can slowly change the surface potential with time (and therefore SPV). This increase or decrease in the SPV is dependent on the ambient conditions. The rate and amount of decrease of the SPV signal in air or oxygen ambient depends on how long the sample has been previously exposed to UV-light in an oxygen-containing environment. The freshly etched sample in Figure 23 exhibits a large decrease of about 0.3 eV in the SPV after 1 h of illumination, whereas the same sample, when it has been previously exposed to UV-light in an oxygen environment for more than 20 h, demonstrates a small decrease of less than 0.1 eV after a 1 h illumination (Figure 24).

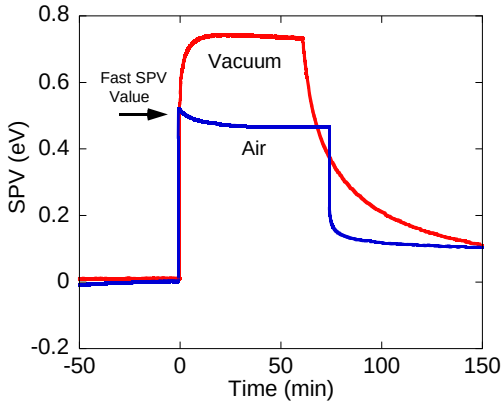

Figure 24 Time dependence of the SPV in air and vacuum for n-type GaN previously exposed for over 20 h to UV light in an oxygen environment, using front-side illumination with band-to-band excitation. UV illumination begins at t = 0 min and stops after 1 h. P_0 =325 nm, 40 mW/cm^2. Sample 2015_HN

We have observed this type of SPV behavior in other n-type GaN samples and have attributed changes in the SPV behavior caused by long UV-expsore to the UV-induced growth of a thicker surface oxide layer, which inhibits electron transfer from the bulk to the surface as the oxide layer increases in thickness.[74] We assume that oxygen, not water, plays a major role in the observed changes of the SPV during UV-illumination, because we observe very similar changes in the SPV in dry oxygen and air ambient.

In the presence of UV light, a physisorbed oxygen species can become chemisorbed after receiving an electron from the bulk over the decreased near-surface barrier. This process results in the slow decrease of the SPV during continuous illumination due to the addition of negative charge to the surface. After many hours of UV-light exposure, however, the chemisorbed oxygen increases the surface oxide thickness. This will inhibit electron transfer from the bulk, which will result in a smaller change in the SPV signal for samples with longer amounts of UV-light exposure.

The amount the SPV decreased under steady-state illumination was measured as a function of previous UV-light exposure. In these experiments after the CPD signal restored to its dark value, the surfaces were exposed to 80 min of UV-illumination. After measuring how much the SPV signal decreased under UV-illumination, the sample was then additionally exposed to a Hg lamp for additional time, to grow a thicker oxide. The sample was then kept in the dark for 1-2 days to reach its dark CPD value before performing another SPV measurement. The above cycle was repeated several times while increasing the total amount of UV-exposure time. After acquiring data for a sample with over 100 h accumulated UV-exposure, it was then cleaned using the cleaning procedure outlined in Chap. 3.3. The SPV behavior during continuous illumination as a function of total UV-exposure is presented in Figure 25 for the initial sample, after UV-exposure, and after being cleaned.

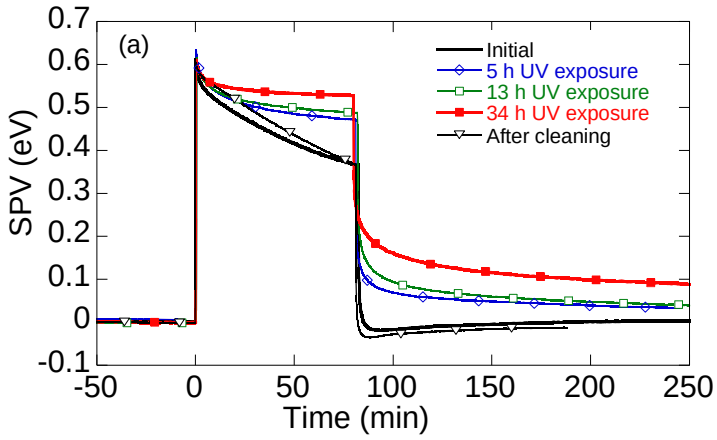

Figure 25 SPV measurements for the initial sample in oxygen, after various times of accumulative UV-exposure, and after etching, where illumination occurred between t = 0 and 80 min. Sample 2015_HN.

In the case of the initial surface, the SPV signal slowly decreased from 0.61 to 0.37 eV during an 80 minute illumination, this behavior is similar to our previous reports on GaN layers grown by molecular beam epitaxy (MBE).[75] For increasing UV-exposure times, the amount the SPV decreases under illumination became smaller, and the steady-state SPV only decreased by about 0.05 eV after 100 h of UV-exposure. The amount the SPV decreased under UV-illumination as a function of total UV-exposure time is plotted in Figure 26. The amount the SPV decreased under UV-illumination has a logarithmic time behavior as a function of total UV-exposure time in hours. After the cleaning procedure, the amount the SPV decreases under UV-illumination returns to its initial as indicated by a red cross.

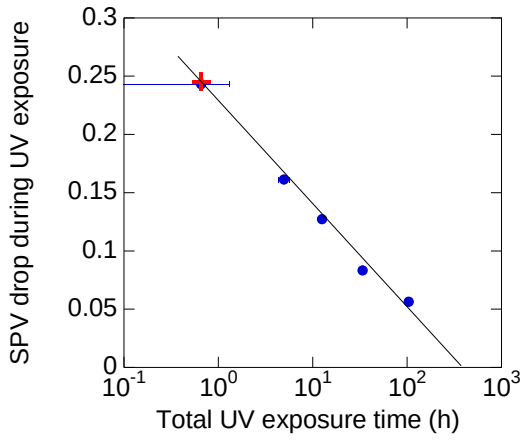

Figure 26 The value of the SPV drop from t = 0 to 80 min. as a function of accumulative UV-exposure time. The value obtained after etching is shown with a cross. Sample 2015_HN.

The SPV behavior as a function of UV-exposure time is consistent with the UV-induced growth of a surface oxide. As the oxide layer increases in thickness, however, this photo-adsorption process slows down since electron transfer from the bulk to the surface becomes more difficult, resulting in less of a decrease in the SPV signal under steady-state illumination. The SPV decay transient, τ, after switching off illumination also becomes slower with increased UV-illumination time. This qualitatively agrees with the growth of an oxide layer, since for thicker oxide layers the transfer of electrons between the oxide and bulk is expected to be slower. Figure 27 shows a schematic diagram of the photo-induced adsorption processes for n-type GaN.

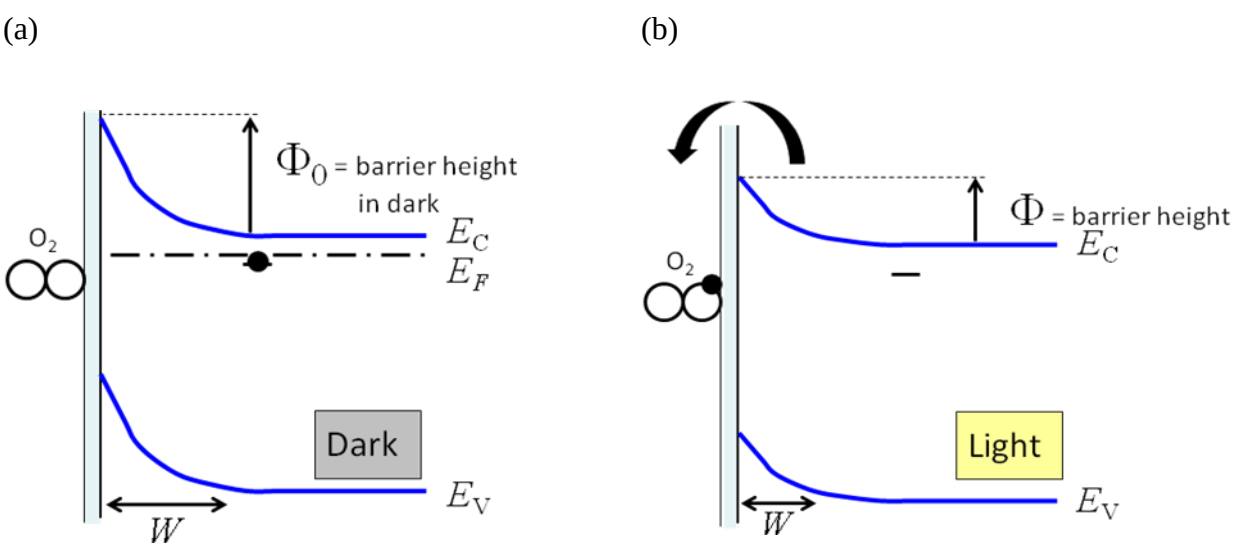

Figure 27 (a) oxygen physisorbed on the surface of n-type GaN in dark conditions. (b) After capturing an electron due to the reduced surface barrier, the oxygen becomes chemisorbed.

In the presence of high intensity UV-light, physisorbed oxygen species can become chemisorbed after receiving electrons from the bulk. Initially, illumination results in the creation of electron-hole pairs in the depletion region, where the electric field causes holes to move toward the surface and electrons toward the bulk. The arriving holes reduce the net negative charge at the surface and thereby the amount of band bending, resulting in an immediate increase of CPD or SPV signal. Because of this decrease in band bending, the flow of bulk electrons to the surface increases exponentially. Some of these electrons may then tunnel through or pass over the potential barrier formed by the oxide layer. The chemisorption of oxygen at the surface therefore becomes more efficient in the presence of UV-light, and the surface oxide can grow much faster under UV-illumination than under dark conditions at room temperature.

In contrast to the SPV behavior in an oxygen containing ambient, the SPV behaviors in a vacuum environment for the etched and UV-exposed GaN are relatively similar (Figure 23 and Figure 24). The SPV quickly reaches a value of about 0.5 eV within the first few seconds and

then increases to about 0.75 eV after 1 h of illumination, due to the photo-induced desorption of negatively charged oxygen species. The SPV behavior appears to show no significant dependence on prior UV-exposure, most likely because electron transfer from the bulk is not necessary for this photo-induced desorption process.

Additional consideration needs to be given to the SPV behavior in vacuum. For some samples, the SPV increases for the first 10-15 min, but then begins to slightly decrease (Figure 23b). We have not been able to determine the cause for the slight decrease in the SPV behavior under continuous UV-illumination. In the past when the lamp and monochromator was used for band-to-band illumination, the SPV increased during illumination for up to 3 h. It was not until we began using the laser and the front side illumination geometry that we observed slight decreases in the SPV signal for n-type GaN in vacuum. Therefore, it may be interesting to perform transient SPV measurements with the front side geometry while reducing the excitation intensity, to determine if the decrease is excitation intensity dependent.

For some samples immediately after the cleaning procedure, the SPV behavior in vacuum was unusual (different pieces of 2015). The SPV signal would both increase and decrease under continuous illumination after the fast initial rise. This type of behavior is attributed to species left over from the cleaning procedure being desorbed under UV-illumination in vacuum. It is important to thoroughly rinse and nitrogen blow dry samples that have been cleaned with chemical methods, as to remove any reactants from the surface as these may affect the SPV behavior.

We have observed the photo-induced adsorption and desorption of negatively charged species on the surface of n-type GaN in air/oxygen and vacuum, respectively. The photo-induced adsorption of oxygen leads to the growth of a thicker oxide layer, and has a logarithmic

dependence on the total UV-exposure time. The behavior in vacuum did not appear to have a dependence on the UV-exposure time because electron transfer from the bulk is most likely not necessary for this photo-induced desorption process.

5.3 Intensity-Dependent SPV Behavior

The intensity of our HeCd laser can be attenuated by more than 9 orders of magnitude by a series of calibrated neutral density filters. The dependence of the SPV signal on excitation intensity for n-type GaN is shown in Figure 28 using front-side illumination. In this figure, the SPV data are plotted vs. the product cP_0, where c is a geometrical factor that accounts for the percentage of photons absorbed in the depletion region and P_0 is excitation intensity. This product is used to estimate the density of electron-hole pairs created in the depletion region during illumination.

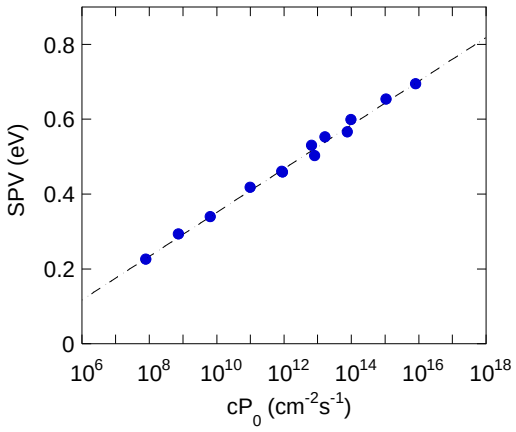

Figure 28 Intensity dependence of the SPV for n-type GaN in air using front-side illumination [325 nm, 40 mW/cm^2]. Dashed line is fit using Eq. (4.20a) with the following parameters: $R_0 = 10^4$ cm^{-2}s^{-1}, $c = 0.194$, and $\eta = 1$ (curve 1). Sample 2015_HN.

The sample exhibits a maximum SPV value of about 0.7 eV under the highest illumination intensity, and the SPV has a logarithmic dependence on excitation intensity. Using Eq. (4.20a) to

fit the data in Figure 28, we can then estimate the value of R_0 as ~10^4 $cm^{-2}s^{-1}$ with $\eta = 1$. The intensity-dependent SPV behavior can be explained by a thermionic model and does exhibit a logarithmic dependence on excitation intensity.

The value of the near-surface band bending in dark, Φ_0, can be estimated using the calculated value of R_0 obtained from fitting the intensity-dependent SPV from Eq. (4.22a). Using s_n = 10^5 cm/s with the uncertainty of 2 orders of magnitude, we estimate that the band bending for the n-type GaN sample is about 1.1 ± 0.2 eV, which is in agreement with previous estimates obtained from an undoped MBE-grown sample (750_BN).[63] The 0.2 eV error in this measurement comes mostly from the uncertainty in surface recombination velocity.

For n-type GaN, it is very difficult to perform the intensity-dependent SPV measurements in vacuum. We observed the desorption of species even at intensities of about 10^{14} $cm^{-2}s^{-1}$ (P_{exc} ~3 μW/cm^2). The only way to minimize the effects of external mechanisms of the SPV is to limit the exposure time. This can be done by only exposing the sample for 1 to 3 s at each excitation intensity. This procedure will prove useful for temperature-dependent SPV measurements, so that we do not change the surface conditions at high temperatures in an oxygen or environment environment.

5.4 Below-Bandgap SPV Behavior

The surfaces could be exposed with a Xe-lamp attached to a monochromater to probe the below-bandgap SPV behavior. When n-type GaN is illuminated with below-bandgap light, electrons can be excited from surface states over the near-surface barrier into the bulk. This movement of charge will reduce the net negative surface charge, and therefore the band bending.

The SPV signal dependence on photon energy is plotted in Figure 29 for using the Xe-lamp and backside illumination. In these experiments, the steady-state SPV was allowed to saturate while attempting to minimize the effect of photo-induced mechanisms.

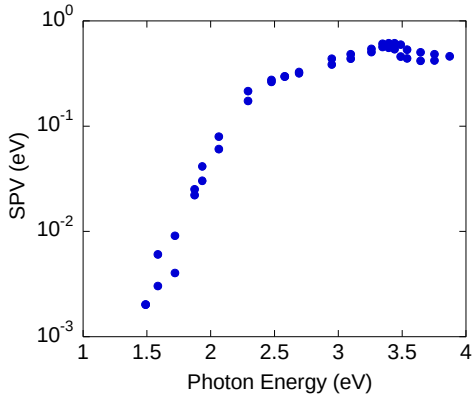

Figure 29 Steady-state SPV spectra for n-type GaN in air using backside illumination (30 mW/cm^2). The spectrum shows a maximum SPV value at a photon energy of about 3.4 eV. The threshold voltage for the n-type GaN sample is about 1.5 eV. Sample 2015_HN.

The SPV spectrum in Figure 29 indicates that n-type GaN has a threshold photon energy of about 1.5 eV and a maximum SPV of about 0.7 eV at a photon energy of 3.4 eV. Photons with this energy are able to pass through the bulk GaN but are absorbed in the depletion region due to the strong electric field in the depletion region. The photons with an energy slightly less than the bandgap can be effectively absorbed in the depletion region via photon-assisted tunneling (Franz-Keldysh effect), thereby increasing the number of photons with energy slightly less than the bandgap absorbed in the depletion region.[76,77,78] The SPV signal decreases above 3.4 eV due to an abrupt rise in the absorption coefficient near the bandgap (3.43 eV): photons with higher energy will not be able to penetrate through the bulk and reach the surface. The SPV signal generated from photon energies above 3.43 eV can be attributed to photoluminescence arising close to the GaN/sapphire interface and/or unfiltered parasitic light from the monochromator

with energy close to 3.4 eV which passes through the GaN bulk and is effectively absorbed in the depletion region.

Although the above mechanism for below-bandgap SPV with surface states reasonably explains the experimental results, we cannot exclude the alternative mechanism of a two-step excitation of electrons in the depletion region via deep-level point defects. In such a two-step mechanism, an electron is first resonantly excited from a deep defect to the conduction band, and then an electron from the valence band is excited to the defect level. To explain the thresholds observed in the SPV spectra, the defect level should appear in the middle of the GaN bandgap, or 1.5 to 2.0 eV from the valence or conduction band. Defects with such levels could be responsible for an observed red luminescence band, but have not been observed in deep-level transient spectroscopy experiments. We consider this two-step mechanism as less likely, because similar SPV spectra were observed in GaN samples not exhibiting a red luminescence band.

The threshold voltages measured from these experiments may also depend on the experimental conditions. It is possible that in these experiments we do not wait enough time for the SPV to saturate, or that the excitation intensity we use limits the threshold voltage. It is possible that if the excitation intensity was increased orders of magnitude, that the threshold voltage would shift to lower energies. It is important to keep this in consideration when performing these types of measurements. It would prove advantageous to preheat samples and measure the SPV spectra a room temperature. This type of measurement has not been performed yet.

5.5 Restoration of the SPV Behavior

After illumination ceases, the band bending will begin to restore to its value in darkness because electrons begin to repopulate the surface. The time dependence of the SPV signal after

ceasing illumination is predicted by Eq. (4.21a). Figure 30 illustrates the SPV restoration behavior in both air and vacuum after short (3 s) and long (1 h) illumination times.

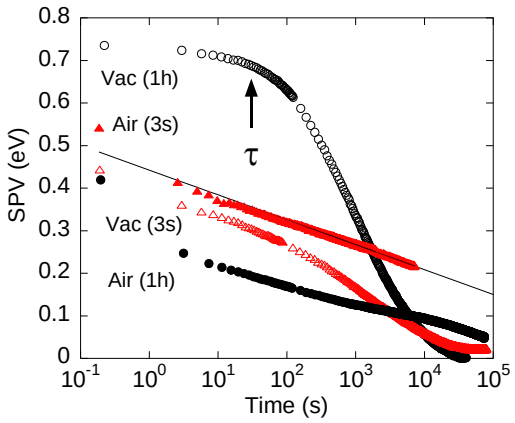

Figure 30 Restorations of the SPV in air and vacuum after short (3 s) or long (1 h) exposure times for n-type GaN. Solid lines are calculated with Eq. (4.21a) using $\eta = 1$, $y_0 = 0.7$ eV, $\tau = 40$ μs. Sample 2015_HN.

In most cases, the SPV data demonstrate logarithmic restoration rates with slopes close to the predicted value of *kT*. All of the SPV restorations have similar rates with $\eta = 1$ and $\tau = 40$ μs [see solid line in Figure 30], except for the case of a 1 h illumination in vacuum. In this latter case, the photo-induced desorption of surface species results in a larger initial SPV, but the restoration behavior exhibits a much longer time delay of $\tau = 100$ s followed by a slope greater than *kT*. The thermionic model predicts that larger SPVs should have exponentially shorter delay times. This, however, is not the case for the 1 h illumination in vacuum. It appears that if photo-induced processes increased the magnitude of the SPV by at least 0.2 eV, then the restoration behavior would have a significantly longer time delay time followed by a higher restoration rate. This type of behavior is not surprising given any change in the surface charge that is not related to electrons overcoming the near surface barrier from bulk to surface or vice versa and holes reaching the surface is not incorporated into the thermionic model use to fit the restorations.

We have observed that changing the number of data points that are being averaged affects the restoration rate (avg of 1 vs. avg 5). We have observed at the point in which we changed the average, the slope of the SPV appears to change, or has shifted the CPD signal. This behavior is not predicted by our model, and is most likely an experimental artifact related to the Kelvin probe software. It is important to only change the interval (the time the system waits in-between measurements) because this will not affect the restoration rate. When the signal average was changed from 1 to 5 in Figure 30 for the 3 s vacuum measurement, the rate of restoration appeared to change.

Overall the SPV restoration behavior is well-predicted by the model for n-type GaN in the case of short illumination times, as well as for longer times where photo-induced processes do not significantly change the steady-state SPV value.

5.6 Temperature Dependent SPV Behavior

a. Transient SPV behavior

Increasing the sample temperature can help elucidate the effect of oxygen, water, and vacuum in the transient SPV behavior. The SPV behavior for band-to-band illumination of the cleaned n-type sample in oxygen and vacuum obtained at 295 and 450 K is shown in Figure 31.

(a) (b)

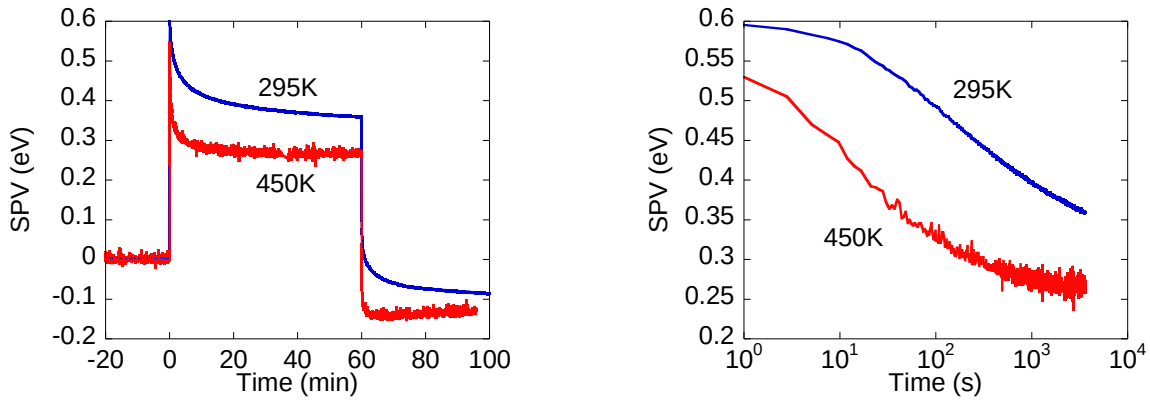

Figure 31 (a) Time dependent SPV behavior for n-type GaN, under continuous band-to-band UV illumination (325 nm, 40 mW/cm^2), in oxygen at 295 and 450 K. Illumination occurs from time t = 0 to t = 60 min. (b) SPV transient in a logarithmic scale. Sample 2015_HN.

As previously observed, in oxygen at 295 K, the SPV signal for band-to-band illumination quickly reaches a positive, maximum value of about 0.60 eV, and then decreases under continuous illumination by about 0.24 eV over 1 h. In oxygen at 450 K, the SPV signal quickly rises to about 0.52 eV and then decreases by about 0.26 eV at a faster rate than observed at 295 K.

This behavior can be explained as follows. In the presence of UV light, a physisorbed oxygen species can become chemisorbed after receiving an electron from the bulk. Since an electron must overcome the near-surface barrier when traveling from the bulk to surface, the rate of this process can be exponentially increased by illumination with band-to-band light (due to a decreased barrier height) or by increasing the sample temperature. This measurement shows that it is oxygen, not water, is the photo-induced adsorbed species. At this high temperature, the probability for water molecules to adsorb onto the surface is low. Since the rate of adsorption of negatively charged oxygen species increased with increasing sample temperature, we predict that

the n-type GaN sample grows an oxide layer significantly faster at higher temperatures under UV-illumination. Simply heating the sample in air/oxygen ambient in dark could also promote the growth of an oxide layer due to the increased number of electrons that are able to overcome the near-surface barrier.

(a) (b)

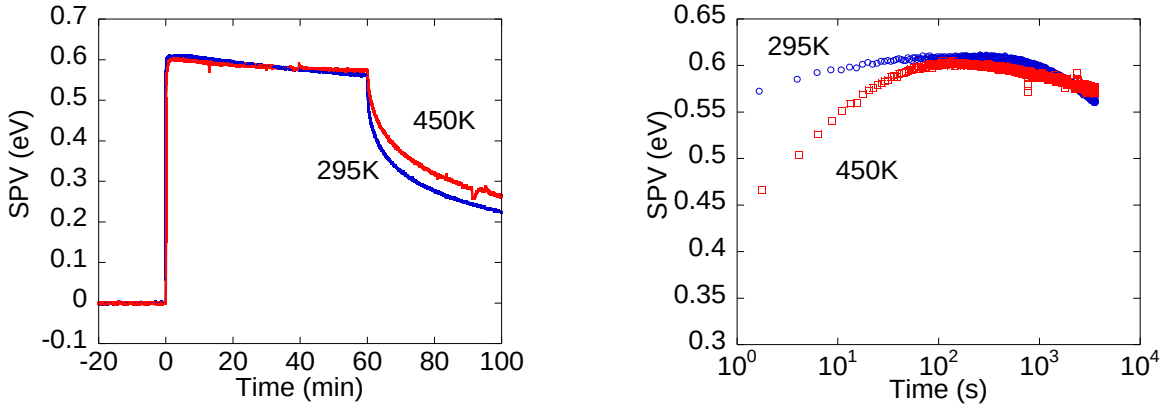

Figure 32 (a) Time dependent SPV behavior for n-type GaN, under continuous band-to-band UV illumination (325 nm, 40 mW/cm^2), in vacuum at 295 and 450 K. Illumination occurs from time t = 0 to t = 60 min. (b) SPV transient in a logarithmic scale. Sample_2015HN

In Figure 32, the time-dependent SPV behavior in vacuum at 295 and 450 K is shown. At 295 K, the SPV immediately rises to about 0.57 eV, increases by about 0.04 eV during the first 5 min., and then slightly decreases during 1 h of illumination. At 450 K, the SPV immediately rises to about 0.50 eV, increases by about 0.10 eV during the first 5 min., and then slightly decreases over 1 h.

In our previous work, we proposed that the surface potential increases in vacuum under continuous band-to-band illumination due to the photo-induced desorption of negatively charged oxygen species.[79] In this study, however, such photo-induced desorption is only observed during the first few minutes of illumination; the origin of the subsequent slow decrease of the SPV is

not yet clear. It appears that temperature did not greatly influence the SPV behavior for n-type GaN in vacuum. However, at both 295 and 500 K, it appears that the restoration rate after illumination is ceased exhibits a longer than usual delay time. The length of the delay time may be attributed to external mechanisms of the SPV since a significant SPV was generated. For a SPV of about 0.6 eV, it is expected that the delay time should be less than a millisecond.

b. Intensity-Dependent SPV Behavior

Increasing the sample temperature will change the values of R_0, and allow us to estimate the values of band bending as a function of temperature. The dependences of the SPV signal on excitation intensity at different temperatures for the n-type HVPE-grown sample are shown in Figure 33. The intensity-dependence was fit with the following expression:

$$y = \eta kT \ln\left(\frac{cP_0}{R_0}+1\right) = \eta kT \ln\left(\frac{cP_0}{s_n N_C \exp\left(-\frac{\Phi_0 + (E_C - F)}{kT}\right)}+1\right), \tag{5.1}$$

where the only fitting parameter was the band bending in dark, Φ_0.

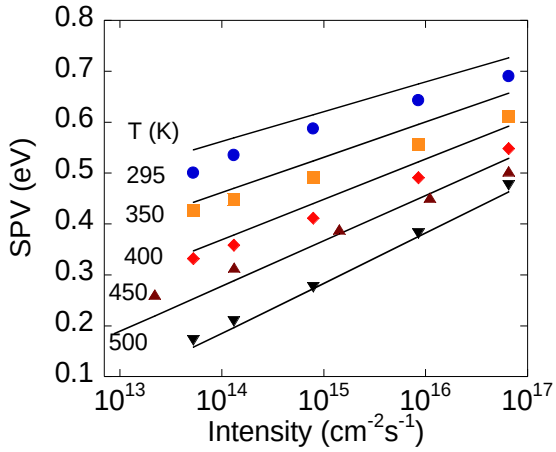

Figure 33 Intensity-dependent SPV measurements of n-type GaN in vacuum taken at various temperatures using band-to-band UV illumination (325 nm). The solid lines are calculated using Eq. (5.1) with the parameters: $\eta = 1$, $c = 0.454$ and $\Phi_0 = 1.05$, E_C-F = 0.076, 0.088, 0.099, 0.112, and 0.124 eV for T = 295, 350, 400, 450, and 500 K, respectively. Sample 2015_HN.

As predicted by Eq. (5.1), the SPV signal increases logarithmically with excitation intensity. Additionally, at any given excitation intensity, the magnitude of the SPV decreases with increasing temperature. This is due to an exponential increase in the rate R_0 with increasing temperature. In these experiments, the UV exposure time was limited to about 1 second to minimize the effect of external mechanisms, such as photo-induced desorption or absorption. The thermionic model predicts that this short exposure time is a sufficient amount of time for the SPV to saturate.

The slopes of the SPV intensity dependence were fit using Eq. (5.1), where the estimated Φ_0 is about 1.05 eV. The band bending appears to be slightly overestimated by no more than 0.05 eV at temperatures below 450 K. The values of band bending therefore change very little with increasing temperature, in agreement with the thermionic model which predicts that band bending is independent of sample temperature. Since the band bending was calculated using the

SPV intensity-dependent behavior as a function of temperature, these results further verify the thermionic model used to fit our SPV measurements.

c. Restoration of the SPV

Increasing the sample temperature should exponentially increase the rate at which the band bending restores to its value in dark. The restoration of the SPV after ceasing illumination is shown in Figure 34 for 295 and 500 K.

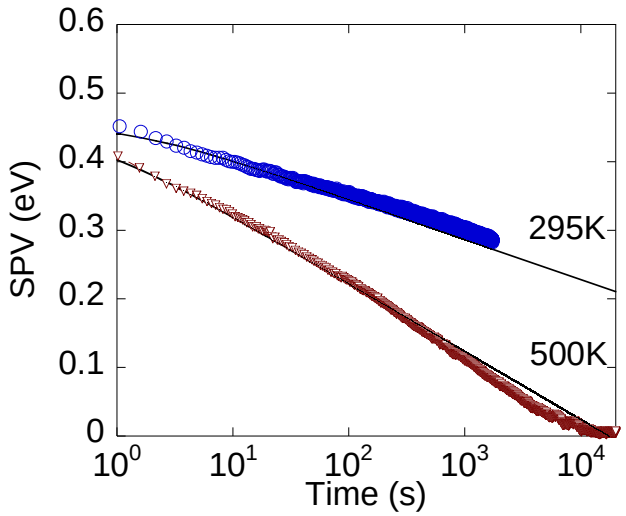

Figure 34 Restorations of SPV in vacuum after short (1 s) UV illuminations at 295 and 500 K and $P_0 = 10^{17}$ $cm^{-2}s^{-1}$. The fits are calculated using Eq. (4.21a) with $\eta = 1$; $y_0 = 0.62$ and 0.45 eV; and $\tau = 0.002$ s and $\tau = 0.5$ s for T = 295 and 500 K, respectively. Sample 2015_HN

As predicted by the thermionic model, the SPV restores as a logarithmic function of time, where the restoration rate increases with increasing temperature. Thus, at high temperatures (500 K), the SPV fully restores after 3 h, whereas at low temperatures (295 K), the SPV may need years to fully restore. From this behavior, we conclude that measurements performed at high temperatures provide more accurate baselines for SPV measurements within reasonable amounts

of time (< 1 day). This is due to the exponential temperature dependence of the rate at which electrons flow over the near surface barrier. As a consequence, we have found that sample heating is required to completely restore surface band bending, within 24 h, for samples with Φ_0 of 1 eV or higher. The thermionic model accurately predicts the rate at which the SPV restored; however, it is important to note that the SPV did not completely restore as fast as the thermionic model predicts (milliseconds compared to 3 h). This is mainly due to the delay time, τ, being orders of magnitude larger than expected.

5.7 Band bending in n-type GaN

The band bending in a Si-doped n-type GaN was calculated using two separate methods, one involving the samples response to illumination (shown in the previous sections), and the other involving the value of the contact potential in darkness.

Assuming that Φ_0 may be different at different temperatures, we repeated the fitting of the data shown in Figure 33 with Eq. (4.20a) in which Φ_0 was a fitting parameter at each temperature. The obtained values of Φ_0 range from 1.06 ± 0.03 eV with a possible systematic error of up to ±0.2 eV (due to possible error in the values of s_n, taken as 10^5 cm/s) over the temperature range from 295 to 500 K (see Figure 35).

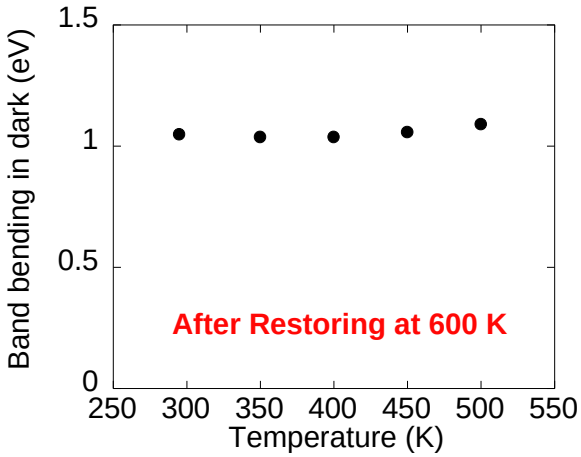

Figure 35 Estimated values of band bending in dark using the best fits of the data in with Eq. (4.20a). T = 295, 350, 400, 450, and 500 K using $E_c - F$ = 0.076, 0.088, 0.099, 0.0112, and 0.124 eV calculated from Eqs. (4.25a) and (4.29a), respectively. Sample 2015_HN.

The band bending was also estimated using the dark CPD signal. The values of the CPD varied from 0.36 to 0.52 eV at temperatures between 295 – 500 K using Eq. (4.25a). The work function of the probe was estimated using two methods: from values reported in the literature and from measuring the CPD of an Au-foil. Using these methods, the work function of the steel probe has the following values: 3.8 and 4.8 eV. The band bending in dark calculated using these work functions is shown in the following table.

Table VIII: Band bending calculated for n-type GaN using the dark CPD signal for sample 2015_HN.

Temperature (K)	*qCPD* (eV)	E_C-F (eV)	Φ_0 if ϕ_M =3.8 (eV)	Φ_0 if ϕ_M =4.8 (eV)
295	0.516	0.076	0.008	1.008
350	0.536	0.088	-0.024	0.976
400	0.436	0.099	0.065	1.065
450	0.278	0.112	0.2	1.2
500	0.360	0.124	0.116	1.116

The estimates of band bending using the work function calculated from the measurement of an Au foil may provide the more accurate values of band bending, because they are consistent with the values obtained from the response to illumination (Φ_0 = 1.06±0.03 eV)

In conclusion, the band bending in the n-type Si-doped sample was measured to be about 1.0 – 1.1 eV at temperatures between 295 – 500 K using a thermionic model and about 0.98 – 1.1 eV using the dark CPD values calibrated relative to an Au foil. This method involving R_0 is assumed to be more accurate than the method which involves the CPD signal in dark because it relies on the samples response to illumination. Figure 36 shows the estimated band bending using both methods.

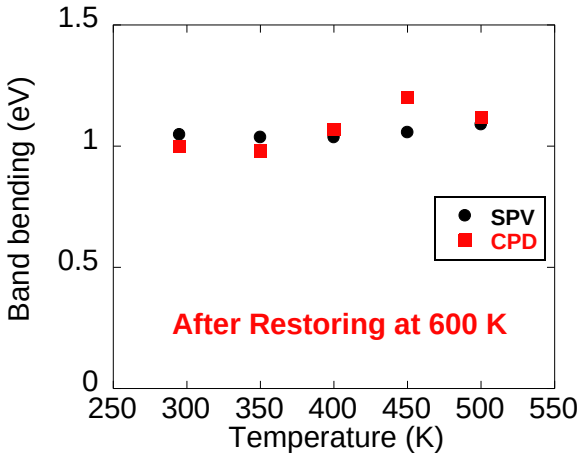

Figure 36 Estimated values of band bending using R_0 values from intensity-dependent SPV measurements and the dark CPD at various temperatures. ϕ_m = 4.8 eV and sample 2015_HN.

These values are in agreement with the literature and show the versatility of the SPV technique and the Kelvin probe method to measure the near-surface band bending.

Chapter 6: SPV Behavior in Polar GaN (0001 and $000\bar{1}$)

In this Chapter we will analyze the SPV behavior from bulk, undoped n-type GaN templates grown by HVPE at Kyma Technologies Inc. In particular, the effects of surface treatment [chemical mechanical polish (CMP) and mechanical polish (MP)] and polarity (Ga- and N-polar) are explored.

6.1 Steady-State SPV Behavior

To test the reactivity of the polar surfaces to oxygen, the surfaces of the as-received GaN templates and HCl-cleaned templates were exposed to UV illumination in oxygen ambient. The steady-state SPV behavior in pure oxygen gas (99.999%) for both the Ga- and N-polar CMP treated GaN surfaces is shown in Figure 37.

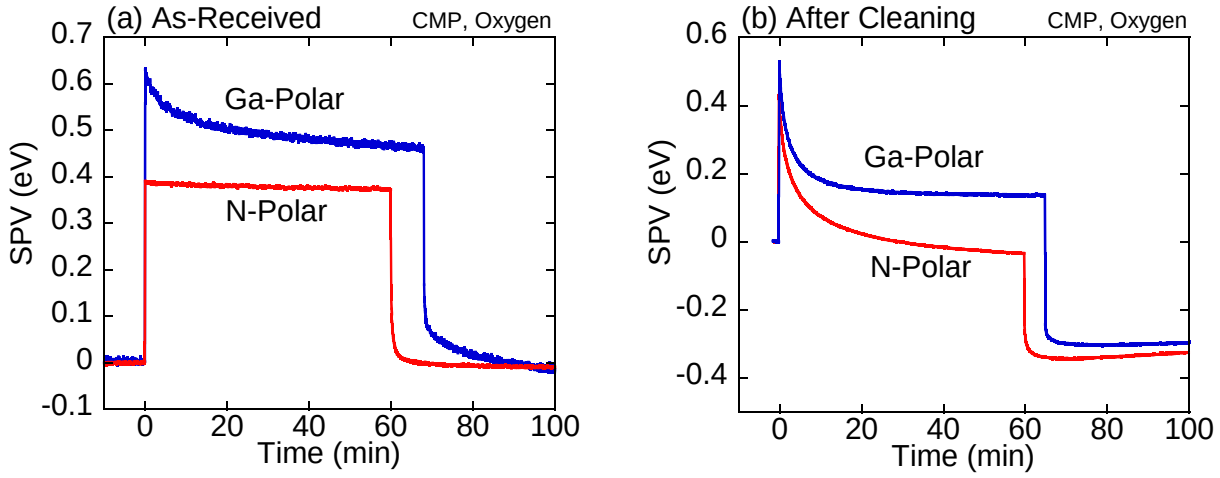

Figure 37 Time dependence of the SPV in oxygen for bulk CMP-treated GaN using the front-side illumination geometry with band-to-band excitation (325 nm, 40 mW/cm^2) for (a) as-received, GaN sample 1305 and (b) GaN samples 1412-3 and 1412-4 after HCl cleaning. UV illumination begins at t = 0 min and stops after 60 min for the N-polar and 65-70 min for the Ga-polar surface.

When illumination begins for the as-received samples (Figure 37a), both the Ga- and N-polar surfaces exhibit an immediate rise in the SPV of about 0.6 and 0.4 eV, respectively. This fast rise corresponds to the accumulation of photo-generated holes reaching the surface (fast internal mechanism). After this initial rise, the SPV signal for the Ga-polar surface decreases by about 0.1 eV over the 1 h illumination. This decrease in the SPV signal during illumination corresponds to the photo-induced adsorption of negatively charged oxygen species (slow external mechanism), which agrees with previous reports. In contrast, the as-received N-polar surface exhibits a constant SPV value during continuous illumination, suggesting the presence of a thick oxide layer which does not facilitate electron transfer or indicating that oxygen is not efficiently adsorbed onto the N-polar surface. From the measurement of the as-received surfaces, it appears that the Ga-polar surface is more prone to the photo-induced adsorption of oxygen species.

To determine if the presence of a thick oxide layer was responsible for the behavior of the N-polar surface observed in Figure 37(a), a similar sample (1412_4) was cleaned with HCl to temporarily remove any native oxide layer. After the cleaning procedure, the sample was loaded into the cryostat with pure oxygen gas and was ready for measurements within 20 min. As expected, when illumination begins, both the Ga- and N-polar surfaces again exhibit an immediate rise in the SPV of about 0.6 and 0.4 eV, respectively. After this initial rise however, the SPV signal substantially decreases by about 0.39 and 0.46 eV for the Ga- and N-polar surfaces during the 1 h illumination, respectively (Figure 37b). From this experiment, we conclude that both Ga- and N-polar surfaces become very susceptible to the photo-induced adsorption of oxygen species after the HCl cleaning both, with the N-polar surface being more susceptible to this process. This result is in agreement with a report from Scheffler *et al.*,[80] who

used density functional theory to predict which surface should be more reactive. They attributed the reactivity of the N-polar surface to the difference in the number of dangling bonds as compared to the Ga-polar surfaces.

In vacuum we expect the slow external mechanism to shift from photo-induced adsorption to desorption. There were no significant differences in the SPV behavior for Ga- and N-polar surfaces under band to band illumination in vacuum. Figure 38 illustrates the effect of continuous illumination in vacuum on the CPD behavior for the as-received, CMP-treated N-polar surface.

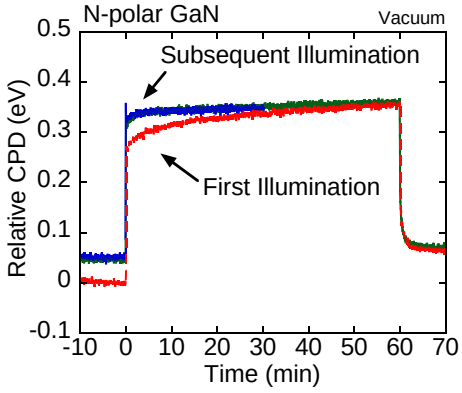

Figure 38 Time dependence of the SPV in vacuum for the N-polar surface of as-received CMP-treated, GaN sample 1305, using front-side illumination with band-to-band excitation (325 nm, 40 mW/cm^2). UV exposure lasts for 1 h, and the sample was kept in dark for 1 h before subsequent illumination.

In this experiment, the sample was first illuminated for 1 h, and then kept in dark for 1 h before being subsequently illuminated for an additional hour. During the initial exposure, the CPD immediately rises to about 0.3 eV and continues to increase by about 0.1 eV over 1 h. This increase in the CPD signal during continuous UV illumination in vacuum is attributed to the photo-induced desorption of negatively charged species. After illumination is ceased and the sample is stored in dark for 1 h, the CPD signal restores to about 0.1 eV higher than the dark

baseline. Note that this value is equal to the amount by which the CPD increased under continuous UV illumination. After the CPD appeared to be fully restored, the sample is then subsequently illuminated for an additional hour to observe the transient behavior of the CPD signal during a second illumination. During the subsequent UV illumination, the CPD signal immediately rises to 0.4 eV, and increases only slightly over 1h (< 0.03 eV). These measurements demonstrate that once negatively charged species are desorbed in vacuum, they are not immediately re-adsorbed when illumination ceases. However, if the sample is illuminated after remaining in dark for several hours, then photo-induced adsorption is again observed. The same type of experiments have been performed on Ga-polar samples, although they are not as beneficial, since the time required for the band bending to fully restore is comparable to the time required for the photo-induced desorbed species to re-adsorb.

6.2 Intensity-Dependent SPV Behavior

The dependence of the steady-state SPV signal on excitation intensity is shown in Figure 39 for all the CMP-treated Ga- and N-polar surfaces.

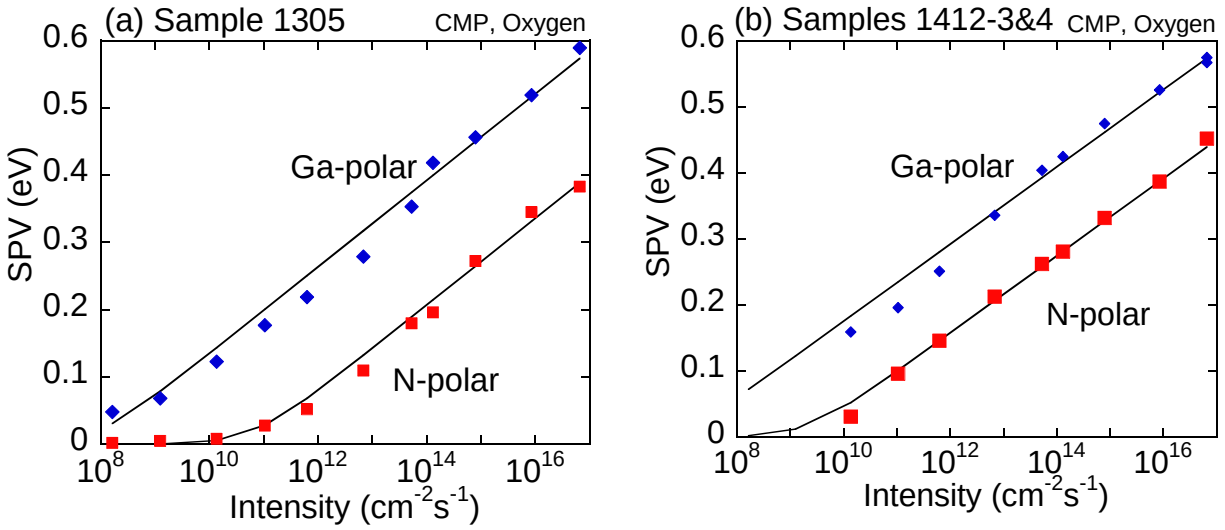

Figure 39 Intensity dependence of the SPV in oxygen for CMP-treated GaN using front-side illumination (325 nm, 40 mW/cm^2). (a) Two faces of sample 1305 and (b) CMP-treated, Ga- and N-polar surfaces of samples 1412-3 and 1412-4, respectively. Solid lines are fits using Eq. (4.20a) with $\eta = 1.1$, $c = 0.99$ and $R_0 = 8\times10^7$ cm^{-2}s^{-1} (Ga-polar) and 6×10^{10} cm^{-2}s^{-1} (N-polar) for (a) and $\eta = 1.0$, $c = 0.99$ and $R_0 = 1\times10^7$ cm^{-2}s^{-1} (Ga-polar) and 2×10^9 cm^{-2}s^{-1} (N-polar) for (b).

In this set of experiments, the UV exposure times are limited to reduce the amount of photo-induced adsorption. At the highest excitation intensity, the SPV signals for the CMP-treated Ga- and N-polar surfaces are about 0.6 and 0.4 eV, respectively. This indicates that the N-polar surface may have smaller band bending. As expected, the SPV data for both the Ga- and N-polar surfaces exhibit a logarithmic behavior as a function of excitation intensity. Using Eq. (4.20a) to fit the SPV intensity-dependent measurements, we estimate that values of R_0 are 10^7 and 10^{10} cm^{-2}s^{-1} for the Ga- and N-polar surfaces, respectively. In these fits, $c = 0.99$ (depletion region width ~550 nm) and $\eta = 1.1$. Using the R_0 values from the fits of the intensity-dependence data with Eq. (4.20a), as well as taking $s_n = 10^5$ cm/s, $N_C = 2\times10^{18}$ cm^3 and $(E_C - F) = 0.16$ eV, we estimate from Eq. (4.22a) that the band bending for the Ga- and N-polar surfaces is 0.74 eV and 0.57eV, respectively. If we assume that the uncertainty in the value of s_n is within the range of 10^3 – 10^7 cm/s, then the error in Φ_0 is about ±0.2 eV. The band bending estimates are in agreement

with the steady-state SPV values, indicating that the band bending is no less than 0.6 and 0.4 eV for Ga- and N-polar GaN surfaces, respectively. If the surface electron recombination velocity is the same for both surfaces, then the band bending for the CMP-treated, N-polar surface is smaller than for the Ga-polar surface. In a report by Jones *et al*.,[81] the band bending of Ga- and N-polar surfaces grown by MBE was measured with SKPM using the dark CPD values. The difference in band bending between the Ga- and N-polar surfaces was measured to be approximately 0.05 eV, with the Ga-polar surface having the larger band bending. They reported that these values may be due to strain within the crystal, but it is possible that the surface oxide affects the measured surface potential values as well. Also, mixed polarity at the surface might have been present for the MBE-grown layers.

The indium contacts on the MP-treated surfaces were highly resistive. This made taking data with the Kelvin probe setup extremely difficult, and we believed to observe downward and upward offsets of the SPV signal on the MP-treated surface (Ga-polar) of sample 1412_4 when the sample was illuminated with band to band light. Data of the MP-treated surface of sample 1412_3 could be obtained because ohmic contacts could be applied to the CMP-treated Ga-polar surface.

6.3 Below-Bandgap SPV and Photoluminescence Behavior

The SPV generated from below-bandgap light arises from electrons that are excited from surface states over the near-surface barrier into the bulk. This emission of electrons from the surface states to the bulk decreases the net negative charge at the surface, and consequently

decreases the band bending. The SPV spectral response measured for both the MP- and CMP-treated, Ga- and N-polar surfaces is shown in Figure 40.

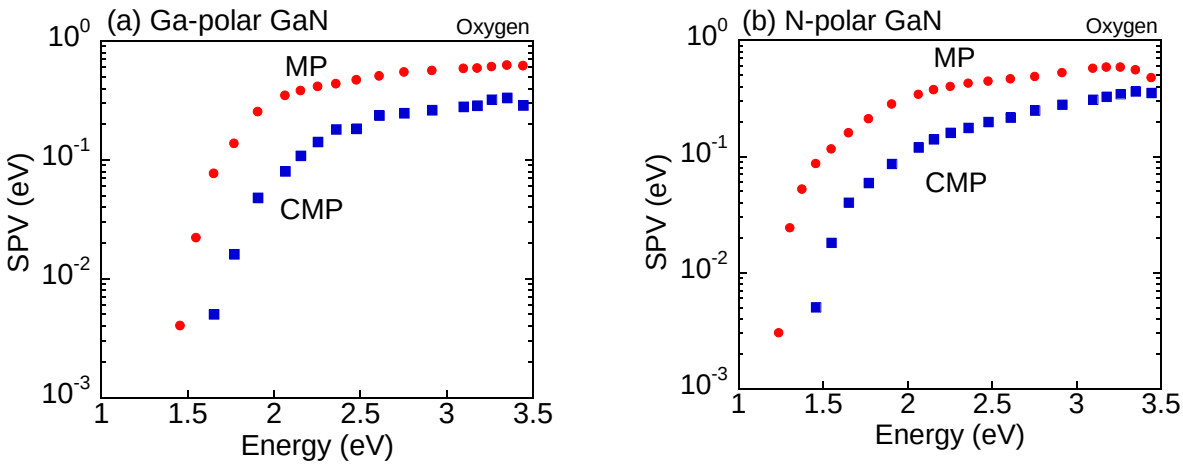

Figure 40 Steady-state SPV spectra in oxygen for (a) Ga-polar and (b) N-polar GaN samples 1412-3 and 1412-4 using backside illumination (30 mW/cm^2). Both spectra for MP-treated surfaces show larger SPV values than for CMP-treated surfaces for all photon energies used. Threshold voltages for the CMP-treated, polar surfaces are about 1.5 eV (Ga face) and 1.3 eV (N face).

The magnitude of the SPV signal from below-bandgap excitation is proportional to the density of charged surface states. The amount of photons absorbed at surface states is predicted by:

$$P_S = \sigma^S{}_{ph} N_s^{\bullet} P_0 \exp(-\alpha D) \tag{6.1}$$

where $\sigma^S{}_{ph}(\hbar\omega)$ is the optical cross-section of the surface states for photons of a given energy, $N_s^{\bullet}$ is the density of occupied surface states, and $\alpha(\hbar\omega)$ is the absorption coefficient for photons of a given energy. From the below-bandgap behavior, it appears that density of negatively charged surface states appears to be larger for both the MP-treated GaN surfaces. It is possible that a continuous distribution of the surface states, rather than a single state, is formed after the MP treatment. In this case, the smaller threshold voltage for the MP-treated surfaces can be explained by a larger number and wider energy distribution of the surface states. Reliable,

quantitative information about the band bending cannot be acquired from these measurements; however, it may be used to qualitatively compare the band bending in these samples.

The room-temperature photoluminescence (PL) spectra from the CMP- and MP-treated, Ga- and N-polar surfaces are shown in Figure 41.

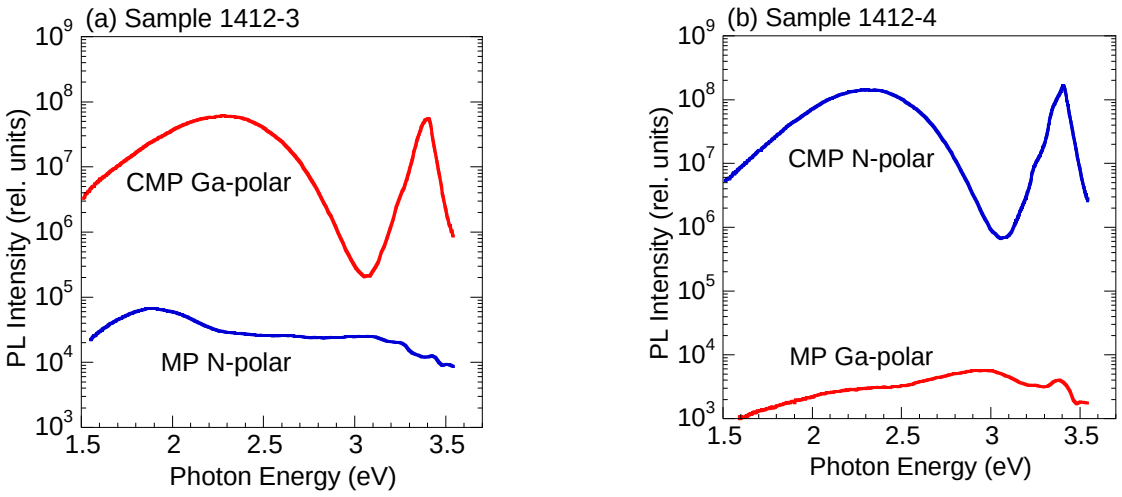

Figure 41 PL spectra at room temperature from GaN samples (a) 1412-3 and (b) 1412-4. Independent of surface polarity, PL from MP-treated surfaces is orders of magnitude weaker than that from CMP-treated surfaces. P_0 = 0.3 W/cm^2.

As is clearly shown, the PL intensity from the CMP-treated surfaces is several orders of magnitude higher than that of the MP-treated surfaces, for both polarities. In addition to the near-bandedge emission peak at 3.406 eV, the PL spectrum for the CMP-treated surfaces contains a broad, yellow-green band with a maximum at about 2.3 eV, which presumably has the same origin as the yellow-green band in previously studied freestanding GaN templates grown by the HVPE technique.[82] The quantum efficiency of PL at room temperature is estimated to be 0.6 and 1.3% for the CMP-treated, Ga- and N-polar surfaces, respectively. In sharp contrast, the quantum efficiency for the MP-treated surfaces is much lower – on the order of 10^{-5}%. This low quantum

efficiency could potentially be due to the presence of a large number of point and extended defects.

The low-temperature PL spectra from the Ga- and N-polar surfaces after CMP treatment contain sharp, excitonic lines at photon energies above 3.2 eV, as well as a yellow-green and a new, red, defect-related band (Figure 42).

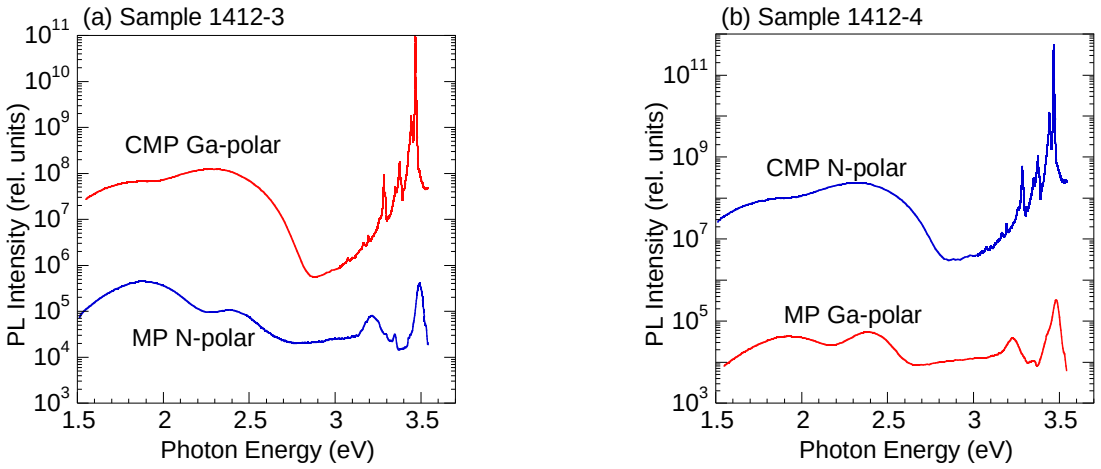

Figure 42 PL spectra at T = 15 K from GaN samples (a) 1412-3 and (b)1412-4. Again, PL from MP-treated surfaces is orders of magnitude weaker than that from CMP-treated surfaces. P_0 = 0.3 W/cm^2.

The red band has a maximum at 1.8 eV and saturates at relatively low excitation intensities, which is seen as a shoulder to the yellow-green band at P_0 = 0.3 W/cm^2 (Figure 42). The quantum efficiency of PL at 15 K is 6% and 28% for the CMP-treated, Ga- and N-polar surfaces, respectively. Again, the PL intensity from the MP-treated surfaces is several orders of magnitude weaker with a quantum efficiency of 5×10^{-4}% and 3×10^{-3}% for the Ga- and N-polar surfaces, respectively. Two defect-related bands could be identified from the low-temperature PL spectrum from the MP-treated surfaces: a red and green band at 1.9 eV and 2.4 eV, respectively. From the shape, position and temperature dependent behavior of these bands, they appear to

originate from the same defects as the RL2 and GL2 bands in high-resistivity Ga-rich GaN grown by the MBE technique.[83]

The large width of the excitonic band and extremely low quantum efficiency from MP surfaces indicates low crystalline quality near the surface and that a large number of defects act as centers of non-radiative recombination. This highly defective region penetrates at least 0.5-1 μm into the bulk, as estimated by the researches at Kyma Technologies. Thus, we may expect a high density of defect states not only at the surface, as shown from the SPV spectral measurements, but also in the depletion region. These defect states may facilitate the transfer of electrons from the bulk to the surface via a hopping mechanism. Based on the PL results, we cannot exclude the possibility that these defect states in the depletion region could contribute to the SPV signal in the case of below-bandgap excitation. The defect states created by the MP treatment may also affect the behavior of the SPV in other measurements. Further investigations are under way to measure the width of this defective region and understand how the defective region affects the electrical and optical properties of a GaN template.

6.4 Restoration of the SPV Behavior

When illumination of the samples is ceased, the band bending is expected to logarithmically restore to its dark value with a rate proportional to temperature. Equation (4.22a) predicts that the SPV should restore logarithmically in time with a rate that is proportional to kT after the delay time τ. The restoration of the SPV in the CMP-treated, Ga-polar and N-polar surfaces is plotted in Figure 43 and is fit by Eq. (4.21a).

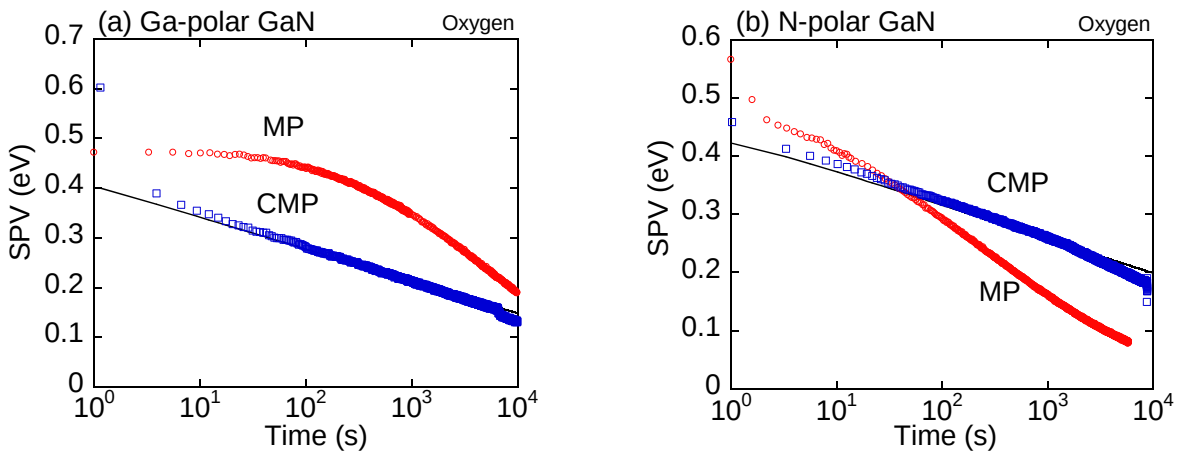

Figure 43 SPV restoration in oxygen for MP- and CMP-treated, surfaces of samples 1412-3 and 1412-4 after short (3 s) exposure times for (a) Ga-polar and (b) N-polar bulk GaN. Solid lines are calculated with Eq. (4.22a) using $\eta = 1.1$, $\tau = 0.1$ s and $y_0 = 0.47$ eV for Ga-polar, and $\eta = 1$, $\tau = 0.1$ s and $y_0 = 0.46$ eV for N-polar surfaces.

The SPVs from the CMP- and MP-treated surfaces restore with a logarithmic time dependence, but with different rates even though they are both kept at 295 K. The restorations of the SPV from the CMP-treated surfaces are fit by Eq. (4.21a) and restore with a rate predicted by the thermionic model. In these fits, the parameter τ was not explicitly calculated and a value of 0.1 s was estimated. The SPVs from the MP-treated surfaces, however, restore with rates that are faster than predicted. The MP-treated, Ga-polar surface SPV exhibits a longer-than-expected delay time, and restores with a rate faster than kT. This surface needs further investigation; however, the poor quality of the contacts make SPV measurements difficult using the Kelvin probe setup. The MP-treated, N-polar surface begins to restore after a short delay time, but with a rate twice as fast as predicted. Differences in the restoration rates between the CMP- and MP-treated surfaces are most likely due to surface or near-surface conditions. The MP-treated surfaces apparently contain a higher density of surface or near-surface defects, which may

facilitate electron hopping between defects toward the surface, thereby increasing the restoration rate.

To examine the temperature dependence of the SPV restoration for both surface treatments, the sample temperature was increased to 425 K. The restoration of the SPV in vacuum from the CMP- and MP-treated, N-polar surfaces at 295 and 425 K are shown in Figure 44.

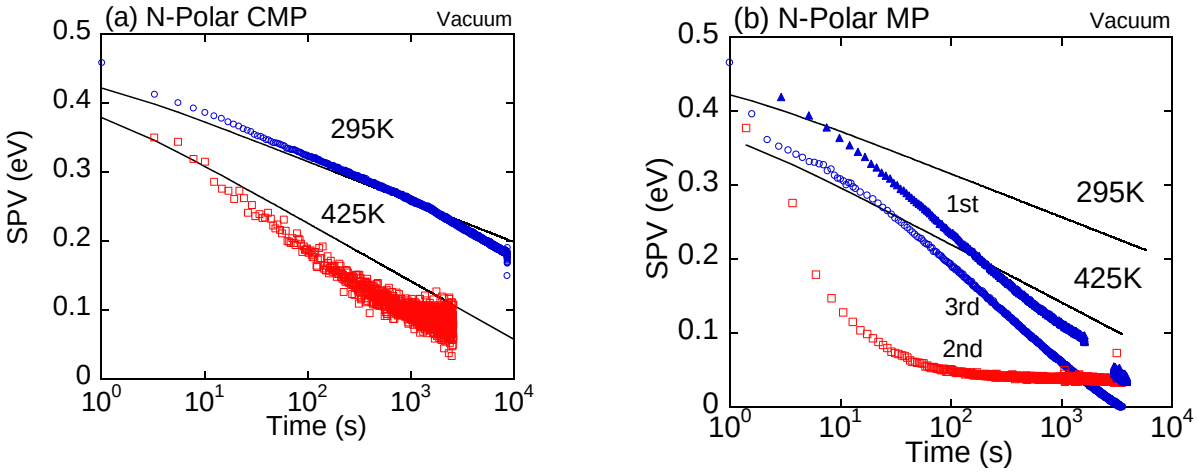

Figure 44 SPV restoration in vacuum for N-polar surfaces of 1412-3 and 1412-4 after short (3 s) UV exposure. (a) CMP-treated surface (sample 1412-4) and (b) MP-treated surface (sample 1412-3). The measurement in (b) was taken in the following order: first, the sample was illuminated for 3 s at 295 K and allowed to restore; second, the sample was heated to 425 K, illuminated for 3 s, and allowed to restore at 425 before being cooled quickly to 295 K; and third, then the sample was illuminated for 3 s at 295 K and allowed to restore. Solid lines are calculated with Eq. (4.22a) using $\eta = 1$, $\tau = 0.1$ s and the following values of $y_0 =$ 0.42 eV (at 295 K) and 0.38 eV (at 425 K).

For the CMP-treated surface at 295 and 425 K, the SPV appears to restore with a rate predicted by the thermionic model. For the MP-treated surface, however, the restoration rate is twice as fast as predicted at 295 K and about 3-4 times faster at 425 K. The complete restoration of the SPV occurs in only about 300 s at 425 K, as opposed to about 30,000 s at 295 K. An experiment was performed after the SPV completely restored at 425 K, where the sample was quickly cooled

back to 295 K. A subsequent SPV was generated and the restoration of the SPV was measured at 295 K. This restoration took about 30,000 s, the same amount of time as the original run at 295 K.

A possible explanation for the faster than predicted restoration rates of the MP-treated surfaces may be due to electron transfer from the bulk to the surface via a highly defective depletion region (via a hopping mechanism). In this mechanism, electrons from the bulk hop between defect states before being captured by a surface state. This is an alternative means of restoring band bending in dark, as opposed to electrons overcoming the near surface barrier, as predicted by a thermionic model. The movement of electrons between these defect states would have a high probability if the defect density in the depletion region and bulk is very high, as is predicted from PL measurements for MP-treated surfaces. This relatively fast transfer of electrons via defect states would be independent of the near-surface barrier height and would have a strong dependence on temperature. This could explain why the SPV restoration rate increases with increasing temperature, but not proportionally to kT. The results from temperature-dependent SPV restoration measurements and the dramatic reduction of PL intensity from MP-treated GaN indicate that surface treatment plays an enormous role in the electrical and optical properties of bulk GaN.

6.5 Calculation of Band Bending Using the SPV, CPD, and XPS Measurements

When comparing the steady-state, intensity-dependent SPV behavior from the chemically mechanically polished Ga- and N-polar surfaces of the same sample, we have established that the band bending from the Ga-polar surface is approximately 0.2 eV larger than that the band bending of the N-polar surface. The estimated band bending values are 0.74 and 0.57 eV for the Ga- and N-polar surfaces, respectively.

Again, the band bending can be calculated using the dark CPD. There was no discernable difference in the surface potentials between the two polarities. The CPD signals in darkness were about ~0.35 eV for both the Ga- and N-polar samples, which provide an estimate of the band bending in dark to be about 1.09 eV.

$$\Phi_0 = 4.8 - 3.2 - 0.16 - 0.35 = 1.09\,eV$$

The values of band bending calculated from the CPD signal are larger than the values predicted by the thermionic model (0.74 and 0.57 eV for Ga- and N-polar, respectively), and may be due to the error associated with measuring the band bending using the CPD signal.

Using the position of the Ga_{3d} peak from XPS measurements of samples 1305 (Figure 45), the band bending appears to be 0.3 and 0.4 eV for the Ga- and N-polar GaN samples.

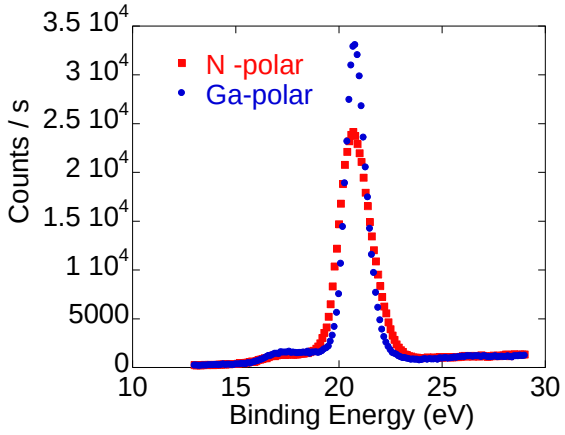

Figure 45 XPS spectra of the Ga_{3d} peak for Ga and N-polar GaN. MgKα source.

The measured peak positions for the Ga_{3d} peak were 20.7 and 20.8 eV for N- and Ga-polar GaN, respectively. The band bending was calculated as

$$\Phi_0 = +E_{Ga3d} + E_{Gap} - (E_{Fbulk}) - Peak\ Position$$
$$\Phi_0 = +17.8 + 3.4 - (0.2) - Peak\ Position$$
$$\Phi_0 = 0.3\,\text{eV (Ga-polar) and } 0.4\,\text{eV (N-polar)}$$

This method of estimating band bending is most likely the least accurate since X-rays generate a SPV which decreases the band bending. In these experiments, we measured the positions of the Ga_{3d} and C_{1s} peaks while changing various experimental parameters. The peaks were measured in dark, under illumination, with no flood-gun (charge compensation), and with the flood-gun. The results of these experiments showed that the position of the Ga_{3d} peak changed no more than 0.05 eV between measurements. However, there was a much larger change in the position of the C_{1s} peak of about 0.2 eV between measurements. It is interesting to note that the two peaks did not shift together, as predicted by the method to calculate band bending.

Chapter 7: SPV Behavior in p-type GaN

In this Chapter we will analyze the SPV behavior from Mg-doped p-type GaN samples grown by HVPE, MBE and MOCVD techniques.

7.1 Transient SPV Behavior

In p-type GaN, downward band bending is caused by excess positive charge at the surface, see Figure 19. The SPV is expected to become more negative for p-type GaN due to electrons reaching to the surface under illumination. The SPV behavior for front-side, band-to-band illumination of HVPE-grown p-type GaN in vacuum and oxygen is shown in Figure 46.

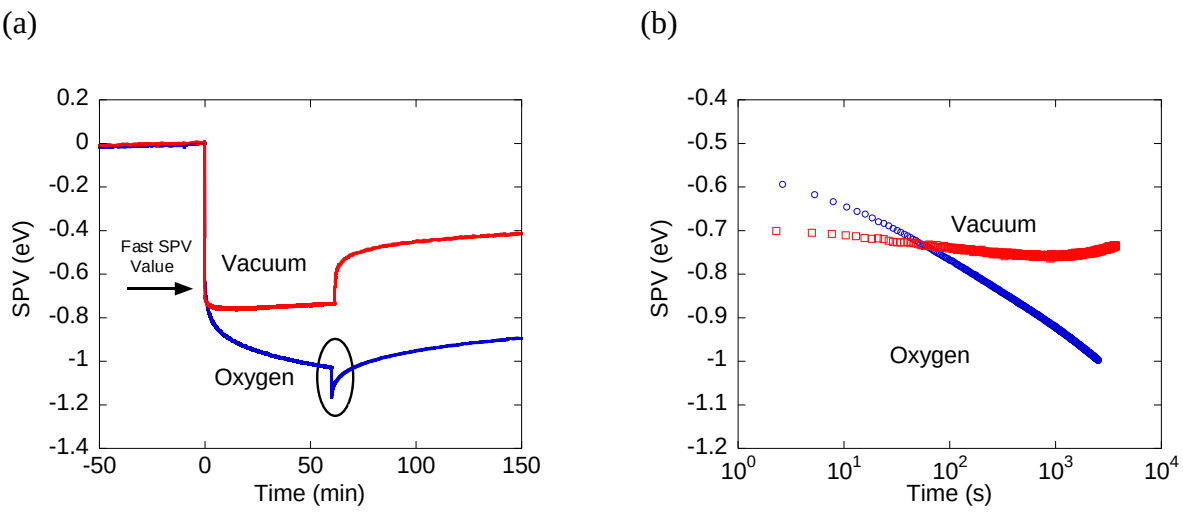

Figure 46 (a) Time dependence of the SPV in air and vacuum for p-type GaN, using front-side illumination with band-to-band excitation (325 nm, 40 mW/cm^2). UV illumination begins at t = 0 and stops after 60 min. (b) SPV transients in a logarithmic scale. Sample 863_HP.

As expected, when illumination begins, the SPV signal quickly reaches a negative value. If the sample is continuously illuminated for longer than 3 s, however, then the SPV can slowly change

as a function of the ambient conditions. In an oxygen environment, the SPV signal continues to become more negative and reaches −1.1 eV after 1 h illumination. This slow decrease can be explained by the photo-induced adsorption of negatively charged oxygen species. Unlike for n-type GaN, the SPV decrease during illumination apparently does not depend on the amount of prior UV-exposure the sample has received. It should be noted that when illumination ceases after one hour, an anomalous downward offset occurs, as indicated by the circled region. This unexpected offset behavior appears to be caused by accidental illumination of the contacts and will be discussed in Chap. 7.5. In a vacuum environment, the SPV signal becomes just slightly more negative during the first 10 min. of illumination, and then becomes slightly more positive. It therefore appears that p-type GaN is not very sensitive to photo-induced processes in vacuum. The steady-state SPV can be seen in more detail in Figure 46b, where the SPV is plotted as a function of time on a logarithmic scale. It appears that the decrease in the SPV signal generated in an oxygen environment does not saturation after 1 h. In vacuum, the SPV decreased slightly for the first 1000 s, then began to increase for the remainder of the illumination.

7.2 Intensity-Dependent SPV Behavior

The dependence of the SPV signal on excitation intensity for p-type GaN grown by HVPE is shown in Figure 47 using front-side illumination. The SPV data are plotted vs. the product cP_0, where c is a geometrical factor and P_0 is excitation intensity. This product is used to estimate the density of electron-hole pairs created in the depletion region during illumination.

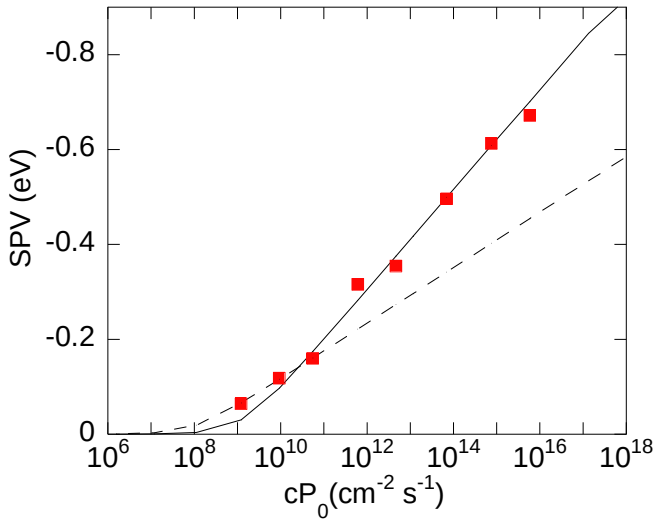

Figure 47 Intensity dependence of the SPV for p-type GaN in vacuum using front-side illumination (325 nm, 40 mW/cm^2, c = 0.134). Solid and dashed lines are fits using Eq. (4.20b) with the following parameters: $R_0 = 10^8$ cm^{-2}s^{-1}, $\eta = 1$ (dashed curve); and $R_0 = 10^9$ cm^{-2}s^{-1}, $\eta = 1.8$ (solid curve). Sample 863_HP.

A fit with $\eta = 1$ is shown in Figure 47 with a dashed line, with a value of $R_0 \sim 10^8$ cm^{-2}s^{-1}. The p-type intensity-dependent data can be described correctly by the thermionic model only at low illumination intensities. The solid line in Figure 47 is a better fit to the data and uses the parameters $R_0 = 10^9$ cm^{-2}s^{-1} and $\eta = 1.8$ (solid curve). Such large values of η are unreasonable and further work needs to be performed to clarify this issue. Also, the data at low intensities could fit the model by coincidence, if the SPV has not been allowed to saturate at these low intensities.

The value of the band bending in dark, Φ_0, can be estimated by using the R_0 values obtained from fitting the intensity data with Eq. (4.20b). We estimate that the band bending in the sample is $\Phi_0 \approx -(0.8 \pm 0.2)$ eV, using values of $R_0 = 10^8 - 10^9$ cm^{-2}s^{-1}, $s_p = 10^5$ cm/s (in the range of 10^3–10^7 cm/s), $N_V \approx 2\times10^{19}$ cm^{-3}, and $E_V - F = -0.15$ eV.

7.3 Below-Bandgap SPV Behavior

As shown in Figure 48, the SPV spectrum has a threshold photon energy of about 2 eV, and a maximum SPV of about –0.7 eV at a photon energy of 3.4 eV. This threshold is about 0.5 eV larger than the one observed for n-type GaN. The threshold photon energies for n- and p-type GaN of about 1.5 eV and 2.0 eV, respectively, are consistent with a single surface state located 1.3 to 1.5 eV below the conduction band.

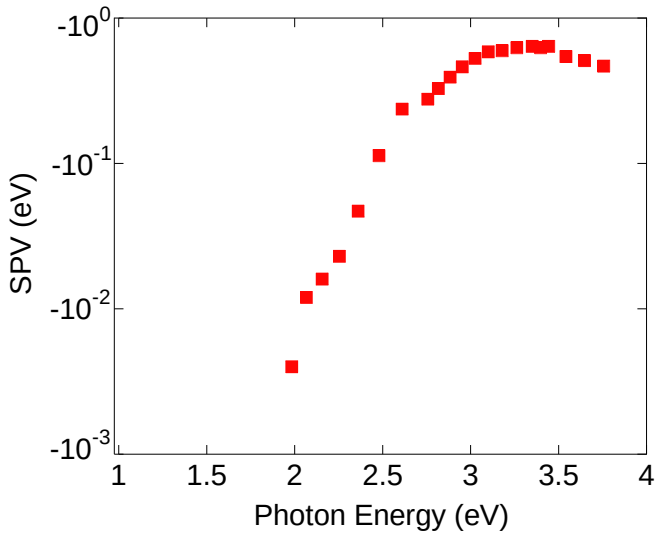

Figure 48 Steady-state SPV spectra for p-type GaN in air using backside illumination (30 mW/cm^2). The spectrum shows a maximum SPV value at a photon energy of about 3.4 eV. The threshold voltage for the p-type GaN sample is about 2.0 eV. Sample 863_HP.

7.4 Restoration of the SPV

After illumination ceases, it is expected that the SPV decays logarithmically to zero. Figure 49 shows the SPV restoration in both air and vacuum after short (3 s) and long (1 h) illumination times.

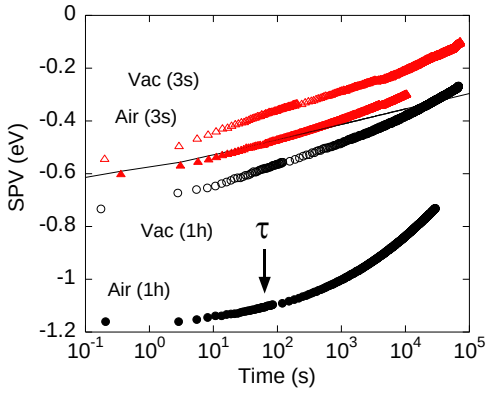

Figure 49 Restorations of the SPV in air and vacuum after short (3 s) or long (1 h) exposure times for p-type GaN. Solid line is calculated with Eq. (4.21b) with $\eta = 1$, $y_0 = -0.67$ eV, $\tau = 40$ ms. Sample 863_HP.

From Figure 49 it appears that even with short illumination of the GaN surface, the SPV in p-type GaN restores slightly faster than predicted by a thermionic model. This again may be attributed to a large number of defects near the surface for p-type GaN films. The η values for the short exposures are about 1.2 – 1.4, which are smaller than the values measured for the MP-treated bulk GaN templates (~2).

The SPV restorations have similar rates with short time delays (~40 ms), except for the case of a long illumination in air. The photo-induced adsorption of surface species for long illumination in air results in a significantly more negative SPV, which then demonstrates a long delay time of $\tau = 200$ s before restoring with a slope greater than kT. As with n-type GaN, when p-type GaN is exposed to UV-illumination in air, this appears to increase the SPV magnitude by at least 0.2 eV. This increase in the SPV then causes the restoration behavior to have a significantly longer time delay time followed by a faster restoration rate than predicted by our phenomenological model. Overall, however, the SPV restoration behavior is well-predicted by the model for p-type GaN in the case of short illumination times, as well as for longer times where photo-induced processes do not significantly change the steady-state SPV value.

7.5 Anomalous Behavior of the SPV Signal

The SPV transients for p-type GaN can exhibit anomalous offsets which shift the measured SPV signal in an opposite direction to the real SPV signal due to electrons reaching the surface. This offsetting behavior for the p-type sample in both front and back illumination geometries is shown in Figure 50.

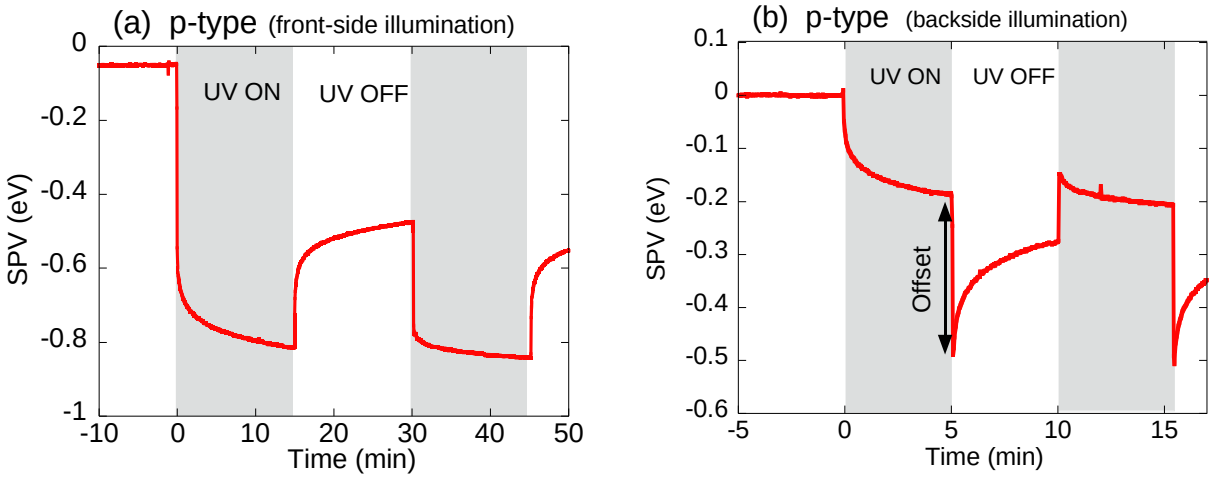

Figure 50 Evolution of the SPV signal with UV light being turned on and off. (a) SPV data for front-side illumination with no exposure of the contacts to laser light and no anomalous behavior. (b) SPV data for backside illumination where the contacts are indirectly exposed to light, resulting in anomalous offsets when the light is turned on or off. Sample 863_HP.

When the sample is illuminated from the front-side without any illumination of the contacts, no offset anomalies occur in the SPV behavior [Figure 50a]. Intentional illumination of the contacts from the front-side do result in significant offset values (data not shown). When the sample is illuminated from the backside and the contacts are indirectly exposed to light, offsets are also observed. In Figure 50b, a downward offset of 0.3 eV occurs when illumination is turned off at t = 5 min, and an upward offset of 0.1 eV occurs when the light is turned on again at t = 10 min. Note that no apparent offset occurs when the light is initially turned on at t = 0 min; however, the

observed SPV value is significantly lower than expected. In this case, a large upward offset does in fact exist, but this offset is smaller than the downward SPV value, and it is the difference between these two values which is observed. One explanation for the existence of these anomalous offset values derives from our observation that such p-type samples show a conversion from p- to n-type surface conduction when performing hot-probe measurements under UV illumination. We therefore believe that this offset behavior may be related to a shift under illumination of the quasi Fermi level near the contact, which is used as the reference potential for the Kelvin probe.

7.6 Temperature-Dependent SPV Behavior

a. Intensity-Dependent Steady-State SPV behavior

Since the intensity-dependent SPV behavior at room temperature did not fit the thermionic model for p-type GaN, high temperature intensity-dependence measurements were performed. The dependences of the SPV signal on excitation intensity at different temperatures for a HVPE-grown, p-type GaN sample is shown in Figure 51. The experiments were conducted over the period of three days, while the sample was heated to 650 K (first measurement), and then cooled to 295 K (last measurement). In all cases to ensure that the band bending fully restored in darkness, the sample was annealed to 650 K before the SPV measurements.

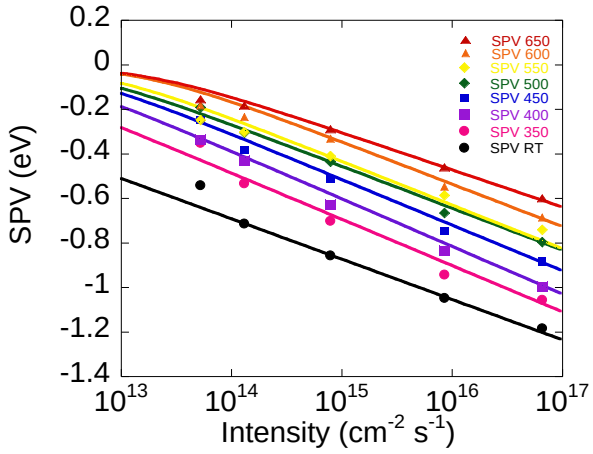

Figure 51 Intensity-dependent SPV measurements of HVPE-grown p-type GaN (863_HP) in vacuum taken at various temperatures using band-to-band UV illumination (325 nm). The solid lines are calculated using Eq. (4.20b) with the parameters: η = 3.1, 3, 2.7, 2.3, 1.9, 1.8, 1.6, and 1.3, c = 0.13 and R_0 = $2\times10^{9,}$ 6×10^{10}, 2×10^{11}, 4×10^{11}, 5×10^{11}, 8×10^{11}, 2×10^{12}, and 2×10^{12} cm^{-2} s^{-1} for T = 295, 350, 400, 450, 500, 550, 600, 650 K, respectively. Sample was pre-heated to 650 K for 1 h before measurements.

As predicted by the thermionic model, the magnitude of the SPV at any given excitation intensity decreases with increasing temperature, and the magnitude of the SPV increases logarithmically with excitation intensity for all temperatures. However, the slope of the SPV versus intensity for all of the temperatures is larger than expected (η ranges from 1.3 to 3.1 at temperatures from 650 to 295 K). The slope of the SPV intensity-dependence does begin to approach the predicted value only at T =650 K, η = 1.3.

The dependence of η on T indicates that the high resistivity in p-type GaN samples may affect the Kelvin probe SPV measurements. At higher temperatures, it is expected that the sample conductivity will greatly increase, and any negative effect due to the high resistivity of the p-type GaN samples should decrease. The increased slope could also be potentially related to the Dember potential, which is due to the different mobilities of electrons and holes in GaN.[84]

The values of R_0 calculated from the highest temperatures are probably the most reliable data, since the value of η is closest to unity.

The dependence of the steady-state SPV on light intensity for a MOCVD-grown, Mg-doped p-type GaN has also been measured and is illustrated in Figure 52. The data were taken using the same procedure as for the HVPE-grown sample.

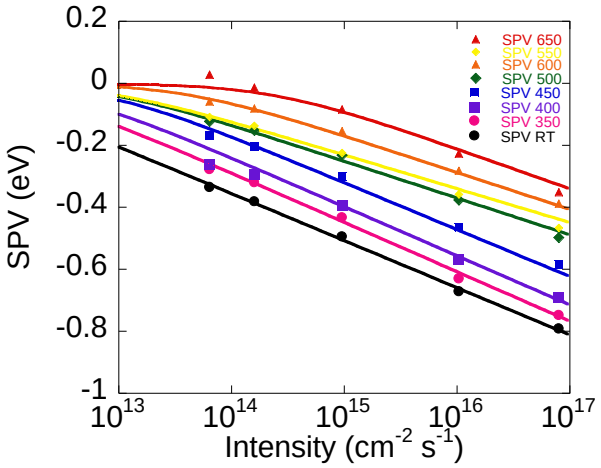

Figure 52 Intensity-dependent SPV measurements of MOCVD-grown p-type GaN (983_MP) in vacuum taken at various temperatures using band-to-band UV illumination (325 nm). The solid lines are calculated using Eq. (4.20b) with the parameters: η = 2.6, 2.3, 2.0, 1.7, 1.2, 1, 1, and 1, c = 0.13 and R_0 = 6×10^{10}, 2×10^{11}, 4×10^{11}, 1×10^{12}, 1×10^{12}, 1×10^{12}, 5×10^{12}, and 3×10^{13} cm^{-2} s^{-1} for T = 295, 350, 400, 450, 500, 550, 600, and 650 K, respectively. Sample was pre-heated to 650 K for 1 h before measurements.

We observe the same phenomena as for the HVPE-grown GaN, namely the value of η decreases from 2.6 to 1.0 as the sample temperature increases from 295 K to 650 K. This type of trend is not predicted by our thermionic model. For the intensity-dependent SPV measurements from this sample, the values of η indeed reach unity at temperatures $\geq$ 550 K. These measurements may also verify that the sample conductivity may play a large role in SPV measurements taken with

our Kelvin probe setup. When the samples are heated, the conductivity greatly increases and the effect from the high-resistivity sample in our circuit is removed.

The steady-state SPV data for a MBE-grown, Mg-doped p-type GaN sample are shown in Figure 53.

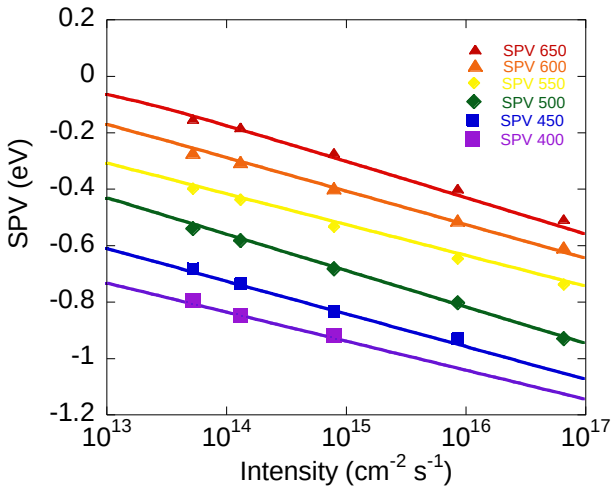

Figure 53 Intensity-dependent SPV measurements of MBE-grown p-type GaN (9591_BP) in vacuum taken at various temperatures using band-to-band UV illumination (325 nm). The solid lines are calculated using Eq. (4.20b) with the parameters: η = 1.3, 1.3, 1.3, 1, 1, and 1, c = 0.13 and R_0 = 1×10^5, 7×10^6, 6×10^8, 2×10^9, 5×10^{10}, and 6×10^{11} cm^{-2} s^{-1} for T = 400, 450, 500, 550, 600, and 650 K, respectively. Sample was pre-heated to 650 K for 1 h before measurements.

Again, we observe that the slope of the intensity-dependence does not fit the model. However, the values of η become unity when the temperature is in the range from 550 K to 650 K.

There was an additional effect observed in the MBE-grown samples: high excitation intensity at a low sample temperature (< 400 K) caused the measured "gradient" (a parameter in the Kelvin probe software) to change. The gradient is mainly proportional to the sample/probe spacing and the measured current in the system, which are both not expected to change under illumination. The high illumination intensities at low temperatures may have induced a current in

the circuit, which may negatively affect the measured CPD. This is the reason why there are fewer data points, and it was not possible to take data below 400 K on sample 9591_MB at the excitation intensities used. Other MBE-grown samples show a similar effect, but the degree to which the gradient changes at low temperature (295 to 400 K) and high excitation intensity appears to be sample dependent (9600_MB and 9599_MB). It should also be noted that the resistance across the contacts of our p-type GaN samples sometimes changed by orders of magnitude (MΩ to KΩ) due to UV-illumination.

To test if the high values of η at room temperature are related to the limitations of the Kelvin probe technique for measuring high-resistivity samples, the intensity-dependent SPV was also measured with an AFM using the SKPM mode. In this experiment, the samples were illuminated with a Hg-lamp and the intensity was varied with a set of calibrated square neutral density filters. The results from this experiment are shown in Figure 54. The light intensity was estimated by accounting for the sample/lamp geometry and then using a power meter. Fitting the intensity dependence with Eq. (4.20b) provides reasonable values of R_0 for all of the sample types. Additionally, the slope of the intensity-dependence is consistent with the thermionic model for the measurements taken with SKPM at room temperature, in contrast to Kelvin probe measurements. The reason for the larger than expected SPV at low excitation intensity (~10^{11} $cm^{-2}s^{-1}$) could be due to stray UV-light that reaches the sample surface. The stray light should not be of sufficiently high intensity to be responsible for the correct value of η, however, due to the logarithmic dependence of excitation intensity on the SPV.

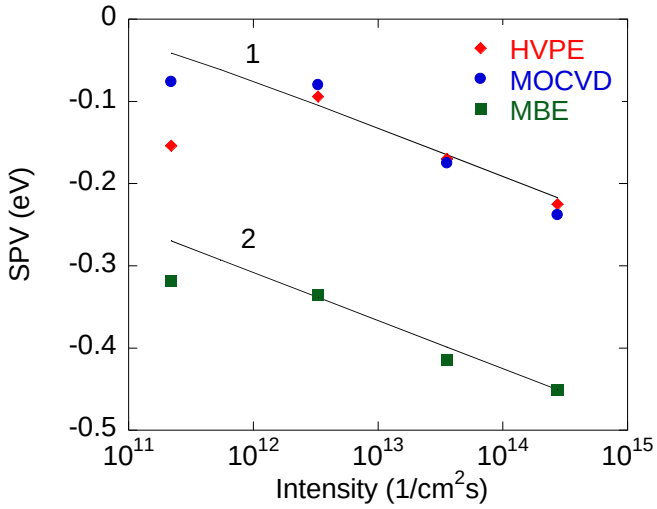

Figure 54 Intensity-dependent SPV measurements of p-type GaN samples (9591_BP, 863_HP, and 983_MP) in vacuum taken at room temperature using SKPM with band-to-band UV illumination (365 nm). The solid lines are calculated using Eq. (4.20b) with the parameters: $\eta = 1$, $c = 0.13$ and $R_0 = 7\times10^5$ (line 2) and 7×10^9 (line 1), cm^{-2} s^{-1} at $T = 295$.

The SPV data taken using the SKPM method exhibited no unusual behavior of the SPV signal; however, in these measurements we could not wait for a stable/reliable baseline in darkness. This would not change the slope of the dependences we measured, but would instead shift the SPV values. It should be noted that no anomalous offsets of the SPV were observed in these measurements, which may be due to the low excitation intensity or that the Fermi-level is not used in the measurement of the CPD.

The time-dependent SPV at 500 K was studied in a MBE-grown sample with our Kelvin probe setup. The SPV behavior under continuous illumination were measured at 100%, 1% and 0.01% of the full excitation intensity for 1 h and are shown in Figure 55.

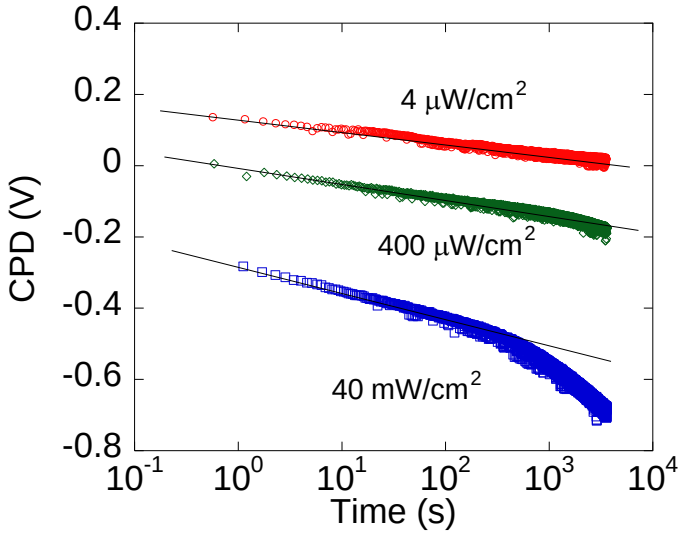

Figure 55 Time-dependent SPV measurement of MBE-grown p-type GaN (9600_MB) in vacuum taken at various intensities using band-to-band UV illumination (325 nm) at T = 500 K. Lines are added to guide the eye.

It is apparent that the SPV at full excitation intensity shows no signs of saturation in vacuum. Instead, at about 10-100 s, it appears that the rate at which the surface becomes more negative increases! We may expect similar behavior for the lower excitation intensities as well, but the behavior would appear after a period of time proportional to the excitation intensity. At an excitation intensity of 40mW/cm^2, it is predicted that the SPV behavior should saturate after less than 1 second. We attribute this behavior to some unknown external mechanism. This type of behavior is another unusual characteristic of the SPV behavior for p-type GaN as measured with a Kelvin probe.

b. Restoration of the SPV

The restoration of the SPV after ceasing illumination for the HVPE-grown sample is shown in Figure 56 for temperatures between 295 and 500 K. As predicted by a thermionic model, the

SPV restores with a logarithmic rate. However, the rate at which the SPV restores is about twice as fast as predicted. This may be due to a high density of defects near the surface, as was observed in the mechanically-polished bulk GaN samples.

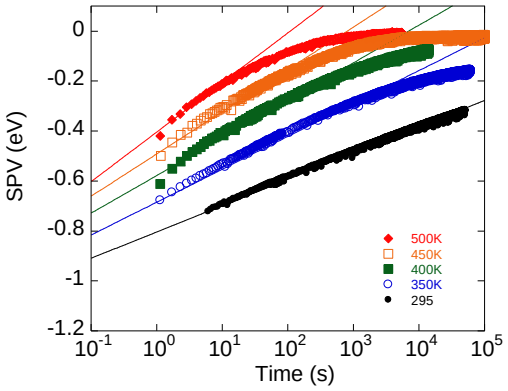

Figure 56 Restorations of SPV for HVPE-grown GaN (863_HP) in vacuum after short (1 s) UV illuminations for temperatures from 295 to 500 K at $P_0 = 10^{17}$ $cm^{-2}s^{-1}$. The fits are calculated using Eq. (4.21b) with y_0 = -1.12, -1.08, -1.03, -1.0, and -0.9 eV; T = 295, 350, 400, 450, and 500 K ; η = 1.8, 1.9, 1.9, 1.9, and 2, for all temperatures respectively; and τ = 0.001 s.

The restoration of the SPV after illumination of the MOCVD grown Mg-doped p-type GaN sample is shown in Figure 57.

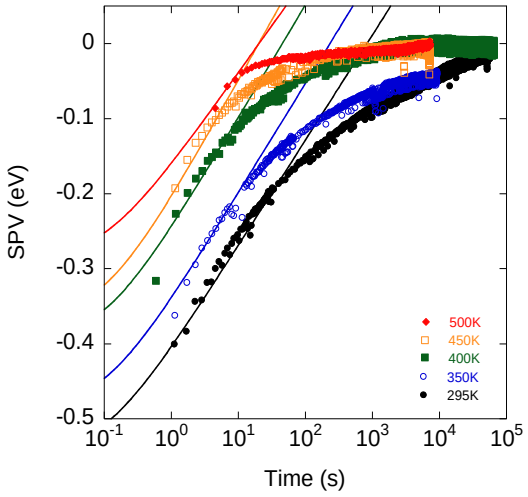

Figure 57 Restorations of SPV for MOCVD grown GaN (983_MP) in vacuum after short (1 s) UV illuminations at temperatures from 295 to 500 K with $P_0 = 10^{17}$ $cm^{-2}s^{-1}$. The fits are calculated using Eq. (4.21b) with y_0 = -0.55, -0.49, -0.4, -0.37, and -0.29 eV; T = 295, 350, 400, 450, and 500 K ; η = 2.4, 2.1, 1.9, 1.8 and 1.2; for all temperatures respectively; and τ = 0.1 s for all samples.

The restoration of the SPV occurs unusually fast at high temperatures, where the SPV appeared to restore after only 50 s. All of the restorations appear to have a fast and slow component, where the fast component lasted for the first 100 s at 295 K and then the SPV slowly restored to zero for the remainder of the measurement. This two-component restoration behavior is more apparent at higher temperatures, where at 500 K the SPV reached a value of about -0.050 eV then slowly restored to zero. This could be an indication that the surface states have multiple energy levels in the band gap. States that are closer to the valence band are expected to restore faster, while states further in the gap will restore more slowly.

The restorations of the SPVs in the MBE-grown sample at high temperature were too fast to be analyzed with the thermionic model and therefore are not shown here. At high temperatures the SPV restored in less than 1 second which has not been observed in any other samples studied. For this reason, the restorations of the MBE-grown samples are not plotted and fit with the

thermionic model. It is, however, interesting that the thermionic model predicts sub-second restorations at high temperatures.

It is important thing to note that if the sample is not heated to higher temperatures, then the band bending will not fully restore. Annealing the samples is crucial to correctly estimating the amount of band bending in dark. At higher temperatures, we are able to observe the complete restoration of band bending, which may not be observable in one's lifetime at 295 K.

7.7 Band Bending in p-type GaN

The band bending in dark, Φ_0, calculated from the fits of the intensity dependence for the HVPE-, MOCVD-, and MBE-grown samples is plotted in Figure 58.

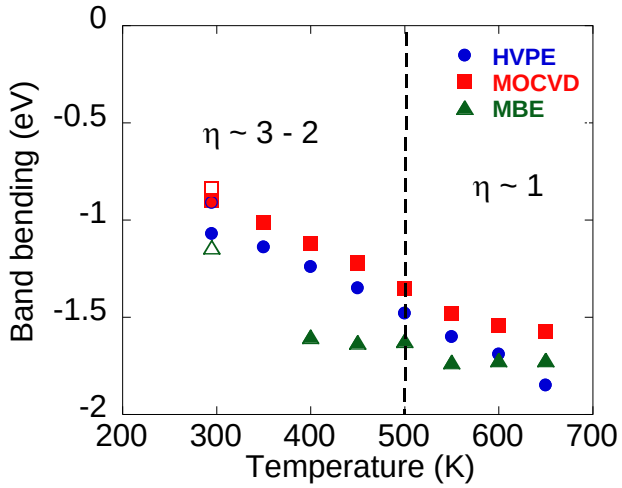

Figure 58 Estimated values of band bending for the HVPE, MOCVD, and MBE p-type GaN samples (863_HP, 983_MP, and 9591_BE) using R_0 values from intensity-dependent SPV measurements at various temperatures. $E_F - E_V$ = 0.19, 0.20, 0.20, 21, 0.21, 0.22, 0.23, and 0.23 eV for sample 863_HP, and, 0.09, 0.09, 0.09, 0.09, 0.09, 0.10, 0.10, and 0.10 eV for sample 983_MP, and N/A, N/A, 0.061, 0.059, 0.057, 0.056, 0.055, and 0.054 eV for sample 9591_BE at T = 295, 350, 400, 450, 500, 550, 600, and 650 K, respectively. The calculated band bending using the AFM are shown with open symbols and is -0.84, -0.91, and -1.14 eV at T = 295 K using $F - E_V$ = 0.15, 0.11 , and 0.073 eV, for the MOCVD, HVPE, and MBE grown samples, respectively. Samples were pre-heated to 650 K for 1 h before measurements.

Using the calculated values of R_0 from the intensity-dependent measurements, the band bending is estimated to range from -0.84 to -2.11 eV when the temperature is varied from 295 to 650 K, respectively. The apparent increase in band bending with temperature needs to be given more consideration since the values of η change with temperature. The intensity-dependent SPV could not be accurately fit by the thermionic model with η close to unity at temperatures below 500 K. If we assume that the measurements at high temperature are the most accurate (based on η values) then the band bending values for the HVPE-, MOCVD-, and MBE-grown samples are -1.85, -1.57, and -1.72 eV at 650 K, respectively.

The values of band bending calculated using the SKPM technique are slightly smaller than the values measured by the Kelvin probe (by ~0.1 eV at 295 K). This may be due to an error in the SPV measurement with the Kelvin probe technique, or that the samples did not restore to their dark values of band bending prior to illumination in the SKPM setup. In the latter case, the samples were kept in ambient lighting in order to solder then to a conductive metal disk. It is possible that the fluorescent lights generated a SPV which could have affected the calculation of band bending. However, these values can be used as the lower end for the downward band bending in p-type GaN.

The band bending was also estimated for a HVPE-grown sample using the raw CPD signal. Using the Eq. (4.26b), and assuming that $N_A = 1.3\times10^{19}$ cm^{-3} and $N_D = 6.5\times10^{18}$ cm^{-3}, the band bending of the HVPE-grown sample can be estimated using the dark CPD. For the MOCVD-grown sample, we assume that $N_A = 8\times10^{19}$ cm^{-3} and $N_D = 1\times10^{18}$ cm^{-3}, which results in $p = 2\times10^{17}$ cm^{-2} at 295 K, as reported to us by our collaborators. Finally, for the MBE-grown sample, we use $N_A = 6\times10^{20}$ cm^{-3} and $N_D = 1.1\times10^{18}$ cm^{-3} to obtain $p = 9\times10^{17}$ cm^{-2} at 295 K,

which was reported to us by our collaborators. Table IX summarizes the results of these calculations.

Table IX: Band bending calculated for the p-type GaN samples using the dark CPD signal. Samples were pre-heated to 650 K for 1 h before measurements.

Sample	Temperature (K)	*qCPD* (eV)	E_g (eV)	E_V-F (eV)	Φ_0 (eV)
863_HP	295	0.068	3.45	-0.182	-1.74
863_HP	350	0.328	3.43	-0.179	-1.98
863_HP	400	0.329	3.40	-0.176	-1.95
863_HP	450	0.328	3.37	-0.174	-1.92
863_HP	500	0.332	3.33	-0.173	-1.89
863_HP	550	0.366	3.30	-0.172	-1.89
863_HP	600	0.376	3.26	-0.172	-1.86
863_HP	650	0.316	3.22	-0.174	-1.76
983_MP	295	0.172	3.45	-0.111	-1.91
983_MP	350	0.09	3.43	-0.104	-1.82
983_MP	400	0.064	3.40	-0.103	-1.76
983_MP	450	0.044	3.37	-0.103	-1.71
983_MP	500	0.043	3.33	-0.104	-1.67
983_MP	550	0.035	3.30	-0.107	-1.63
983_MP	600	-0.036	3.26	-0.110	-1.51
983_MP	650	0.085	3.22	-0.115	-1.59
9591_BP	400	0.037	3.40	-0.062	-1.78
9591_BP	450	0.063	3.37	-0.059	-1.77
9591_BP	500	0.045	3.33	-0.057	-1.72
9591_BP	550	0.030	3.30	-0.056	-1.67
9591_BP	600	0.034	3.26	-0.055	-1.64
9591_BP	650	0.086	3.22	-0.054	-1.65

The results of these calculations are shown in Figure 59.

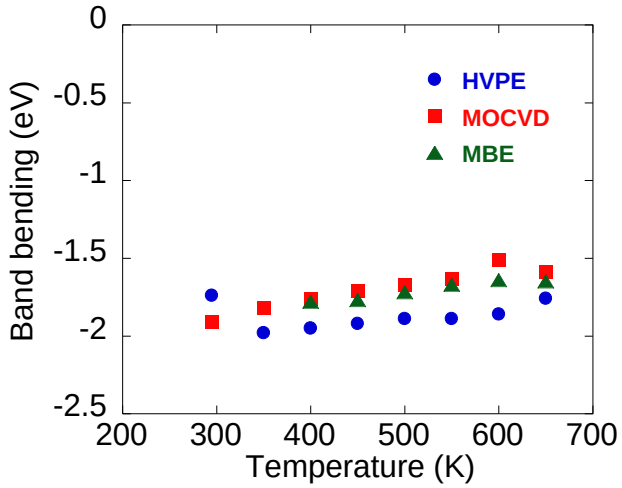

Figure 59 Estimated values of band bending for the HVPE, MOCVD, and MBE grown p-type GaN samples (863_HP, 983_MP, and 9591_BE) using CPD measurements. Samples were pre-heated to 650 K for 1 h before measurements.

The values of band bending in dark from the CPD measurements are similar to the values calculated at higher temperatures with the SPV technique. The CPD data indicate that the absolute value of band bending slightly decreases with increasing sample temperatures. The thermionic model predicts that the band bending should be constant with changing temperature. However, both the SPV and CPD methods of calculating the band bending in dark appear to indicate that the downward band bending in p-type GaN is larger than 1 eV.

In conclusion, we have measured the SPV behavior for p-type GaN grown by three different methods. We observed that illumination of the contacts (either directly from the front side with a laser or indirectly from the back side with the lamp) will cause anomalous offsets of the SPV signal. These offsets will make the SPV to appear to behave as n-type GaN. The slope of the SPV did not scale according to the thermionic model for intensity-dependent measurements at temperatures below 500 K. This behavior was attributed to the high resistivity in p-type GaN. Using intensity-dependent measurements from the Kelvin probe and SKPM, the

band bending was estimated to be between -0.8 and -2.1 eV, where the band bending increases with increasing sample temperatures. From the CPD measurements, the band bending is between -1.5 and -2.0 eV, where the band bending slightly decreased with temperature. Further work needs to be performed to answer this discrepancy at temperatures below 500 K.

7.8 Low-Temperature SPV Measurements

In addition to performing SPV measurements at higher temperatures to distinguish if experimental artifacts were responsible for η values greater than unity in the intensity-dependent SPV measurements, the SPV behavior was also measured at low temperatures. The SPV behavior as a function of temperature for the MOCVD grown p-type GaN sample is shown in Figure 60.

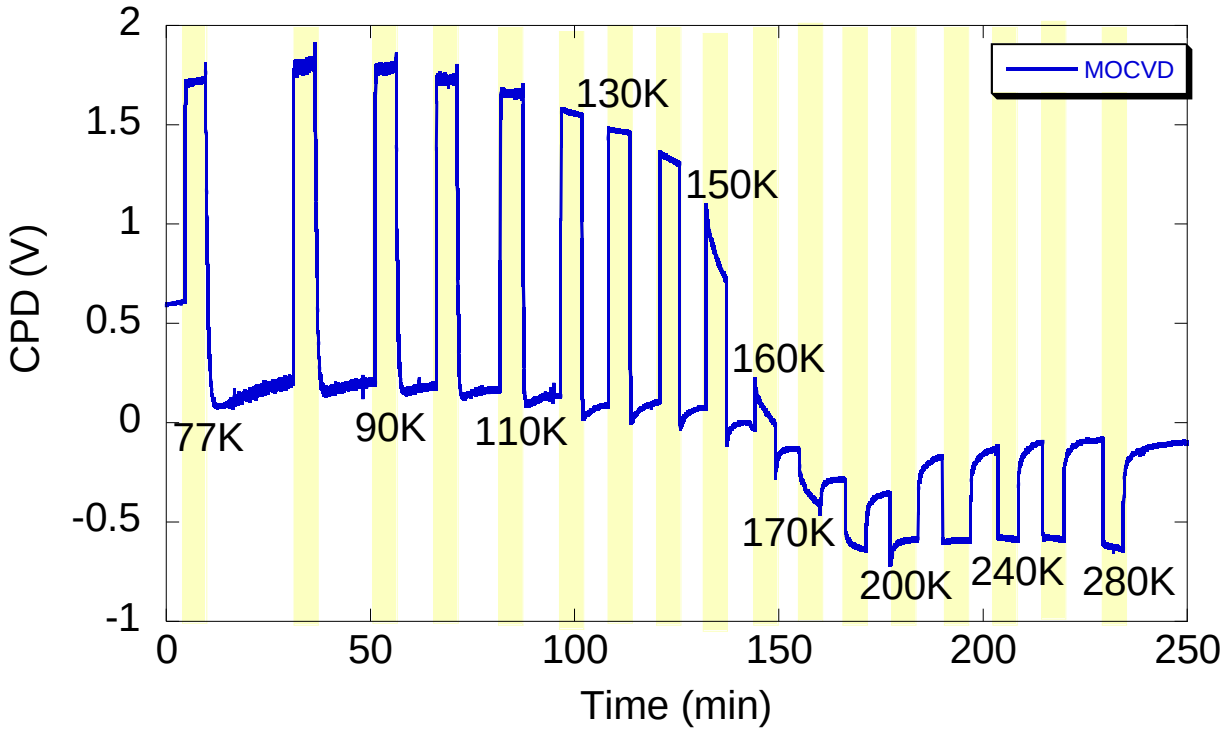

Figure 60 Real time SPV temperature-dependent SPV measurement with variation of the temperature from 77 to 280 K. Periods in which the sample is illumination are shown with a yellow shadow.

While performing SPV measurements at 77 K, it appeared that when the temperature increased from 77 to 295 K, that there was a conversion from "n-type" at low temperatures to "p-type" behavior at high temperatures. In Figure 60, at temperatures below 160 K, the CPD increases under UV illumination. It is until about 170 – 180 K that the CPD decreases under UV illumination, as expected for p-type GaN samples. Not only was the CPD positive at low temperatures, but when illumination was ceased and the CPD restores, it slowly decreases (unlike the fast offset downward observed at 295 K). This behavior can potentially be explained by a thermionic model used to fit PL data by Reshchikov *et al.*[85] In this model, it was predicted that at low temperatures and high excitation intensities there is a larger concentration of free electrons than free holes. It is expected that electrons will saturate a non-radiative defect, which

will cause a population inversion. At higher temperatures, holes become unbound from deep acceptors and then are able to "unplug" the non-radiative channel. With the Kelvin probe, the observation of "p-type" to "n-type" SPV behavior has also been observed for MOCVD- and MBE-grown samples. The temperatures at which the behaviors change are in approximate agreement with the values expected by Reshchikov *et al*.[85]

Chapter 8: X-ray Photoelectron Spectroscopy & Hall Measurements

8.1 XPS Measurements on n-type GaN

To confirm the presence of a UV-induced surface oxide layer, XPS data were taken of both the initial and 100 h UV-exposed samples. Figure 61 contains survey spectra for both samples, where corrections for charge shifting were done based on the C_{1s} peak position at 284.6 eV (shifted the spectra by +1.3 eV).

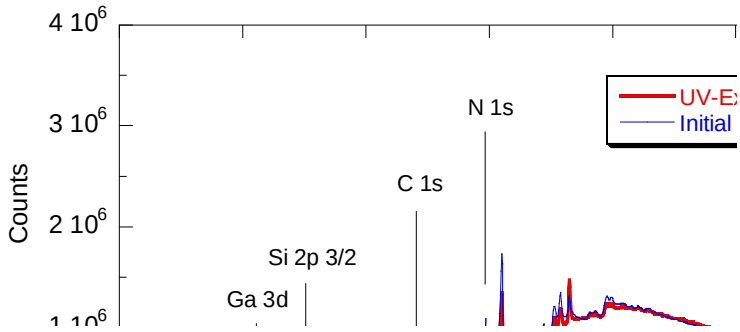

Figure 61 XPS survey spectra of the initial and UV-exposed samples. 2015_HN excited with MgKα X-rays.

The most significant differences between the spectra are the presence of smaller Ga_{2p} peaks and a larger O_{1s} peak for the UV-exposed vs. initial sample. The relative differences of these peaks indicate the growth of a thicker oxide on the surface.

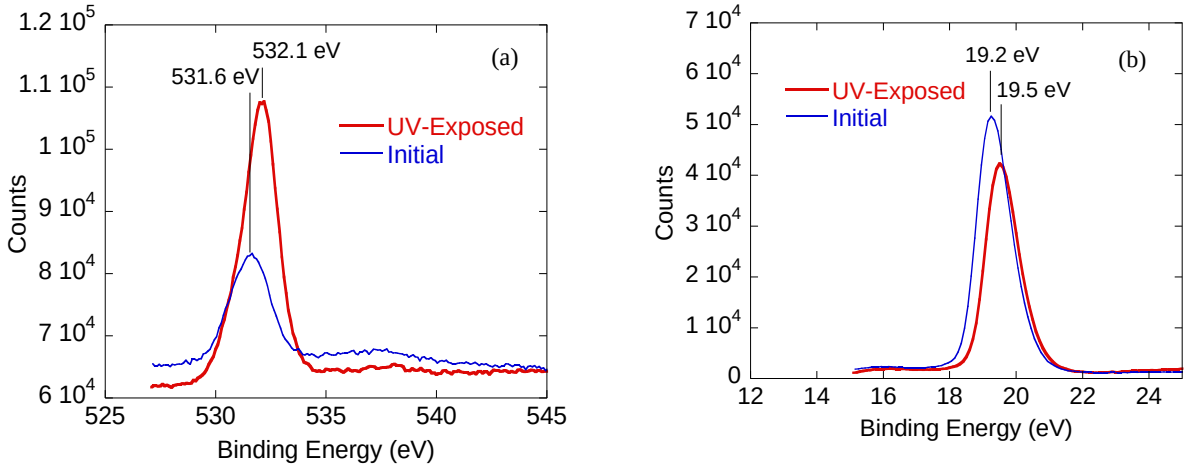

Figure 62 Higher resolution spectra of the (a) O_{1s} and (b) Ga_{3d} peaks for the initial and UV-exposed samples. Both peaks are shifted to higher binding energy for the UV-exposed sample.

Figure 62 shows high-resolution data for the oxygen O_{1s} peak near 532 eV and Ga_{3d} peak near 19 eV. The oxygen peak is more pronounced for the UV-exposed sample and has a shift of ~0.5 eV to higher binding energy, indicating a different chemical environment. A similar shift of ~0.3 eV is also observed for the Ga_{3d} peak. XPS data therefore support the presence of a thicker surface oxide for the sample with extended UV exposure in air.

We can estimate band bending using the Ga_{3d} peak with the described method in the literature review where:

$$(E_F - E_V)_{Surface} = E_{F\,Surface} = Ga_{3d} - 17.76 \tag{8.1}$$

and

$$\Phi_0 = E_{F\,Surface} - E_{F\,Bulk}. \tag{8.2}$$

Using this expression, the band bending was calculated using the positions of the Ga_{3d} peak and the bulk Fermi-level positions provide values of 1.3 and 1.6 eV for the initial and UV-exposed surfaces, respectively. These values are about 0.2 – 0.5 eV larger than the values

measured by the Kelvin probe using the dark CPD and the SPV technique. There is possible error in these measurements that comes from shifting the XPS spectra for carbon. It is assumed that the Fermi-levels between sample and spectrometer are aligned, so there should be no need for shifting. In this early work, we did not mount the sample such that it would be in good electrical contact with the XPS setup. Also, it is important to note that these calculated values of band bending are the lower limits, since the X-rays generate a SPV during measurement of the Ga_{3d} peak.

8.2 Temperature-dependent Hall Effect Measurements

Temperature-dependent Hall effect measurements were performed to determine the concentration of free electrons, n, and electron mobility, μ, of sample 2015_HN. Previously, we found that $n = 3\times10^{18}$ cm^{-3} at room temperature;[86] however, the temperature-dependent measurements in this study indicate that there exists a highly conductive layer near the GaN/sapphire interface which alters the measured mobility and concentration of free electrons.[87] Applying a two layer model used by Look *et al.*,[88] we have now corrected the measurements of mobility and concentration of free electrons, as shown in Figure 63.

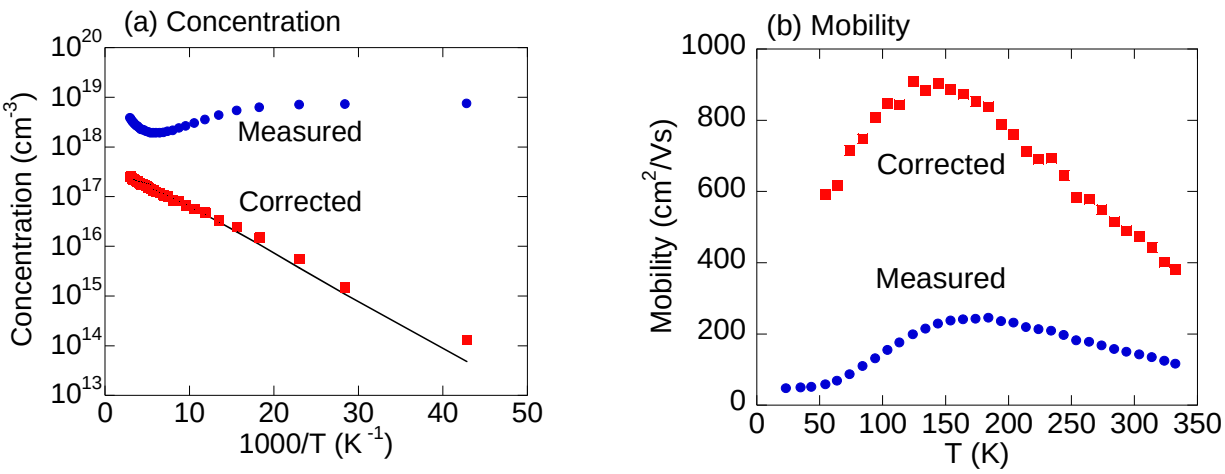

Figure 63 Temperature-dependent Hall measurements of (a) concentration of free electrons n and (b) electron mobility μ for sample 2015_HN. Measured values (blue circles) were corrected using a 2-layer model (red squares) with $\mu = 43.5$ cm^{2}Vs and $n = 2\times10^{20}$ cm^{-3} for the degenerate interface layer. The solid line was fit using $N_A = 5\times10^{16}$ cm^{-3}, $N_D = 4\times10^{17}$ cm^{-3}, and $E_D = 0.020$ eV from Ref. [87].

The correction was obtained by assuming that at low temperatures, the degenerate interface layer is the primary conducting channel, and that values measured at low temperatures are from only the degenerate region. This provides values of $\mu = 43.5$ cm^{-2}Vs and $n = 2\times10^{20}$ cm^{-3} for the degenerate layer, assuming it has a thickness of 200 nm, as in Ref. [87]. The corrected value of n for the bulk region of sample 2015_HN is then about 3×10^{17} cm^{-3} at room temperature, which is an order of magnitude smaller than previously determined. The depletion region is subsequently estimated to be about 50 nm wide.

Chapter 9: Conclusions and Future Directions

This dissertation has discussed the characterization of the surfaces of GaN using various techniques, mainly the surface photovoltage technique based on the Kelvin probe method. We began by analyzing the SPV behavior in n-type GaN under continuous illumination in oxygen and vacuum. In oxygen, illumination of the sample with UV-light aids physisorbed oxygen to become chemisorbed after it receives an electron from the bulk, which reduces the band bending. In vacuum, we observed the subsequent desorption of negatively charged species under illumination. When measuring the intensity-dependent SPV behavior, the SPV increased logarithmically with light intensity as predicted by a thermionic model. Using this dependence, the band bending in an HVPE-grown GaN was estimated to be about 1.1 eV upward. The band bending was also estimated using the dark CPD, which provided values close to 1 eV as well. The restoration of the band bending was logarithmic in time as predicted by a thermionic model. However, the delay time after which the logarithmic dependence began depended on how long the sample was exposed with UV-light at high intensity, which can be attributed to slow external processes.

We discussed the effect of polarity and surface treatment on the SPV behavior in HVPE-grown bulk GaN templates. When analyzing the steady-state SPV behavior in oxygen, we established that the HCl-cleaned, N-polar surface is more prone to the photo-induced adsorption of oxygen species. The band bending in Ga-polar GaN is about 0.2 eV larger than the that in N-polar GaN. The SPV spectra obtained with below-bandgap excitation revealed that the mechanically polished surfaces generated larger SPVs due to a larger number of defects near the surface. In photoluminescence measurements, the mechanically polished surfaces exhibited PL

intensities several orders of magnitude smaller than the chemically mechanically polished surfaces. This further indicates that there exists a large concentration of defects near the surface of the mechanically polished samples. Furthermore, in the experiments measuring the SPV restoration after short illumination of the mechanically and chemically mechanically polished surfaces, it was found that the restoration rate was about twice as fast as expected for the mechanically treated surfaces. This behavior was attributed to electron hopping between defects, thereby assisting electrons to reach the surface.

For p-type GaN, we observed that illumination of the contacts (either directly from the front-side with a laser or indirectly from the back side with the lamp) will cause anomalous offsets of the SPV signal. The slope of the SPV as a function of excitation intensity was inconsistent with a thermionic model at temperatures below 500 K. Using intensity-dependent measurements from the Kelvin probe and SKPM, the band bending was estimated to be between -0.8 and -2.1 eV, where the band bending appeared to increase with increasing sample temperatures. From the CPD measurements, we determined that the band bending is between -1.6 and -2.0 eV, with no significant temperature dependence. Pre-heating the samples at 650 K for 1 h in dark proved vital in correctly measuring the value of band bending in dark.

In summary, we have studied the surface properties of GaN using the SPV technique based on the Kelvin probe method. A thermionic model has been developed to explain the results. Specifically, we found that: (1) oxygen is photo-adsorbed onto the surface of GaN; (2) the oxide layer grows due to extended exposure of GaN to UV-light in air ambient; (3) the band bending in n-type GaN is about 1 eV at T = 295 – 650 K; (4) the SPV behavior in n-type GaN can be well-described by a thermionic model; (5) the cleaned N-polar surface is more prone to the adsorption of oxygen and has about 0.2 eV smaller band bending than Ga-polar; (6) the

surface preparation (type of polishing) can affect the steady-state SPV values and SPV restoration due to the introduction of defects at the surface; (7) the difficulties measuring the SPV behavior of p-type GaN under UV-illumination due to experimental artifacts; (8) the band bending for p-type GaN varies from -0.8 to -2.3 eV, with the largest value at 600 K; (9) that pre-heating the samples in darkness allowed the band bending in p-type GaN to fully restore, and (10) p-type GaN may convert locally to n-type GaN at low temperatures and high UV-excitation. Finally, this dissertation illustrated the versatility of the Kelvin probe method to characterize the surface of wide band gap semiconductors.

References

[1] S. Nakamura, T. Mukai, M. S. Senoh, Jap. J. Appl. Phys. **30**, L1998 (1991).

[2] http://www.blu-raydisc.com/en/Technical/FAQs/HistoryandAssociation.aspx

[3] H. Morkoç, *Nitride Semiconductors and Devices*, Springer-Verlag Berlin Heidelberg (1999).

[4] T. Harafuji and J. Kawamura , *Appl. Phys.* **96**, 2501(2004).

[5] D. A. Stocker, E. F. Schuber, and J. M. Redwing, Appl. Phys. Lett. **73,** 2654-2656 (1998).

[6] S Nakamura, T. Mukai, M. Senoh, Appl. Phys. Lett. **64**, 13 (1994).

[7] S. Mohammad, A. Salvador, H. Morkoc, *Proceedings of the IEEE* , vol.83, no.10, pp.1306-1355, Oct 1995.

[8] J. Neugebauer and C. G. Van de Walle, *Appl. Phys. Lett*. **69**, 503 (1996).

[9] W. C. Johnson, J. B. Parson, and M. C. Crew, J. Phys. Chem. **36**, 2561 (1932).

[10] I. Vurgaftman, J. R. Meyer, and L. R. Ram-Mohan, J. Appl. Phys. 89, 5815 (2001).

[11] K. Hiramatsu, S. Itoh, H. Amano, I. Akasaki, N. Kuwano, T. Shiraishi and K. Oki, J. Crystal Growth **115**, 628-633 (1991).

[12]M. Lin, S. Strite, A. Agarwal, A. Salvador, G. Zhou, N. Teraguchi, A. Rockett, and H. Morkoç, Appl. Phys. Lett. **62**, 702-704 (1993).

[13] H. P. Maruska and J. J. Tietjen, Appl. Phys. Lett. **15**, 327 (1969).

[14] H. Amano, M. Kito, K. Hiramatsu, and I. Akasaki, Jpn. J. Appl. Phys. **28**, L2112-L2114 (1989).

[15] S. Nakamura, M. Senoh, S. Nagahama, N. Iwasa, T. Yamada, T. Matsushita, H. Kiyoku, and Y. Sugimoto, Jpn. J. Appl. Phys. **35**, L74-L76 (1996).

[16]H. Morkoc, S. Strite, G. B. Gao, M. E. Lin, B. Sverdlov, M. Burns, J. Appl. Phys. **76**, 1363 (1994).

[17] V. M. Bermudez, J Appl. Phys. **80**, 1190 (1996).

[18] C. I. Wu and A. Kahn, J. Vac. Sci. Technol. B **16**, 2218 (1998).

[19] H. W. Jang, J. H. Lee, and J. L. Lee, Appl Phys. Lett. **80**, 3955 (2002).

[20] S. Nakamura, IEICE Transactions on Electronics **E83-C,** 529 (2000).

[21] E. Feltin, B. Beaumont, M. Laügt, P. de Mierry, P. Vennégues, H. Lahrèche, M. Leroux, and P. Gibart, Appl. Phys. Lett. **79**, 3230 (2001).

[22] S. Mohammad and H. Morkoc, Proceedings of the IEEE **83**, 1306 (1995).

[23] T. Sasaki and T. Matsuoka, J. Appl. Phys. **64**, 4531 (1988).

[24] S. D. Wolter, B. P. Luther, D. L. Waltemyer, C. Onneby, S. E. Mohney, and R. J. Molnar, Appl. Phys. Lett. **70** (16), 21 (1997).

[25] http://www.kelvinprobe.info/.

[26] Z. W. Deng, R. W. M. Kwok, W. M. Lau, and L. L. Cao, Appl. Surf. Sci. Volume **158**, 58-63 (2000).

[27] J. Cui, R. Graupner, J. Ristein, and L. Ley, Diam. Relat. Mater. **8**, 748-753 (1999).

[28] F. S. Aguirre-Tostado, M. Milojevic, K. J. Choi, H. C. Kim, C. L. Hinkle, E. M. Vogel, J. Kim, T. Yang, Y. Xuan, P. D. Ye, and R. M. Wallace, Appl. Phys. Lett. **93**, 061907 (2008).

[29] K. Kakushima, K. Okamoto, K. Tachi, J. Song, S. Sato, T. Kawanago, K. Tsutsui, N. Sugii, P. Ahmet, T. Hattori, and H. Iwai, J. Appl. Phys. **104**, 104908 (2008).

[30] R. Schlaf, P. G. Schroeder, M. W. Nelson, B. A. Parkinson, P. A. Lee, K. W. Nebesny, and N. R. Armstrong, J. Appl. Phys. **86**, 1499-1509 (1999).

[31] W. M. Lau, R. W. M. Kwok, and S. Ingrey, Surf. Sci. **271**, 579-586 (1992).

[32] T. Hashizume, S. Ootomo, S. Oyama, M. Konishi, and H. Hasegawa, J. Vac. Sci. Technol. B. **19**, 1675-1681 (2001)

[33] http://physics.nist.gov/PhysRefData/XrayMassCoef/ComTab/gallium.html

[34] J. R. Waldrop and R. W. Grant, Appl. Phys. Lett. **68**, 2879 (1996).

[35] S. Bloom, G. Harbeke, E. Meier, and I. B. Ortenburger, Phys. Status Solidi B **66**, 161 (1974)

[36] G. Martin, S. Strite, A. Botchkarev, A. Agarwal, A. Rockett, H. Morkoç W. R. L. Lambrect, and B. Segall, Appl. Phys. Lett. **65**, 610 (1994).

[37] K. M. Tracy, W. J. Mecouch, R. F. Davis, and R. J. Nemanich, J. Appl. Phys. **94**, 3163 (2003).

[38] S. W. King, J. P. Barnak, M. D. Bermser, K. M. Tracey, C. Ronning, R. F. Davis, and R. J. Nemanic, J. Appl. Phys, **84** 5248 (1998).

[39] M. Alonso, R. Cimino, and K. Horn, Phys. Rev. Lett. **64**, 1947 (1990).

[40] H. Sezen, E. Ozbay, O. Aktas, and S. Suzer, Appl. Phys. Lett. **98**, 111901 (2011).

[41] V. M. Bermudez, T. M. Jung, K. Doverspike, and A. E. Wickenden, J. Appl. Phys. **79**, 110 (1996).

[42] S. Kitamura and M. Iwatsuki, Appl. Phys. Lett. **72**, 3154-3156 (1998).

[43] J. A. Nichols, D. J. Gundlach, and T. N. Jackson, Appl. Phys. Lett. **83**, 2366-2368 (2003).

[44] B. S. Simpkins, E. T. Yu, and P. Waltereit, J. Appl. Phys. **94**, 1448-1453 (2003).

[45] S. Chevtchenko, X. Ni, Q. Fan, A. A. Baski, and H. Morkoç, Appl. Phys. Lett. **88**, 122104 (2006).

[46] M. A. Reshchikov, S. Sabuktagin, D. K. Johnstone, A. A. Baski, and H. Morkoç Phys. Sol. Stat. **2**, 2813-2816 (2005).

[47] G. Koley and M. G. Spencer J. Appl. Phys. **90**, 337, (2001).

[48] J. A. Smart, A. T. Schremer, N. G. Wiemann, O. Ambacher, L. F. Eastman, and J. R. Shealy, Appl. Phys. Lett. **75**, 388 (1999).

[49] S. Sabuktagin, M. A. Reshchikov, D. K. Johnstone, and H. Morkoç, Mat. Res. Soc. Symp. Proc. **798**, Y5.39.1 (2004).

[50] K. A. Bulashevich and S. Y. Karpov Phys. Stat. Sol. C. **3**, 2356-2359 (2006).

[51] S. Barbet, R. Aubry, M.A. di Forte-Poisson, J.C. Jacquet, D. Deresmes, T. Mélin, and D. Théron, Appl. Phys. Lett. **93**, 212107 (2008).

[52] B. S. Simpkins, D. M. Schaadt, E. T. Yu, and R. J. Molnar J. Appl. Phys **91**, 9924 (2002).

[53] J. D. Wei, S. F. Li, A. Atamuratov, H.H. Wehmann, and A. Waag, Appl. Phys. Lett. **97** 172111 (2010).

[54] L. Kronik and Y. Shapira, Surf. Interface Anal. **31**, 954-965 (2001).

[55] M. Eyckeler, W. Monch, T. U. Kampen, R. Dimitrov, O. Ambacher, and M. Stutzmann, J. Vac. Sci. Technol B **16**, 2224 (1998).

[56] I. Shalish, Y. Shapira, L. Burstein, and J. Salzman, J. Appl. Phys. **89**, 390-395 (2001).

[57] J. P. Long and V. M. Bermudez, Phys. Rev. B. **66**, 121308 (2002).

[58] G. Koley and M. G. Spencer, J. Appl. Phys. **90**, 337 (2001).

[59] M. Eyckeler, W. Mönch, T. U. Kampen, R. Dimitrov, O. Ambacher, and M. Stutzmann, J. Vac. Sci. Technol. B **16**, 2224 (1998).

[60] C. I. Wu and A. Kahn, J. Appl. Phys. **86**, 3209 (1999).

[61] McAllister Technical Services, Kelvin Probe users manual, (1999-2007).

[62] http://www.kelvinprobe.info/technique-theory.htm

[63] M. A. Reshchikov, M. Foussekis, and A. A. Baski, J. Appl. Phys. **107**, 113535 (2010).

[64] S. M. Sze, *Physics of Semiconductor Devices*, 2nd ed.,Wiley, New York, 1981.

[65] W. J. Moore, J. A. Freitas, Jr., and R. J. Molnar, Phys. Rev. B **56**, 12073 (1997).

[66] K. Jarasiunas, "Nonlinear optical characterization of photoelectrical properties of wide bandgap semiconductors by time-resolved four-wave mixing technique", *Wide Bandgap Materials and New Developments*, Ed. M. Syvajarvi and R. Yakimova (2006).

[67] V. Bougrov, M. E. Levinshtein, S. L. Rumyantsev, and A. Zubrilov , in *Properties of Advanced SemiconductorMaterials GaN, AlN, InN, BN, SiC, SiGe* . Eds. Levinshtein M.E., Rumyantsev S.L., Shur M.S., John Wiley & Sons, Inc., New York, 2001, 1-30.

[68] J. I. Pankove, S. Bloom, and G. Harbeke, *RCA Rev.*, **36**, 163 (1975).

[69] H. Nienhaus, M. Schneider, S. P. Grabowski, W. Monch, R. Dimitrov, O. Ambacher, and M. Strutzmann, Mater. Res. Soc. Symp. Proc. **680**, E4.5 (2001).

[70] C. H. Su, W. Palosz, S. Zhu, S.L. Lehoczky, I. Grzegory, P. Perlin, T. Suski, Journal of Crystal Growth, **235**, 111-114 (2002).

[71] D. C. Look, *Electrical Characterization of GaAs Materials and Devices* (Wiley, New York, 1989), App. B.

[72] J. D. McNamara, M. Foussekis, H. Liu, H. Morkoç, M. A. Reshchikov, and A. A. Baski Proc. SPIE 8262, 826213 (2012).

[73] M. A. Reshchikov, G. –C. Yi, and B. W. Wessels, Phys. Rev. B **59**, 13176 (1999).

[74] J. D. Ferguson, M. A. Foussekis, M. D. Ruchala, J. C. Moore, M. A. Reshchikov, and A. A. Baski, Mat. Res. Soc. Symp. **1202**, I04-01 (2009).

[75] M. Foussekis, J. D. Ferguson, A. A. Baski, H. Morkoç, and M. A. Reshchikov, Physica B: Condensed Matter **404**, 4892-4895 (2009).

[76] F. Binet, J. Y. Duboz, E. Rosencher, F. Scholz, and V. Harle, Phys. Rev. B. **54**, 11 (1996).

[77] W. Franz and Z. Naturforschung **13a**, 484(1958).

[78] L. V. Keldysh, Sov. Phys. JETP **7**, 788 (1958).

[79] M. Foussekis, A. A. Baski, and M. A. Reshchikov, Appl. Phys. Lett. **94**, 162116 (2009).

[80] T. K. Zywietz, J. Neugebauer, and M. Scheffler, Appl. Phys. Lett. **74**, 1695 (1999).

[81] K. M. Jones, P. Visconti, F. Yun, A. A. Baski, and H. Morkoç, Appl. Phys. Lett. **78**, 2497 (2001).

[82] M. A. Reshchikov, H. Morkoç, S. S. Park, and K. Y. Lee, Appl. Phys. Lett. **81**, 4970 (2002).

[83] M. A. Reshchikov and H. Morkoç, J. Appl. Phys.97, 061301 (2005).

[84] L. Kronik, Y. Shapira, Surface Science Reports **37** 1-206 (1999).

[85] M. A. Reshchikov, A. A. Kvasov, M. F. Bishop, T. McMullen, A. Usikov, V. Soukhoveev, and V. Dmitriev, Phys. Rev. B. **84**, 075212 (2011).

[86] M. Foussekis, A. A. Baski, and M. A. Reshchikov Physa. Stat. Sol. (c) **8**, 2148-2150 (2011)

[87] D. C. Look, C. E. Stutz, R. J. Molnar, K. Saarinen, and Z. Liliental-Weber, Sol. St. Comm. **117**, 571 (2001).

[88] D. C. Look and R. J. Molnar, Appl. Phys. Lett. **70**, 3377-3379 (1997).